Impacts of Climate Change, Land Management Practices and Land Cover on Water Resources at the Watershed Scale

by

Xiaoyu Kang

BSc, Beijing Forestry University, 2016

MSc, Beijing Forestry University, 2019

A Dissertation Submitted in Partial Fulfillment of the Requirements for the Degree of

Doctor of Philosophy

in the Graduate Academic Unit of Forestry and Environmental Management

Supervisors:	Fan-Rui Meng, Ph.D., Dept. of Forestry and Environmental Management
	Charles P.-A. Bourque, Ph.D., Dept. of Forestry and Environmental Management
Examining Board:	Paul A. Arp, Ph.D., Dept. of Forestry and Environmental Management
	Guohua Yan, Ph.D., Dept. of Mathematics and Statistics
	Alexa Alexander Trusiak, Ph.D., Dept. of Biology
External Examiner:	Wanhong Yang, Ph.D., Dept. of Geography, Environment & Geomatics, University of Guelph

This dissertation is accepted by the Dean of Graduate Studies

THE UNIVERSITY OF NEW BRUNSWICK

August 2024

ABSTRACT

Water resources are critical to sustaining terrestrial ecosystems and socio-economic systems globally. However, global water supplies are threatened by deforestation and conversion to agricultural lands. Assessing the impacts of landcover change at the watershed scale poses significant challenges. Difficulty arises from inherent variability associated with the interaction of complex land-surface conditions due to variation in watershed characteristics and landuse/landcover, daily-to-annual response of watersheds to changing local-to-regional weather. It also comes with small sample sizes typically obtained with traditional watershed experiments. Consequently, comprehensive, integrated models of watershed hydrology is used in assessing impacts of climate change, land management, and landcover on water resources in watersheds. Hydrological models have their own limitations, as they are developed and refined according to pre-existing knowledge of hydrological processes. In this study, a comprehensive hydrological model (i.e., SWAT) in combination with experimental data and statistical methods was used to assess the impacts of climate change, landuse practices, and landcover variances on water resources at the watershed scale. This hybrid approach overcomes the limitations existing in both field experiments and watershed models. Here, three scientific questions associated with the application of the model are addressed. Climate change is shown to have a negative impact on crop yields under three emission scenarios, Representative Concentration Pathways (RCPs) 2.6, 4.5, and 8.5. Under RCP 8.5, a significant reduction in crop yield is projected to ensue from 2060 to 2099, i.e., 13–23% from historical yields. Present research also indicates the impacts of elevated ambient CO_2 concentrations on water yield can be distinguished at watershed level and was shown to be responsible for a 1.6% increase in

water yield over 23-year. The gradual, annual application of flow diversion terraces in the same watershed caused a measurable reduction in water yield by about 29% at the end of the study period. It was also found that forested watersheds had lower peak flow during the snowmelt seasons, and this flow was delayed by at least 7–17 days following the peak flow observed in an agricultural watershed. The results from this study have profound implications for water-resource management, landuse planning, and flood-risk management.

ACKNOWLEDGEMENT

I would like to acknowledge the support from my supervisor, Dr. Fan-Rui Meng, throughout my research journey. Dr. Meng has been instrumental in providing expert assistance in designing my dissertation. His ideas and guidance in the usage of hydrological models and statistical analysis methods have been fundamental for my dissertation. Moreover, Dr. Meng's advice and direction have been crucial in navigating my Ph.D. program. I appreciate the academic and financial support provided by Dr. Charles P.-A Bourque, my co-supervisor. His instruction in meteorology and hydrology has been foundational to my education. Dr. Bourque has not only guided me in conducting academic research but has also profoundly influenced my analytical skills. Furthermore, his mentorship in the art of constructing, writing, and revising scholarly papers has been invaluable. I also extend my appreciation to Dr. Junyu Qi, a member of my advisory committee, for his guidance on structuring my papers and dissertation. His teachings have not only enlightened me on the principles of systemic thinking but also paved my way into academics. Additionally, I am indebted to Dr. Sheng Li, another member of my advisory committee, for his generous funding, support, and invaluable contributions to my academic research. Dr. Li's provision of experimental data and mentorship on research methods have been instrumental in my scholarly journey.

I extend my appreciation to the faculty members of the Faculty of Forestry and Environmental Management (ForEM), especially Dr. Paul A. Arp for his invaluable instruction in hydrology and soil sciences, and Mr. Jae Ogilvie, for his expert support on matters associated with the usage of ArcGIS. My appreciation also goes out to the entire staff of ForEM for their assistance across the different facets of my program. Furthermore,

I am thankful to the staff of the Soil and Hydrology team at the Fredericton Research and Development Centre for their generosity in providing additional data. Their collective support has significantly contributed to my academic journey.

I am grateful for the support from my parents throughout my Ph.D. program. I also wish to extend my thanks to Dr. Meng's wife, for her assistance in my daily life and for being an exemplary role model in fostering positive habits. Additionally, my gratitude goes to all my colleagues in Drs Meng and Bourque's research lab, especially Dr. Kang Liang and his wife who have offered me exceptional care since my arrival.

I would like to acknowledge the financial support from (1) Natural Sciences and Engineering Research Council (NSERC), New Brunswick Environmental Trust Fund (NBETF) and Environment and Climate Change Canada (ECCC) through project GCXE21P014; (2) province of New Brunswick through project J-002472, entitled "Modeling the effects of water stress and supplemental irrigation on potato production in New Brunswick under climate change"; (3) Agriculture and Agri-Food Canada through project J-001754 entitled "Landscape integrated soil and water conservation (LISWC) on sloping fields under potato production in Atlantic Canada"; and (4) Faculty of Forestry and Environmental Management, UNB, for license and computer support for ESRI ArcGIS™ and other software employed in this study. I also thank Sylvie Lavoie, Yulia Kupriyanovich, John Monteith, and Lionel Stevens for their technical support in data collection and sample analyses.

X. Kang

March 2024

TABLE OF CONTENTS

LIST OF TABLES

LIST OF FIGURES

LIST OF ABBREVIATIONS

AAFC	Agricultural and Agri-Food Canada
AC	Atlantic Canada
AP	Agriculture-based Parameters
BBW	Black Brook Watershed
BCCAQv2	Bias Correction/Constructed Analogues with Quantile mapping reordering
BL	Baseline
BMLR	Bayesian Multiple Linear Regression
BMPs	Best Management Practices
CMIP5	Coupled Model Intercomparison Project Phase 5
CN	Curve Number
CO_2	Carbon Dioxide
DEM	Digital Elevation Model
DOY	Day of Year
EARI	Enabling Agricultural Research and Innovation
EP	Parameters associated with the evapotranspiration process
ET	Evapotranspiration
FDTs	Flow Diversion Terraces
FP	Parameters associated with forests
GCMs	General Circulation Models, Global Climate Models
GHGs	Global Greenhouse Gases
GP	Parameters associated with groundwater discharge
GRW	Grande Rivière Watershed
HRU	Hydrologic Response Unit
HSD	Honestly Significant Difference
IQR	Interquartile Range
IRW	Iroquois River Watershed
LAI	Leaf Area Index
LiDAR	Light Detection and Ranging

LISWC	Landscape Integrated Soil and Water Conservation
MCMC	Markov Chain Monte Carlo
MLR	Multiple Linear Regression
NB	Province of New Brunswick
NSERC	Natural Sciences and Engineering Council of Canada
PCIC	Pacific Climate Impacts Consortium
RCPs	Representative Concentration Pathways
SD	Standard Deviation
SM	Supplementary Material
SP	Parameters associated with the snowmelt process
SUFI-2	Sequential Uncertainty Fitting algorithm *v.* 2
SWAT	Soil and Water Assessment Tool
SWAT-CUP	Soil and Water Assessment Tool, Calibration and Uncertainty Procedures
USDA	United States Department of Agriculture
USJR	Upper Saint John River
WUE	Water Use Efficiency

CHAPTER 1

INTRODUCTION

1.1 Background

Water resources are critical for securing human life, sustaining socio-economic development, and maintaining the stability of ecosystems (Rozas-Vásquez et al., 2019). However, issues including increases in human populations, expansion of agricultural food production, rapid urbanization, as well as other economic activities, interrupt natural water cycles and pose threats to water supplies globally (Hurkmans et al., 2009; Kiptala et al., 2013; Marcal et al., 2021; Yu and Bourque, 2022), contributing to water scarcity in many regions of the world. It is recognized that insufficient soil water is an important limitation on local food production and security (Kang et al., 2009; Tijjani et al., 2024). These interests are severely impacted by (i) climate change, particularly as air and land surface temperatures increase, the consumption of water vapor by the atmosphere increases, and precipitation patterns change (Martínez-Valderrama et al., 2023), and (ii) landuse measures that alter landcover characteristics and associated water supplies (Potter, 1991; Roy et al., 2024). Therefore, a systematic understanding of hydrological processes and their influencing factors at watershed scales can facilitate the formulation of appropriate water-resource management strategies and the prediction of future water supplies.

However, these influencing factors are naturally confounded and not easily isolated as to their specific role in defining hydrological processes. In many experimental studies, watershed experiments are commonly used to separate the influencing factors on water resources, because these experiments (i) offer a comprehensive and realistic approach to provide understanding informing sustainable land management practices and water resources planning; (ii) capture the complexity of hydrological processes occurring in response to different controlling factors, such as those associated with variable climate, soil

properties, physiographic variability, and vegetation cover; (iii) allow researchers to study watershed-process alterations by landuse effects, not only for the immediate area but also for the entire watershed for the reason that landuse changes in one part of the watershed may have cascading effects downstream, accounting for the accumulated impacts on downstream water quantity and quality; and (iv) facilitate the direct measurement of waterflow, including surface runoff and discharge. Previous long-term watershed experiments have accumulated large amounts of observed data, assisting our understanding of major hydrological processes at the watershed scale (e.g., Udawatta et al., 2002; Gomyo and Kuraji, 2016). However, all field experiments, e.g., paired-watershed experiments (Gomyo and Kuraji, 2016; Tomer, 2018), pre- and post-treatment experiments (Troendle and King, 1985), and edge-of-field experiments (Daniels et al., 2018), have their limitations. Since hydrological processes are complex with massive year-to-year variations, assessing the impact of forest tree removal on water yield, for instance, may require large sample sizes. Restricted by the costs of experiments and expansive labor requirements, difficulties exist in acquiring sufficient data for analysis. Furthermore, these experimental approaches are limited by their scope, posing challenges when applied to large areas (Jin et al., 2023).

Consequently, comprehensive, process-based models of watershed hydrology, e.g., MIKESHE (Wang et al., 2013), WetSpa (Safari et al., 2012), SWAT (Arnold et al., 1998; Saravanan et al., 2022), and other comparable models, are widely used to compensate for limitations in field experiments (Leavesley, 1994; Jayakrishnan et al., 2005). While process-based models are comprehensive, efficient, and capable of extrapolating experimental data to broader spatial scales, their merit and precision as to the assessment of cause-and-effect relationships hinge on the accuracy with which the models can

represent salient biophysical processes. It has been observed that process-based models can introduce considerable uncertainty in evaluating the effects of climate, land management practices, and landcover type, stemming from the intricate interaction among these elements and models' limited capacity. Uncertainties come from model structure (Qi et al., 2016a, 2016b, 2017b; Karki et al., 2023; Li et al., 2023; Liang et al., 2023a; Mu et al., 2023; Zhang et al., 2023b), parameterization (Wu et al., 2012a, 2012b; Haas et al., 2022; Garna et al., 2023), and input data used (Qi et al., 2017a, 2022; Zeng et al., 2023; Zhang et al., 2023a; Zhu et al., 2023; Liu et al., 2024), posing some limitations on model accuracy. However, improvements to reduce model uncertainties are strongly connected to field data acquired from field experiments for understanding hydrological processes and model calibration.

In brief, both field-watershed experiments and hydrological models bring their own sets of limitations in estimating the controlling factors of water-yield dynamics in rivers and streams. This study proposes two new approaches of analysis (Chapters 3 and 4), considering ambiguity in the models' ability to assess all shared effects associated with variable weather, on-land management practices, and landcover type differences on monthly water yields. These methods rely on the predictions produced with a well-established, process-based model (i.e., SWAT, Soil Water Assessment Tool, in this case) in developing baseline scenarios. Results from these studies are then compared to historical field data using various analytical techniques (e.g., residual analysis based on Bayesian techniques and model regionalization) to isolate the roles of selected influencing factors, either (i) not accounted for in current model structure (Chapter 3), or (ii) involving watershed-wide differences in landcover expression not easily quantified (Chapter 4).

Employing these approaches cannot only assist in isolating influencing factors efficiently for these two problems but can also help identify important processes that should be featured in hydrological models for improved performance under new circumstances.

1.2 Objective

The main objective of this dissertation is to assess the impacts of future climate change, on-land management practices, and different landcover type on water resources in Atlantic Canada (AC). Specifically, three main research areas being addressed, include: (i) predicting the impacts of climate change (i.e., changes in air temperature and precipitation) and ambient CO_2 concentrations on future crop yields (Chapter 2); (ii) separating the impact of ambient elevated CO_2 concentrations and construction of flow diversion terraces on streamflow dynamics by means of residual analysis (Chapter 3); and (iii) quantifying differences in hydrological response associated with variances in landcover type, particularly agriculture- *vs.* forest-dominated watersheds using model regionalization (Chapter 4).

1.3 Process-based model of choice

A process-based model that embraces hundreds of equations and parameters that describe the sophistication of watershed processes, associated with snow accumulation and melt, groundwater flow, surface runoff generation, and evapotranspiration processes (Golmohammadi et al., 2014; Sun et al., 2023). Among the many hydrological models that presently exist, SWAT is widely used in scientific research and water-resource assessment and watershed management (Yang et al., 2009a, 2009b; Qi et al., 2016a, 2016b, 2017a; Liang et al., 2023a, 2023b; Oduor et al., 2023; Tola and Shetty, 2023). It is commonly used as a decision-support tool in evaluating the impacts of best management practices (BMPs)

and landcover change on water resources in large ungauged watersheds (Qi et al., 2018; Izady et al., 2021; Silva et al., 2024). Recently, the model was extended to estimate the effect of climate change on water yields associated with different greenhouse gas (i.e., GHG) scenarios (Kang et al., 2022; Li et al., 2022). SWAT discretizes the watershed into subwatersheds, which are further subdivided into hydrological response units (HRUs) with homogeneous physiographic features, landuse/landcover type, and soil properties (Neitsch et al., 2011). The model calculates the water balance, including surface and shallow, subsurface runoff, infiltration, percolation, groundwater recharge and discharge (baseflow), evapotranspiration, and transmission losses, crop growth, nutrient cycling, and pesticide-residue transfer within individual HRU. Waterflow, sediment, and nutrient loadings from each HRU are then summed, with the resulting loadings being routed through watershed-specific determinations of channels, ponds, and reservoirs to the watershed outlet. Model outputs include scales from HRU to subwatersheds, to the entire watershed. Observed hydrological data are subsequently used for the calibration and validation of SWAT for extended time horizons through adjustment of parameters linked to specific hydrological processes (Arnold et al., 2012; Mengistu et al., 2019).

1.4 Dissertation structure

Fig. 1.1 provides a schematic of the dissertation structure. The dissertation consists of five chapters. Chapter 1 gives the research background and research objective. Chapters 2–4 address three scientific questions regarding (i) the degree climate change will influence crop yields in AC via a straightforward application of SWAT, (ii) the role of two unaccounted variables in model structure, and (iii) the impact landcover differences may

have on streamflow dynamics. Chapter 5 provides a summary of the study's major scientific contributions and recommendations for further research.

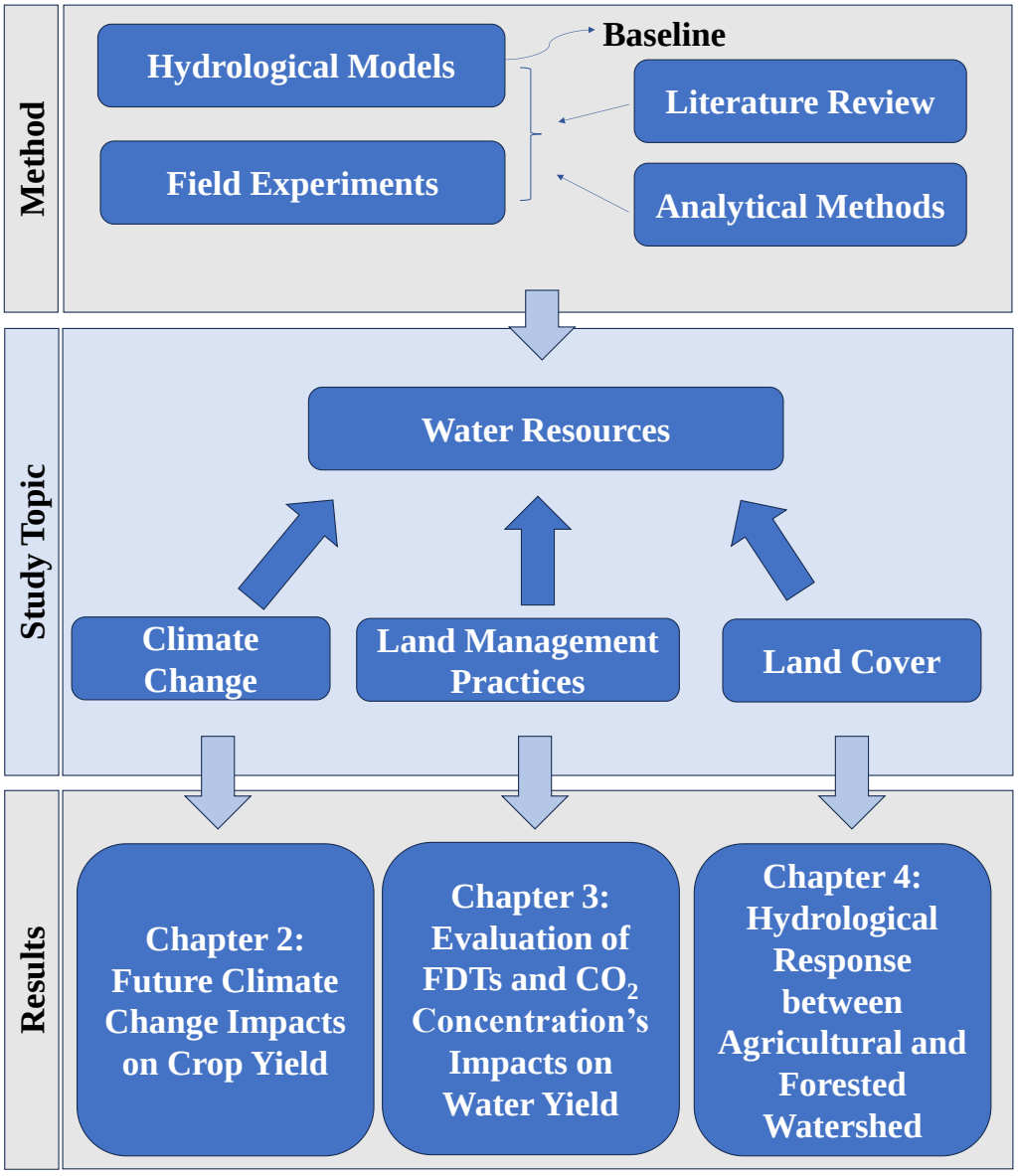

Fig. 1.1 Dissertation structure and relationship between chapters.

References

Arnold, J. G., Srinivasan, R., Muttiah, R. S., and Williams, J. R. (2007). Large area hydrologic modeling and assessment part I: Model Development. Journal of the American Water Resources Association, 34 (1), 73–89. https://doi.org/10.1111/j.1752-1688.1998.tb05961.x.

Arnold, J.G., Moriasi, D.N., Gassman, P.W., Abbaspour, K.C., White, M.J., Srinivasan, R., Santhi, C., Harmel, R., Van Griensven, A., and Van Liew, M.W. (2012). SWAT: Model use, calibration, and validation. Transactions of the ASABE, 55(4), 1491–1508. https://doi.org/10.13031/2013.42256

Daniels, M. B., Sharpley, A., Harmel, R. D., and Anderson, K. (2018). The utilization of edge-of-field monitoring of agricultural runoff in addressing nonpoint source pollution. Journal of Soil and Water Conservation, 73(1), 1–8. https://doi.org/10.2489/jswc.73.1.1.

Garna, R. K., Fuka, D. R., Faulkner, J. W., Collick, A. S., and Easton, Z. M. (2023). Watershed model parameter estimation in low data environments. Journal of Hydrology: Regional Studies, 45, 101306. https://doi.org/10.1016/j.ejrh.2022.101306.

Golmohammadi, G., Prasher, S., Madani, A., and Rudra, R. (2014). Evaluating three hydrological distributed watershed models: MIKE-SHE, APEX, SWAT. Hydrology, 1(1), 20–39. https://doi.org/10.3390/hydrology1010020.

Gomyo, M. and Kuraji, K. (2016). Effect of the litter layer on runoff and evapotranspiration using the paired watershed method. Journal of Forest Research, 21(6), 306–313. https://doi.org/10.1007/s10310-016-0542-5.

Haas, H., Reaver, N. G. F., Karki, R., Kalin, L., Srivastava, P., Kaplan, D. A., and Gonzalez-Benecke, C. (2022). Improving the representation of forests in hydrological models. Science of The Total Environment, 812, 151425. https://doi.org/10.1016/j.scitotenv.2021.151425.

Hurkmans, R. T. W. L., Terink, W., Uijlenhoet, R., Moors, E. J., Troch, P. A., and Verburg, P. H. (2009). Effects of landuse changes on streamflow generation in the Rhine basin. Water Resources Research, 45(6), W06405. https://doi.org/10.1029/2008WR007574.

Izady, A., Joodavi, A., Ansarian, M., Shafiei, M., Majidi, M., Davary, K., Ziaei, A. N., Ansari, H., Nikoo, M. R., Al-Maktoumi, A., Chen, M., and Abdalla, O. (2021). A scenario-based coupled SWAT-MODFLOW decision support system for advanced water resource management. Journal of Hydroinformatics, 24 (1), 56–77. https://doi.org/10.2166/hydro.2021.081.

Jayakrishnan, R., Srinivasan, R., Santhi, C., and Arnold, J. G. (2005). Advances in the application of the SWAT model for water resources management. Hydrological Processes. 19 (3), 749–762. https://doi.org/10.1002/hyp.5624.

Jin, C., Zha, T., Guo, X., Li, X., Liu, X., Jiang, Y., Guo, Z., and Bourque, C. P.-A. (2023). Forest-cover-loss control on year-round river flow dynamics in the upper Saint John River (Wolastoq) basin, Northeastern North America from 2001 to 2019. Journal of Hydrology, 623, 129776. https://doi.org/10.1016/j.jhydrol.2023.129776.

Kang, X., Qi, J., Li, S., and Meng, F.-R. (2022). A watershed-scale assessment of climate change impacts on crop yields in Atlantic Canada. Agricultural Water Management, 269, 107680. https://doi.org/10.1016/j.agwat.2022.107680.

Kang, Y., Khan, S., and Ma, X. (2009). Climate change impacts on crop yield, crop water productivity and food security – A review. Progress in Natural Science, 19(12), 1665–1674. https://doi.org/10.1016/j.pnsc.2009.08.001.

Karki, R., Qi, J., Gonzalez-Benecke, C. A., Zhang, X., Martin, T. A., and Arnold, J. G. (2023). SWAT-3PG: Improving forest growth simulation with a process-based forest model in SWAT. Environmental Modelling and Software, 164, 105705. https://doi.org/10.1016/j.envsoft.2023.105705.

Kiptala, J. K., Mohamed, Y., Mul, M. L., and Van der Zaag, P. (2013). Mapping evapotranspiration trends using MODIS and SEBAL model in a data scarce and heterogeneous landscape in Eastern Africa. Water Resources Research, 49(12), 8495–8510. https://doi.org/10.1002/2013WR014240.

Leavesley, G. H. (1994). Modeling the effects of climate change on water resources - a review. Climatic Change, 28, 159–177. https://doi.org/10.1007/BF01094105.

Li, B., Tan, L., Zhang, X., Qi, J., Marek, G. W., Li, Y., Dong, X., Zhao, W., Chen, T., Feng, P., Liu, D. L., Srinivasan, R., and Chen, Y. (2023). Modeling streamflow response under changing environment using a modified SWAT model with enhanced representation of CO_2 effects. Journal of Hydrology: Regional Studies, 50, 101547. https://doi.org/10.1016/j.ejrh.2023.101547.

Li, X., Tan, L., Li, Y., Qi, J., Feng, P., Li, B., Li Liu, D., Zhang, X., Marek, G. W., Zhang, Y., Liu, H., Srinivasan, R., and Chen, Y. (2022). Effects of global climate change

on the hydrological cycle and crop growth under heavily irrigated management – a comparison between CMIP5 and CMIP6. Computers and Electronics in Agriculture, 202, 107408. https://doi.org/10.1016/j.compag.2022.107408.

Liang, K., Qi, J., Zhang, X., Emmett, B., Johnson, J. M. F., Malone, R. W., Moglen, G. E., and Venterea, R. T. (2023a). Simulated nitrous oxide emissions from multiple agroecosystems in the U.S. Corn Belt using the modified SWAT-C model. Environmental Pollution, 337, 122537. https://doi.org/10.1016/j.envpol.2023.122537.

Liang, K., Zhang, X., Liang, X.-Z., Jin, V. L., Birru, G., Schmer, M. R., Robertson, G. P., McCarty, G. W., and Moglen, G. E. (2023b). Simulating agroecosystem soil inorganic nitrogen dynamics under long-term management with an improved SWAT-C model. Science of The Total Environment, 879, 162906. https://doi.org/10.1016/j.scitotenv.2023.162906.

Liu, Y., Cui, W., Ling, Z., Fan, X., Dong, J., Luan, C., Wang, R., Wang, W., and Liu, Y. (2024). The impact of satellite soil moisture data assimilation on the hydrological modeling of SWAT in a highly disturbed catchment. Remote Sensing, 16(2), 429. https://doi.org/10.3390/rs16020429.

Marcal, J., Antizar-Ladislao, B., and Hofman, J. (2021). Addressing water security: an overview. Sustainability, 13(24), 13702. https://doi.org/10.3390/su132413702.

Martínez-Valderrama, J., Olcina, J., Delacámara, G., Guirado, E., and Maestre, F. T. (2023). Complex policy mixes are needed to cope with agricultural water demands under climate change. Water Resources Management, 37, 2805–2834. https://doi.org/10.1007/s11269-023-03481-5.

Mengistu, A. G., van Rensburg, L. D., and Woyessa, Y. E. (2019). Techniques for calibration and validation of SWAT model in data scarce arid and semi-arid catchments in South Africa. Journal of Hydrology: Regional Studies, 25, 100621. https://doi.org/10.1016/j.ejrh.2019.100621.

Mu, D., Xun, Y., Gao, Y., Ren, D., Sun, C., Ma, X., Huang, G., and Xu, X. (2023). A modified SWAT model for mechanistic simulation of soil water-salt transport and the interactions with shallow groundwater. Hydrological Processes, 37(9), e14980. https://doi.org/10.1002/hyp.14980.

Neitsch, S., Arnold, J., Kinry, J. R., and Williams, J. R. (2011). Soil and Water Assessment Tool theoretical documentation, Version 2011. https://swat.tamu.edu/media/99192/swat2009-theory.pdf

Oduor, B. O., Campo-Bescós, M. Á., Lana-Renault, N., Kyllmar, K., Mårtensson, K., and Casalí, J. (2023). Quantification of agricultural best management practices impacts on sediment and phosphorous export in a small catchment in southeastern Sweden. Agricultural Water Management, 290, 108595. https://doi.org/10.1016/j.agwat.2023.108595.

Potter, K. W. (1991). Hydrological impacts of changing land management practices in a moderate-sized agricultural catchment. Water Resources Research, 27(5), 845–855. https://doi.org/10.1029/91WR00076.

Qi, J., Kang, X., Li, S., and Meng, F.-R. (2022). Evaluating impacts of detailed land use and management inputs on the accuracy and resolution of swat predictions in an experimental watershed. Water, 14(15), 23–52. https://doi.org/10.3390/w14152352.

Qi, J., Li, S., Bourque, C. P.-A., Xing, Z., and Meng, F.-R. (2018). Developing a decision support tool for assessing landuse change and BMPs in ungauged watersheds based on decision rules provided by SWAT simulation. Hydrology and Earth System Sciences, 22(7), 3789–3806. https://doi.org/10.5194/hess-22-3789-2018.

Qi, J., Li, S., Yang, Q., Xing, Z., and Meng, F.-R. (2017a). SWAT setup with long-term detailed landuse and management records and modification for a micro-watershed influenced by freeze-thaw cycles. Water Resources Management, 31, 3953–3974. https://doi.org/10.1007/s11269-017-1718-2.

Qi, J., Li, S., Jamieson, R., Hebb, D., Xing, Z., and Meng, F.-R. (2017b). Modifying SWAT with an energy balance module to simulate snowmelt for maritime regions. Environmental Modelling and Software, 93, 146–160. https://doi.org/10.1016/j.envsoft.2017.03.007.

Qi, J., Li, S., Li, Q., Xing, Z., Bourque, C. P.-A., and Meng, F.-R. (2016a). Assessing an enhanced version of SWAT on water quantity and quality simulation in regions with seasonal snow cover. Water Resources Management, 30, 5021–5037. https://doi.org/10.1007/s11269-016-1466-8.

Qi, J., Li, S., Li, Q., Xing, Z., Bourque, C. P.-A., and Meng, F.-R. (2016b). A new soil-temperature module for SWAT application in regions with seasonal snow cover. Journal of Hydrology, 538, 863–877. https://doi.org/10.1016/j.jhydrol.2016.05.003.

Roy, S. K., Alam, M. T., Mojumder, P., Mondal, I., Kafy, A. A., Dutta, M., Ferdous, M. N., Al Mamun, M. A., and Mahtab, S. B. (2024). Dynamic assessment and prediction of landuse alterations influence on ecosystem service value: A pathway

to environmental sustainability. Environmental and Sustainability Indicators, 21, 100319. https://doi.org/10.1016/j.indic.2023.100319.

Rozas-Vásquez, D., Fürst, C., and Geneletti, D. (2019). Integrating ecosystem services in spatial planning and strategic environmental assessment: The role of the cascade model. Environmental Impact Assessment Review, 78, 106291. https://doi.org/10.1016/j.eiar.2019.106291.

Safari, A., Smedt, F., and Moreda, F. (2012). WetSpa model application in the distributed model intercomparison project (DMIP2). Journal of Hydrology, 418–419, 78–89. https://doi.org/10.1016/j.jhydrol.2009.04.001.

Saravanan, S., Singh, L., Sathiyamurthi, S., Sivakumar, V., Velusamy, S., and Shanmugamoorthy, M. (2022). Predicting phosphorus and nitrate loads by using SWAT model in Vamanapuram River Basin, Kerala, India. Environmental Monitoring and Assessment, 195, 186. https://doi.org/10.1007/s10661-022-10786-2.

Silva, T. P., Bressiani, D., Ebling, É. D., and Reichert, J. M. (2024). Best management practices to reduce soil erosion and change water balance components in watersheds under grain and dairy production. International Soil and Water Conservation Research, 12(1), 121–136. https://doi.org/10.1016/j.iswcr.2023.06.003.

Sun, G., Wei, X., Hao, L., Sanchis, M. G., Hou, Y., Yousefpour, R., Tang, R., and Zhang, Z. (2023). Forest hydrology modeling tools for watershed management: A review. Forest Ecology and Management, 530, 120755. https://doi.org/10.1016/j.foreco.2022.120755.

Tijjani, S. B., Qi, J., Giri, S., and Lathrop, R. (2024). Crop production and water quality under 1.5 °C and 2 °C warming: plant responses and management options in the mid-Atlantic region. Science of The Total Environment, 907, 167874. https://doi.org/10.1016/j.scitotenv.2023.167874.

Tola, S. Y. and Shetty, A. (2023). Quantification of change in land cover and rainfall variability impact on flood hydrology using a hydrological model in the Ethiopian river basin. Environmental Earth Sciences, 82, 254. https://doi.org/10.1007/s12665-023-10929-9.

Tomer, M. D. (2018). A twice-paired watershed experimental design to assess stacked practices through field-edge monitoring. Journal of Soil and Water Conservation, 73(1), 58–61. https://doi.org/10.2489/jswc.73.1.58.

Troendle, C. A. and King, R. M. (1985). The effect of timber harvest on the Fool Creek Watershed, 30 years later. Water Resources Research, 21(12), 1915–1922. https://doi.org/10.1029/WR021i012p01915.

Udawatta, R. P., Krstansky, J. J., Henderson, G. S., and Garrett, H. E. (2002). Agroforestry practices, runoff, and nutrient loss. Journal of Environmental Quality, 31(4), 1214–25. https://doi.org/10.2134/jeq2002.1214.

Wang, S., Zhang, Z., R. McVicar, T., Guo, J., Tang, Y., and Yao, A. (2013). Isolating the impacts of climate change and landuse change on decadal streamflow variation: assessing three complementary approaches. Journal of Hydrology, 507, 63–74. https://doi.org/10.1016/j.jhydrol.2013.10.018.

Wu, Y., Liu, S., and Abdul-Aziz, O. I. (2012a). Hydrological effects of the increased CO_2 and climate change in the Upper Mississippi River Basin using a modified SWAT. Climatic Change, 110, 977–1003. https://doi.org/10.1007/s10584-011-0087-8.

Wu, Y., Liu, S., and Gallant, A. L. (2012b). Predicting impacts of increased CO_2 and climate change on the water cycle and water quality in the semiarid James River Basin of the Midwestern USA. Science of The Total Environment, 430, 150–160. https://doi.org/10.1016/j.scitotenv.2012.04.058.

Yang, Q., Zhao, Z., Chow, T., Rees, H., Bourque, C. P.-A., and Meng, F.-R. (2009a). Using GIS and a digital elevation model to assess the effectiveness of variable grade flow diversion terraces in reducing soil erosion in northwestern New Brunswick, Canada. Hydrological Processes, 23(23), 3271–3280. https://doi.org/10.1002/hyp.7436.

Yang, Q., Meng, F.-R., Zhao, Z., Chow, T. L., Benoy, G., Rees, H. W., and Bourque, C. P.-A., (2009b). Assessing the impacts of flow diversion terraces on stream water and sediment yields at a watershed level using SWAT model. Agriculture, Ecosystems and Environment, 132(1–2), 23–31. https://doi.org/10.1016/j.agee.2009.02.012.

Yu, X. and Bourque, C. P.-A. (2022). Controls of contemporary (2001–2018) springtime waterflow dynamics in a large, snowmelt-dominated basin in northeastern North America. Journal of Hydrology X, 14, 100117. https://doi.org/10.1016/j.hydroa.2021.100117.

Zeng, J., Zhou, T., Qu, Y., Bento, V. A., Qi, J., Xu, Y., Li, Y., and Wang, Q. (2023). An improved global vegetation health index dataset in detecting vegetation drought. Scientific Data, 10, 338. https://doi.org/10.1038/s41597-023-02255-3.

Zhang, R., Bento, V. A., Qi, J., Xu, F., Wu, J., Qiu, J., Li, J., Shui, W., and Wang, Q. (2023a). The first high spatial resolution multi-scale daily SPI and SPEI raster dataset for drought monitoring and evaluating over China from 1979 to 2018. Big Earth Data, 7(3), 860–885. https://doi.org/10.1080/20964471.2022.2148331.

Zhang, Y., Liu, H., Qi, J., Feng, P., Zhang, X., Liu, D. L., Marek, G. W., Srinivasan, R., and Chen, Y. (2023b). Assessing impacts of global climate change on water and food security in the black soil region of Northeast China using an improved SWAT-CO_2 model. Science of The Total Environment, 857, 159482. https://doi.org/10.1016/j.scitotenv.2022.159482.

Zhu, L., Qi, J., Wang, H., Zhou, M., Ye, Y., Li, Y., Tong, C., Deng, X., He, S., and Wang, K. (2023). Coupling SMAP brightness temperature into swat hydrological model for 30-m resolution soil moisture retrievals. IEEE Journal of Selected Topics in Applied Earth Observations and Remote Sensing,16, 8319–8333. https://doi.org/10.1109/JSTARS.2023.3310197.

CHAPTER 2

A WATERSHED-SCALE ASSESSMENT OF CLIMATE CHANGE IMPACTS ON CROP YIELDS IN ATLANTIC CANADA

Kang, X., Qi, J., Li, S., and Meng, F.-R. (2022). A watershed-scale assessment of climate change impacts on crop yields in Atlantic Canada. Agricultural Water Management, 269, 107680. https://doi.org/10.1016/j.agwat.2022.107680.

Abstract

Agriculture in Atlantic Canada (AC) is dominated by a rain-fed potato production system, with potatoes typically alternating with cereal crops, such as barley and oats. Under rain-fed conditions, crop yields are sensitive to weather and its variations and are thus affected by climate change. Previous research regarding climate change impacts on crop yields in AC has been limited to a regional-scale assessment, mostly focusing on climate without considering real-world field conditions (e.g., soil and topography). In this study, an enhanced version of the Soil and Water Assessment Tool (SWAT) was used to estimate crop yields at the watershed scale under climate change conditions projected for the period of 2020 to 2099 using global climate models with three different greenhouse gas (GHG) emission scenarios, Representative Concentration Pathways 2.6, 4.5, and 8.5. Results suggest that climate change will negatively impact potato and barley yields under all three scenarios. Under RCP 8.5, there will be significant reductions (13–23%) in crop yields between 2060 and 2099. The leading cause of crop yield reductions is attributed to soil water stress resulting from increased temperatures and evapotranspiration during the growing season due to climate change. Elevated carbon dioxide (CO_2) concentrations could potentially increase crop yields due to the CO_2 fertilization effect. However, it is not enough to offset the negative impacts of soil water stress. My results suggest that on top of controlling GHG emissions to below the RCP 4.5 level, it is critical to develop and adapt crop, soil, and water management practices, such as adaptation to new crop-rotation systems, early planting dates, and supplementary irrigation to maintain future crop yields in AC.

Keywords: Atlantic Canada, climate change, crop yield, CO_2 fertilization, SWAT

2.1 Introduction

The increase in fossil fuel consumption generates elevated atmospheric carbon dioxide (CO_2) concentrations, which in turn traps heat and warms the earth's surface, leading to rising temperatures, losses in snowpack/ice, and changing precipitation patterns (Rajib et al., 2016; Ahiablame et al., 2017; Pathak et al., 2018). Rising atmospheric CO_2 concentrations will further influence the distribution of precipitation and increase the frequency and intensity of extreme weather events, such as flooding and drought (Harrison et al., 2014). These ongoing changes in climate may have great impact on water budgets, increasing water demands by agricultural crops (Vaghefi et al., 2014; Paul, 2016). Projected changes in seasonal temperature and precipitation distributions can have pronounced impacts on crop growth at different growing stages (Vaghefi et al., 2014; Ahiablame et al., 2017). Studies have indicated that an increase in atmospheric CO_2 concentrations is expected to promote plant growth through the CO_2 fertilization effect (Cure and Acock, 1986; Idso and Idso, 1994). However, other studies have found that stomatal closure responses to elevated ambient CO_2 concentrations can lead to reduced evapotranspiration and CO_2 uptake (Raymundo et al., 2018; Chen et al., 2019). The overall impact of climate change on crop yields is thus complicated, requiring further investigation.

Future changes in annual and seasonal temperature and precipitation patterns and their implications on different agricultural production systems can vary regionally. For instance, in the semi-arid northern High Plains of Texas, Chen et al. (2019) predicted reductions in corn and sorghum yields under future climatic conditions. Smith et al. (2013) indicated that cereal yields would decrease under the influence of future climate change in northern Europe. However, wheat yields were projected to increase in the Taihang

Mountain region of East Asia (Rashid et al., 2019). Paul et al. (2020) also predicted that corn yields would decline in both the mid- and late-21st centuries, whereas soybean yields were predicted to increase in the mid-21st century but decline by the late-21st century in Mid-Atlantic USA. Motha and Baier (2005) found that all major unirrigated crops would experience decreases in yield generalized over the USA. In Canada, spring wheat, winter wheat, and corn yields were projected to increase in the west (Smith et al., 2013). However, corn yields in more humid regions of central Canada were found to decrease (He et al., 2018). It is thus important to assess the impacts of climate change on local water resources and crop yields to evaluate and implement adaptive agricultural management practices needed to maintain a uniform crop productivity (Ozturk et al., 2017).

Potatoes (*Solanum tuberosum L.*) are the largest non-cereal food crop, ranked as the fourth most important food crop in the world (FAO, 2019). It is also the most important horticultural crop, accounting for one third of all vegetable farm revenues in Canada (PotatoPro, 2018). Atlantic Canada (AC) is the most important potato production region in Canada, producing more than 40% of the country's potatoes (Mukezangango, 2017). Barley (*Hordeum vulgare L.*) is the most frequently used rotation crop with potato in AC. It also accounts for the second most important field crop in Prince Edward Island, the largest barley production area in AC (Statistics Canada, 2017). Historical records show that the climate in AC has become progressively warmer over the past hundred years (Zhang et al., 2000; Motha and Baier, 2005). Intensified water stress associated with higher temperatures in the future can adversely affect the growth and yields of potatoes and barley.

There are few studies of climate change's impacts on crop yields to inform agricultural water management in AC. There is a lack of information about rain-fed regions

influenced by seasonal snow cover, where climate change is projected to have an elevated impact. To address this knowledge gap, a modeling approach has been employed to assess the impacts of future climate change on hydrology and crop yields at the watershed scale in AC's environment. Hydrological models incorporating crop growth modules are widely used to assess the change in crop yields under future climate change (Srivastava et al., 2012; Chen et al., 2019; Ahmad et al., 2020). They have the advantages of low cost, high efficiency, and easy control of variables compared with field/laboratory experiments, particularly for agricultural watersheds (Chen et al., 2019; Paul et al., 2020). Among these models, the Soil and Water Assessment Tool (SWAT) has been widely used to investigate climate change effects at the watershed scale worldwide (Arnold et al., 1998). SWAT has been modified to better address AC's environment so it can be adopted to investigate climate change impacts on crop yields in AC (Qi et al., 2016b, 2019b; Wang et al., 2020b). The objectives of this study are to: (1) investigate future climatic conditions as impacted by elevated atmospheric CO_2 concentrations; (2) evaluate the performance of an enhanced version of SWAT in simulating hydrology and crop growth in a small experimental watershed; and (3) predict the impacts of climate change on crop yields with major economic importance (i.e., potatoes and barley) and identify the key drivers for crop yield changes in AC. In this study, three Representative Concentration Pathway (RCP) emission scenarios (i.e., RCPs 2.6, 4.5, and 8.5) are considered, based on projections from five Global Climate Models (GCMs) to represent future conditions for different adaptation strategies.

2.2 Materials and methods

2.2.1 Study site and data collection

Black Brook Watershed (BBW) is in northwestern New Brunswick, Canada (47°5′ to 47°9′N, 67°44′ to 67°48′W), with elevations ranging from 150 to 242 m above mean sea level (Fig. 2.1). The region is characterized as a typical watershed in AC, strongly influenced by marine weather (Chow et al., 2011). The average temperature is 3.7℃, and the annual precipitation is 1037.4 mm, of which about one third of the annual precipitation is in the form of snow. Melting snow in spring is the major source of surface runoff and groundwater recharge (Chow and Rees, 2006; Qi et al., 2017). The area of the watershed is 14.5 km^2, with agricultural, forest, and residential land accounting for 65%, 21%, and 14% of the total area, respectively (Chow et al., 2011). The main crop within BBW is potatoes in rotation with barley. Soils in BBW are classified into six mineral soil classes, namely, Grand Falls, Holmesville, Interval, Muniac, Siegas, and Undine, and one organic soil, Saint-Quentin (Mellerowicz, 1993). These soils are developed from glacial till and are generally very stony. Soil texture ranges from sandy loam, loam, to clay loam.

A water monitoring station at the outlet of BBW (MS#1, Fig. 2.1) has been in operation since 1992. Recorded flow rates have been used to calculate discharge from 1992 to 2015 (Chow et al., 2011). Weather data, including daily precipitation, air temperature, relative humidity, solar radiation, and wind speed from 1992 to 2015 were acquired from the St. Leonard Environment Climate Change Canada weather station, approximately 5 km from BBW (Fig. 2.1). As part of a long-term research effort, field-level landuse information on crop rotation, fertilizer application, management practices, planting and harvest dates, and crop yields from individual farms have been collected via annual surveys since 1992

(Liang et al., 2019). We arranged the SWAT-project with individual hydrologic response unit (HRU) explicitly representing farms within BBW, and management practices were configured according to long-term detailed records at the HRU level (Qi et al., 2017). A high-resolution digital elevation model (1-m resolution) was used, based on elevation data collected with airborne light detection and ranging technology (Qi et al., 2016a, 2016b, 2018). Soil data were extracted from a detailed soil survey map (Mellerowicz, 1993).

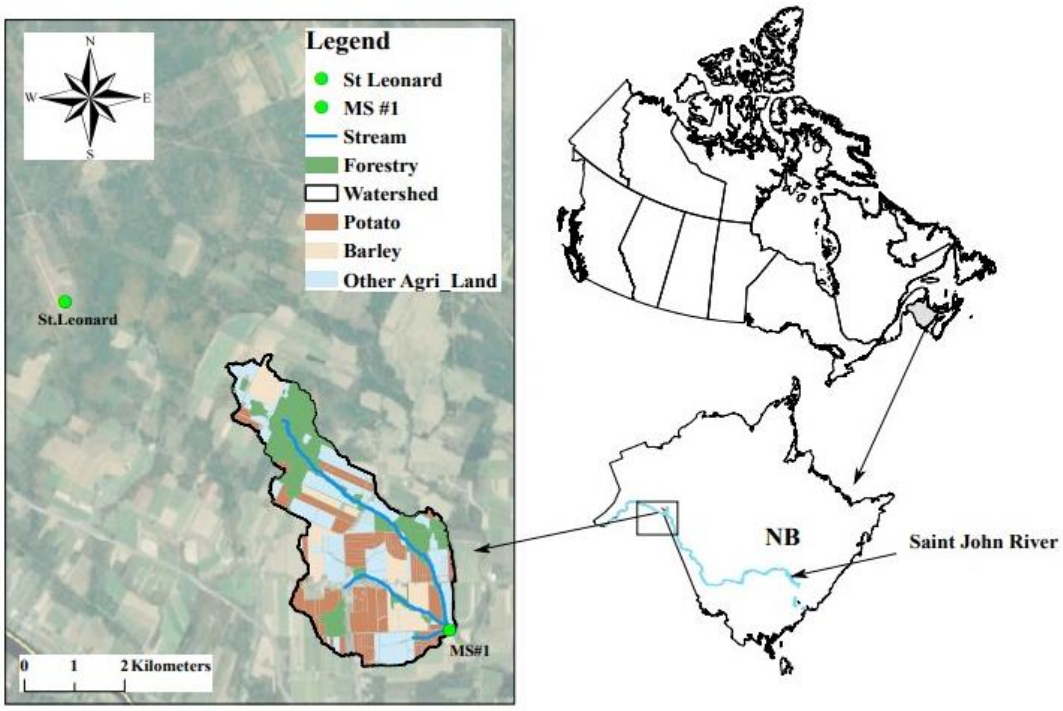

Fig. 2.1 Locations of Black Brook Watershed (BBW) and associated weather (St. Leonard) and water-monitoring (MS#1) stations. Major landcover types are also shown, see legend.

2.2.2 Model description

2.2.2.1 Enhanced SWAT model

SWAT has the capability of predicting hydrological processes, water quality, plant biomass growth, and crop yields as impacted by climate change and landuse management

(Arnold et al., 1998). The model is a semi-distributed and processed-based watershed model providing a flexible framework for simulating the efficacy of a broad range of beneficial management practices (Gassman et al., 2005; Ullrich and Volk, 2009; Qi et al., 2020; Wang et al., 2020a). Major model components include a weather simulator, and modules of hydrology, plant growth, and land management, as well as modules of loads and fluxes of sediment, nutrients, pesticides, bacteria, and pathogens. Neitsch et al. (2011) provides a detailed description of the model.

The first generation of SWAT used an empirical equation to calculate soil temperature (Neitsch et al., 2011), which was found to severely underestimate soil temperatures during winter in regions with substantial snow cover (Qi et al., 2016b). This is because the insulating effects of snow, reducing heat loss of the soil surface, were not considered by the empirically-based expression of soil temperature in older versions of SWAT (Qi et al., 2016b). To address this issue, a physically-based soil temperature module was developed and integrated in SWAT to account for these effects due to freeze-thaw cycles of soil water (Qi et al., 2016a, 2016b, 2019a, 2019b). The enhanced model has proven to dramatically improve snow-dominated hydrological responses to rising temperatures (Wang et al., 2020a, 2020b, 2021), thus increasing the reliability of climate change impacts on agriculture in AC. The time lag in snowmelt was also addressed by calibrating relevant parameters against measured high flows in early spring. The lag was assumed not to be impacted by climate change. Qi et al. (2016b) provides additional information regarding some of these model algorithms and their corresponding parameter calibration.

2.2.2.2 Hydrology and crop yield simulation

The hydrological process in the soil profile simulated by SWAT is based on the water balance equation (Eq. 2.1), which includes the processes of precipitation, surface runoff, infiltration, evapotranspiration, lateral flow, and percolation (Arnold et al., 1998; Neitsch et al., 2011):

$$SW_t = SW_o + \sum_{i=1}^{n}(R_{day} - Q_{surf} - E_a - Q_{lat} - w_{seep}), \quad (2.1)$$

where SW_t is the final soil water content at time t (day), SW_o the soil water content at the start of a timestep, R_{day} the amount of precipitation (or snowmelt), Q_{surf} surface runoff, E_a actual evapotranspiration, Q_{lat} lateral flow, and w_{seep} percolation on day i (all in mm).

Surface runoff is estimated using a modified Soil Conservation Service curve number (Mishra and Singh, 2013). A kinematic storage model is used to calculate lateral flow (Sloan and Moore, 1984). Soil water movement is modeled using a "tipping-bucket" algorithm. Water is allowed to percolate downwards if soil water content exceeds field capacity, and the layer below is not saturated. The amount of water moving downwards from one layer to an adjoining soil layer is calculated using the storage routing method (Arnold et al., 2011; Neitsch et al., 2011). Water percolating out of the lowest soil layer enters the vadose zone, eventually recharging aquifers. In SWAT, evapotranspiration can be calculated with three different methods, including the Penman-Monteith (Monteith, 1965), Priestley-Taylor (Priestley and Taylor, 1972), and Hargreaves method (Hargreaves and Samani, 1985). In this study, the Penman-Monteith method was used to simulate evapotranspiration. The heat unit theory was used to regulate plant growth based on SWAT-specific input parameters summarized in a plant-growth database (Boswell, 1926; Magoon

and Culpepper, 1932). Actual growth was then deducted from potential growth due to environmental stresses caused by extreme temperatures and/or deficits in water and nutrients, particularly nitrogen and phosphorus. Plant growth in the model was controlled by the leaf area index (LAI) of the crop canopy, light intercepted, and conversion of intercepted light into biomass by radiation use efficiency, defined as the amount of dry biomass produced per unit of intercepted solar radiation. Lastly, SWAT partitioned crop yield from the total biomass based on a harvest index with a fraction of plant dry biomass removed as dry economic yield (Arnold et al., 2011).

2.2.3 Climate data

Future climate scenarios, including daily precipitation and maximum-minimum temperatures for BBW, projected by the Coupled Model Intercomparison Project Phase 5 (CMIP5) (Taylor et al., 2012) were downloaded for 1980–2099 (via https://data.pacificclimate.org/portal/downscaled_gcms/map/, last accessed on August 2020) and statistically downscaled to a spatial resolution of 10 km by the Pacific Climate Impacts Consortium (PCIC), University of Victoria (Feb 2019) using the Bias Correction/Constructed Analogues with Quantile mapping reordering (BCCAQv2; Cannon et al., 2015; Werner and Cannon, 2016; Hiebert et al., 2018). The BCCAQv2 is a hybrid downscaling technique developed by PCIC, combining BCCA (Maurer et al., 2010) and quantile delta mapping (Cannon et al., 2015). Data from five representative GCMs for northeastern North America, i.e., CNRM-CM5 (CNRM-CERFACS, France), CSIRO-Mk3-6-0 (CSIRO-QCCCE, Australia), CanESM2 (CCCMA, Canada), MRI-CGCM3 (MRI, Japan), and GFDL-ESM2G (NOAA GFDL, USA) were employed in this study (Cannon et al., 2015).

Three RCP-emission scenarios (RCPs 2.6, 4.5, and 8.5) were selected, representing different greenhouse gas (GHG) emission scenarios to assess hydrological fluxes and crop yields. RCP 2.6 represents the lowest projected emission, with a peak in net radiative forcing of ~3 W m^{-2} in the mid-century before declining to 2.6 W m^{-2} by 2100. RCP 4.5 represents a stabilization in net radiative forcing at 4.5 W m^{-2} by 2100. RCP 8.5 represents the highest global emission scenario with a rise in net radiative forcing of 8.5 W m^{-2} by 2100. Atmospheric CO_2 concentrations for each scenario were downloaded from the Integrated Assessment Modeling Consortium database (http://tntcat.iiasa.ac.at/RcpDb/). The WXGEN weather generator model embedded in SWAT (Sharpley and Williams, 1990) was used to simulate future daily solar radiation, wind speed, and relative humidity. This weather generator assumes that the characteristics of solar radiation, wind speed, and relative humidity remain constant at current levels for the different future scenarios, implying that temperature and precipitation are the dominant drivers of future hydrology and crop growth and yield (Somura et al., 2009; Lopes et al., 2021).

2.2.4 Statistical analysis and model performance evaluation

To predict future climate change impacts on hydrological fluxes and crop yields, measured streamflow and crop yields for BBW were used to calibrate and validate SWAT. For streamflow, model performance was assessed based on the relative error (R_e), coefficient of determination (R^2), and Nash-Sutcliffe efficiency (NS):

$$R_e = \frac{(P_{avg} - O_{avg})}{O_{avg}} \cdot 100\%, \quad (2.2)$$

$$R^2 = \left(\frac{\sum_{i=1}^{n}(O_i - O_{avg})\cdot(P_i - P_{avg})}{[\sum_{i=1}^{n}(O_i - O_{avg})^2 \cdot \sum_{i=1}^{n}(P_i - P_{avg})^2]^{0.5}}\right)^2, \text{ and} \quad (2.3)$$

$$NS = 1 - \frac{\sum_{i=1}^{n}(O_i - P_i)^2}{\sum_{i=1}^{n}(O_i - O_{avg})^2}, \quad (2.4)$$

where O_i and P_i are the observed and predicted values and O_{avg} and P_{avg} their corresponding averages, respectively.

Crop yields at individual HRUs were not separately calibrated because it was technically impractical to do so, given the total number of HRUs for BBW was 887. Instead, simulated and observed crop yields over multiple HRUs were averaged for crop calibration (Sun and Ren, 2014; Sinnathamby et al., 2017; Shahvari et al., 2019). To compare with SWAT-simulated dry biomass measurements, actual potato yields were adjusted by multiplying an average dry mass conversion (~0.23%) determined from experiments based on four varieties of potato (i.e., *Russet Burbank*, *Goldrush*, *Prospect*, and *Shepody*; Liang et al., 2019). Since SWAT does not take potato variety into consideration, we only examined the trend in average potato yields at the watershed level for different climate scenarios. Regarding barley, because of the absence of experiments in AC, actual and simulated yields were directly compared because the dry mass conversion (%) of barely was ~85.2–89.8% (Poulsen et al., 2012), compared to 15–25% for potatoes (Kapoor et al., 2019). R_e was used to assess model performance for crop yields for BBW.

Water use efficiency (WUE) was used to understand how climate change would affect plant water use and growth (Hatfield and Dold, 2019); WUE is defined as the amount of biomass or grain produced per unit of water consumed by crops (Briggs and Shantz, 1913), and

$$WUE = 1000 * yield/ET, \quad (2.5)$$

where WUE is the water use efficiency (kg ha^{-1} mm^{-1}), *yield* the crop yield (tons ha^{-1}), and ET an estimate of evapotranspiration (mm).

After model evaluation with historical data in terms of hydrology and crop yields for BBW, climate data projected with the five GCMs were used to drive SWAT following calibration, simulating hydrological processes and crop yields from 1980 to 2099. Model simulations were summarized for four future periods, i.e., P1 (2020–2039), P2 (2040–2059), P3 (2060–2079), and P4 (2080–2099). Changes in hydrological fluxes and crop yields based on the downscaled results of the five GCMs and three RCP scenarios were compared against fluxes and yields for a 20-year baseline period (BL) from 2000 to 2019. CO_2 fertilization effects on crop yields were summarized for 40-year periods, as discussed in Section 2.4. Forty-year periods (i.e., 2020–2059 and 2060–2099) were used here, rather than 20-year periods, due to the difficulty in configuring ambient CO_2 concentrations for model input. Ambient concentrations in SWAT were not specified as monthly timeseries, like they were for precipitation and temperature, but as multiple-year averages of concentration.

Tukey's honestly significant difference (HSD) test (Tukey, 1949), a single-step multiple comparison procedure and statistical test, was used to identify the difference between the mean values of different periods using the *multcompView* package in R *v.* 4.0.3. Tukey (1949) and the Supplementary Material (SM) provide detailed explanations regarding Tukey's HSD tests.

2.3 Results

2.3.1 Atmospheric CO_2 concentration and climate projections

Although atmospheric CO_2 concentrations in AC are projected to increase relative to BL (330 ppm) for all future periods and RCP scenarios, their trajectories are vastly different among RCP scenarios (Fig. 2.2). For RCP 2.6, ambient CO_2 concentrations are expected to increase from P1 to P2, then decrease from P2 to P4, with P2 having a maximum of 454 ppm. Ambient CO_2 concentrations are expected to increase monotonically from P1 to P4 under RCP 8.5, with a maximum of 1084 ppm. Under RCP 4.5, ambient CO_2 concentrations are projected to increase from P1 to P3 then slightly decrease from P3 to P4, with a peak concentration of 567 ppm during P3.

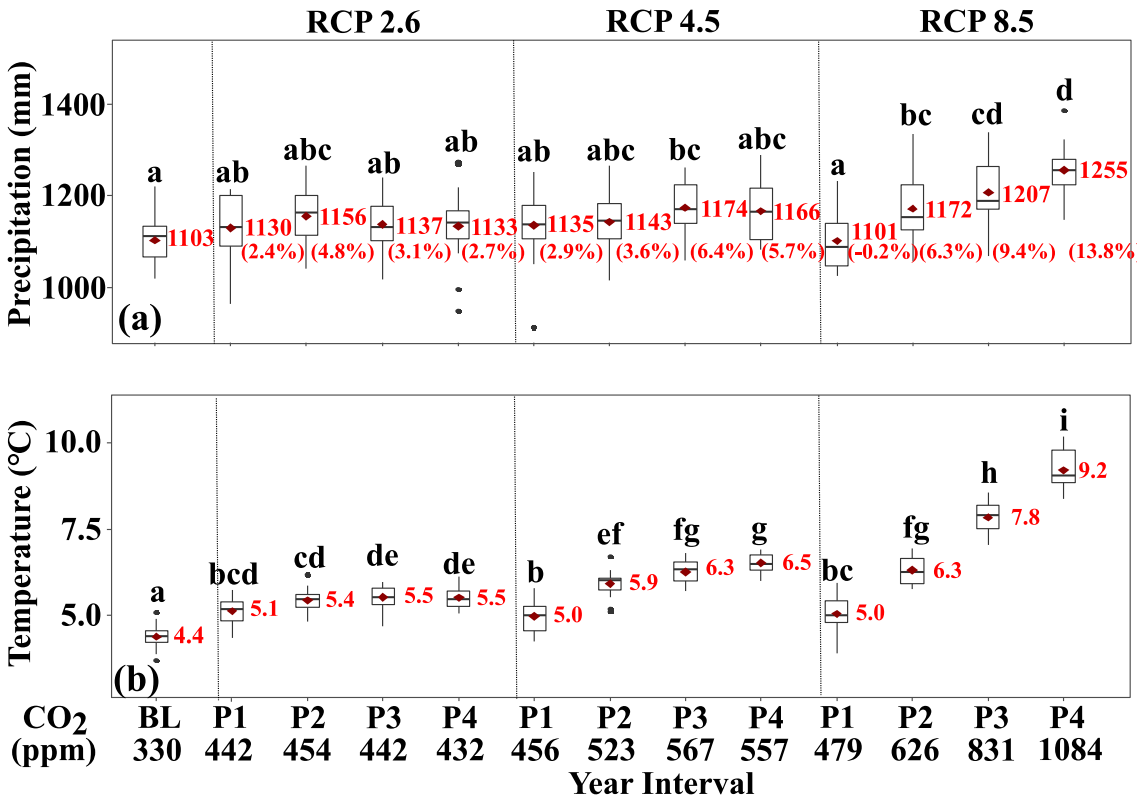

Fig. 2.2 (a) Average annual precipitation and (b) mean air temperature for 20-year time periods in the 21st-century under RCPs 2.6, 4.5, and 8.5. P1, P2, P3, and P4 represent time periods from 2020–2039, 2040–2059, 2060–2079, and 2080–2099, respectively. BL is the baseline period (2000–2019). Percents in parentheses under each average annual precipitation amount in (a) are the percent changes in annual precipitation relative to BL. Corresponding average CO_2 concentrations are also given. The box in each box-and-whisker plot shows the interquartile range, and the horizontal line in the box marks the median. The red dot in the box is the mean value (specified in red on the right-hand side of the box). The whiskers are lines extending from the top and bottom of each box, showing maximum and minimum values, respectively. The black dots beyond the whiskers are outliers. Different letters on top of each box plot indicate that the means are significantly different (p<0.05) from other means based on Tukey's HSD tests.

Projected average annual precipitation amounts simulated by the five GCMs are greater than those during BL period (1103 mm) for all future periods and RCP scenarios except for a slight reduction in P1 under RCP 8.5 (Fig. 2.2a). Changing patterns of precipitation follow those of atmospheric CO_2 concentrations under the different RCP scenarios, with a maximum percent increase of 4.8, 6.4, and 13.8% during P2, P3, and P4

under RCP 2.6, 4.5, and 8.5, respectively. However, increases in average annual precipitation relative to BL are significant (p<0.05) only in RCP 4.5-P3 and in RCP 8.5-P2, -P3, and -P4, due to the greater year-to-year variation in projected precipitation among GCM projections.

Projected percent changes in average monthly precipitation during P1 vary around the BL, without clear trends for any of the RCP scenarios (Fig. 2.3a and b; and Table S2.1 and S2.2 in SM). In P2, no clear differences are seen in average monthly precipitation under all RCPs scenarios. However, they all predict substantial increases in precipitation in the winter months (February–March) and decreases in August (Fig. 2.3c and d). During P3 and P4, greater differences in average monthly precipitation are projected to occur in the winter months. Differences extend into spring, with variability in precipitation gradually decreasing from RCP 8.5 to RCP 2.6 (Fig. 2.3e, f, g, and h). During the growing season, no clear increase is detected in June and July, but a noticeable decrease is seen in August when crops have their greatest need for water. Annual percent increases in precipitation mainly occur during winter and early spring under RCP 8.5.

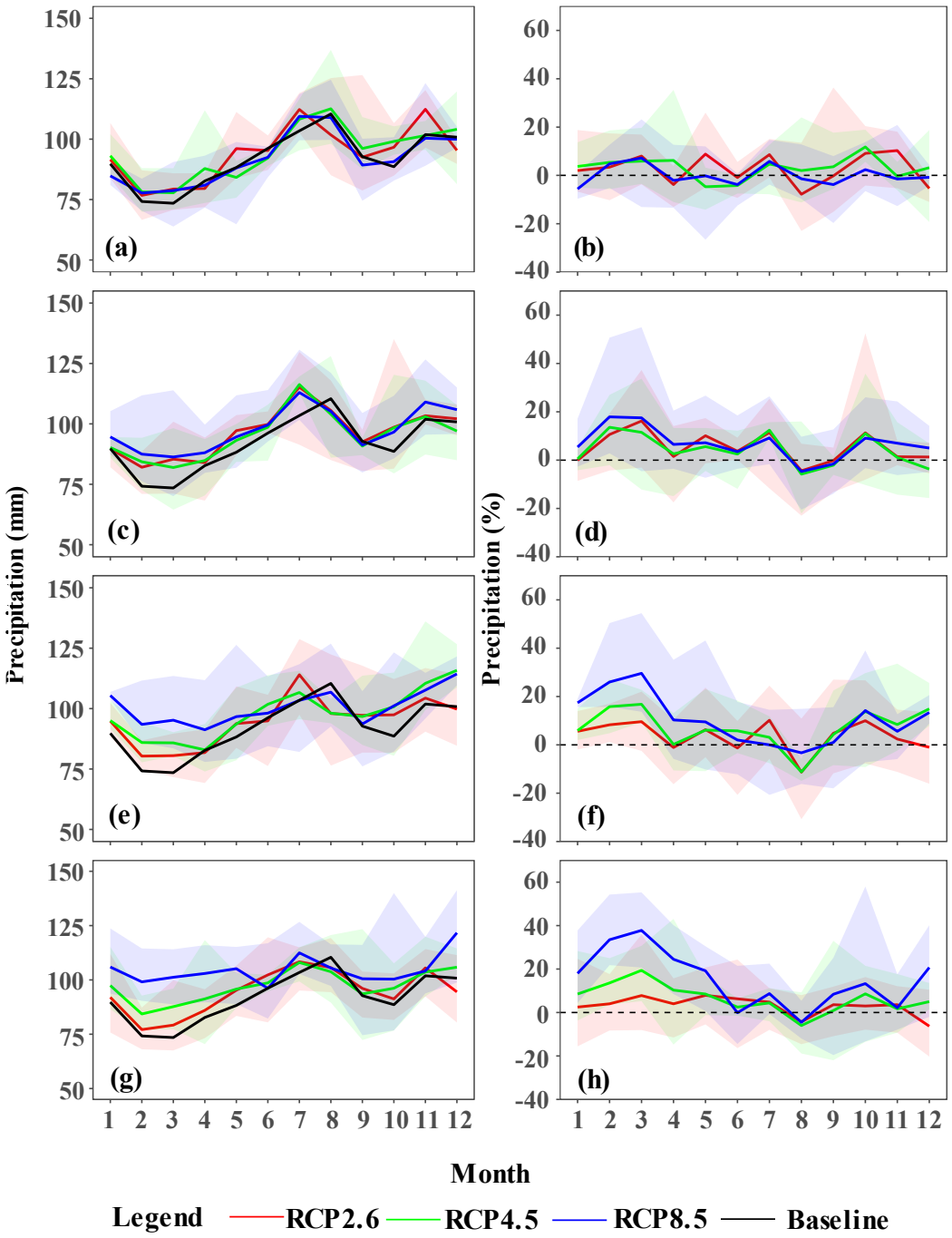

Fig. 2.3 Actual and percent change in average monthly precipitation under the three RCP scenarios during four time periods relative to the baseline period (2000–2019). Panels (a) and (b), (c) and (d), (e) and (f), and (g) and (h) show results for periods P1 (2020–2039), P2 (2040–2059), P3 (2060–2079), and P4 (2080–2099), respectively. The left-hand column shows actual average monthly precipitation, and the right-hand column percent change in average monthly precipitation (dashed lines highlight 0%). The solid lines indicate the mean values of actual and percent change in monthly average precipitation, and shaded areas show the range in minimum to maximum values generated with the five GCMs.

Projected average annual temperatures simulated with the five GCMs are significantly greater (p<0.05) than those projected for the BL period (4.4°C) for all future periods and RCP scenarios (Fig. 2.1b). Different from those of ambient CO_2 concentration and precipitation, average annual temperature increases with time, with maximum increases of 1.1, 2.1, and 4.8°C during P4 for all RCP scenarios. There appears to be a significant lag in ambient CO_2 concentration and temperature so that the greatest average annual temperature occurs during P3 and P4 under RCPs 2.6 and 4.5. Variation in average annual temperature appears low, with more variability under higher atmospheric CO_2 concentrations. There are also significant differences (p<0.05) in temperature increase between the different future periods under conditions projected for RCP 8.5. However, this is not the case for the other RCP scenarios. For example, there is no significant difference between the different future periods between P3 and P4 for RCP 2.6 and between P2 and P3 for RCP 4.5.

Average monthly temperatures reach their respective maxima in July and August under all RCP scenarios, with no obvious difference between RCP scenarios during P1 for all months (Fig. 2.4; and Table S2.3 and S2.4 in SM). After P2, average monthly temperatures projected under RCP 8.5 become greater than those of the other two RCP scenarios, particularly from July to February of the following year. Differences in temperature in spring and early summer (March–June) are not as obvious as in other seasons. Additionally, RCP 8.5 has the greatest seasonal variation in average monthly temperature increases than the other RCP scenarios (Fig. 2.4). These results imply that elevated temperatures in winter under RCP 8.5 could reduce snowfall and accelerate

snowmelt, causing significant flooding in spring. Seasonal variations in temperature exhibit greater uncertainty under high GHG-emission scenarios.

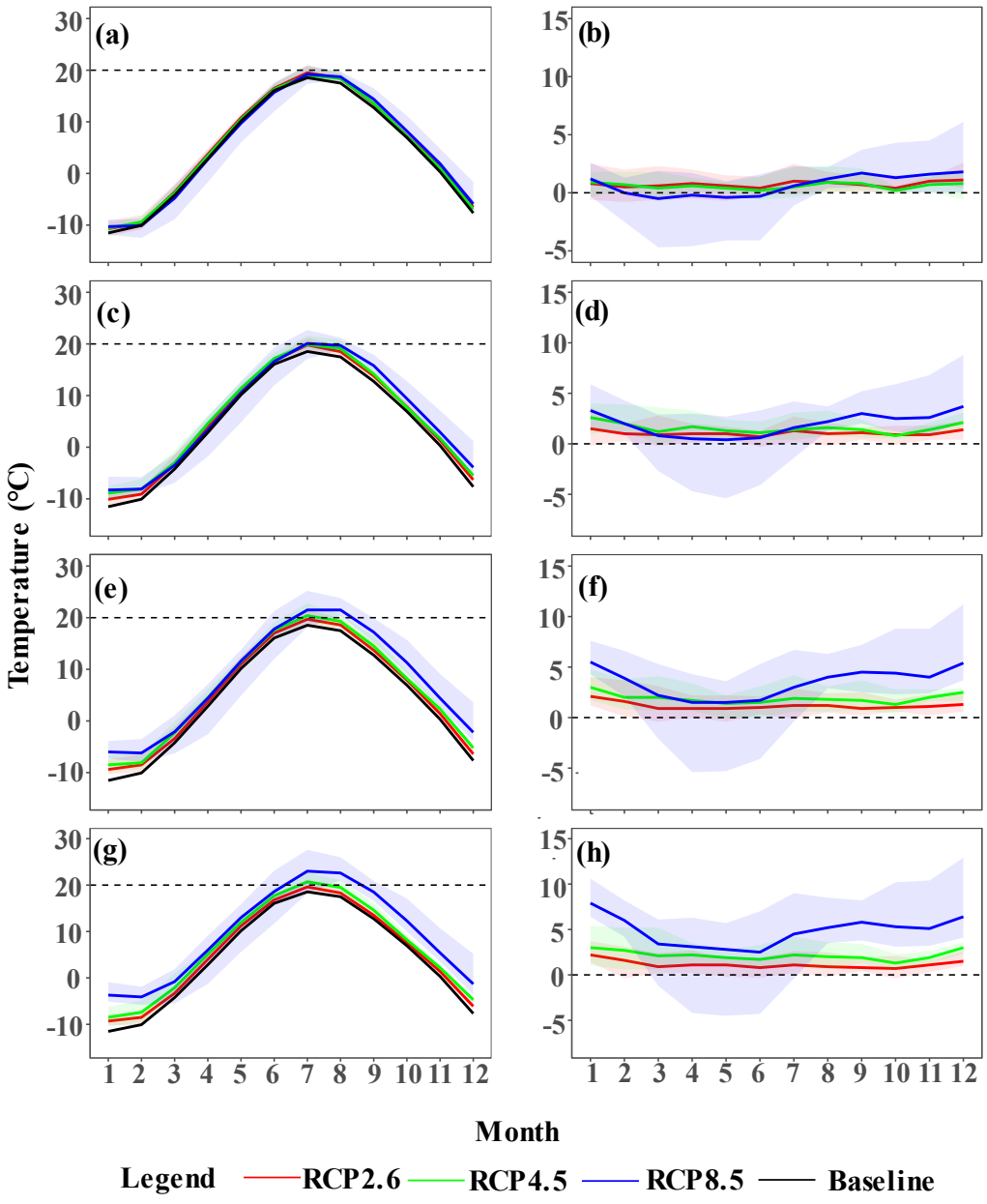

Fig. 2.4 Same as Fig. 2.3 but for temperature. The panels on right-hand side of the figure show changes in average monthly temperature, with the dashed lines referencing 0°C.

2.3.2 Model calibration and validation

To predict climate change's impacts on hydrology and crop yields, SWAT must first be calibrated and validated. Figure 2.5 shows that simulated monthly streamflow matches observations well in terms of the magnitudes of high and low flows during the calibration (1992–2001) and validation (2001–2015) periods. Statistical indices follow the model performance evaluation criteria provided by Moriasi et al. (2007), with R_e = -5%, R^2 =0.76, and NS = 0.76 for the calibration period, and R_e = -3%, R^2 = 0.84, and NS = 0.84 for the validation period.

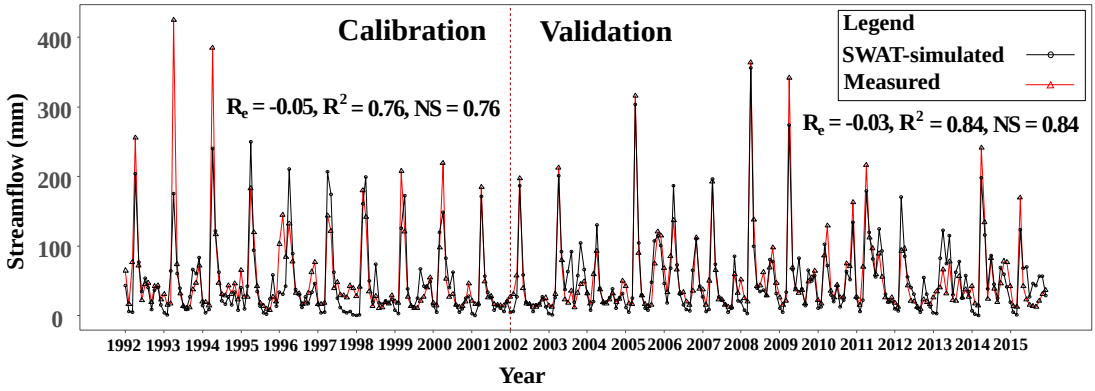

Fig. 2.5 Observed (in red) and simulated monthly streamflow using the enhanced SWAT model (in black) during the calibration (1992–2001) and validation (2002–2015) periods at the outlet of BBW. R_e represents the relative error, R^2 represents the coefficient of determination, and NS represents the Nash-Sutcliffe efficiency.

Previous studies have reported that SWAT can predict crop yields with an acceptable accuracy without calibration (Srinivasan et al., 2010). However, my results indicate that the calibration of crop-growth-related parameters is necessary to improve the accuracy of predicted crop yields. This is likely because the unique biophysical conditions in AC differ from those used in the development of SWAT. We adjusted two crop-growth-related parameters, namely the radiation use efficiency (BIO_E) and the maximum leaf area index

(BLAI) following Sumathy et al. (2017). For potatoes, we increased BIO_E and BLAI from 25 to 30 and 4 to 5, respectively. For barley, we decreased BIO_E from 35 to 30 and kept BLAI constant at 4. Figure 2.6 shows that the model performs reasonably well, predicting yields of both crops during the calibration and validation periods with particularly low absolute R_e (< 5%) for barley during both periods, and for potatoes during the validation period.

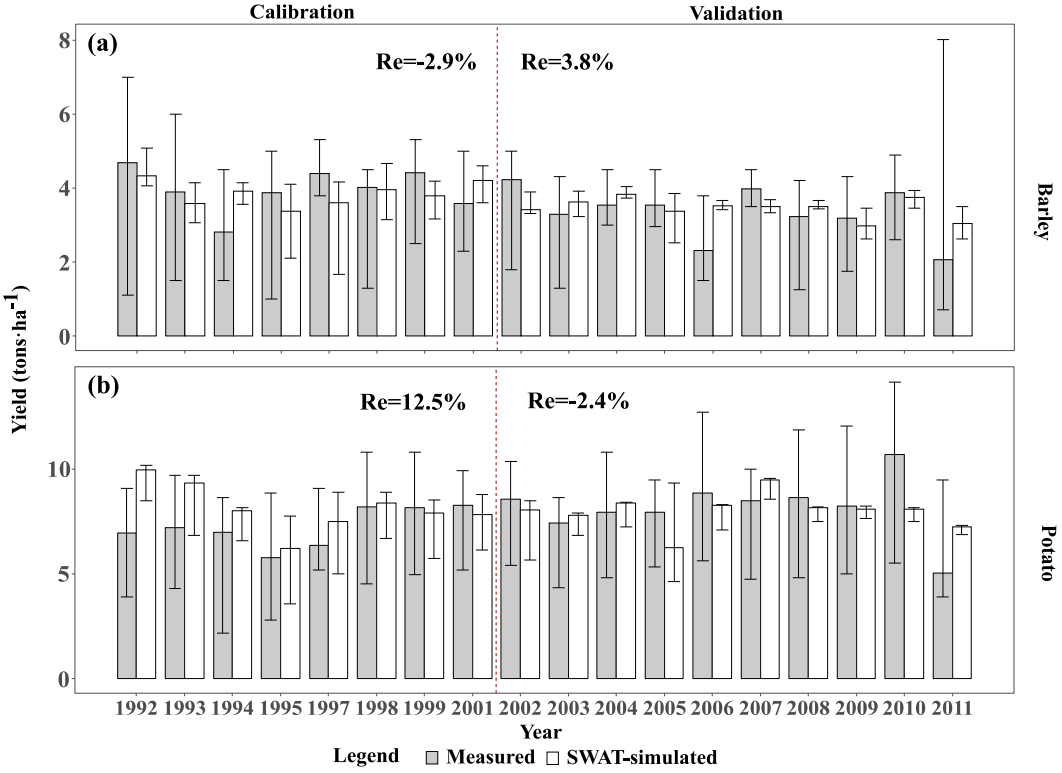

Fig. 2.6 Observed and simulated average crop yields for (a) barley and (b) potatoes for BBW during the calibration (1992–2001) and validation (2002–2011) periods. The whiskers extend through average crop yields to the observed and simulated maximum or minimum crop yields of HRUs. R_e represents the relative error.

2.3.3 Future crop yields

Average annual barley and potato yields are predicted to reduce relative to BL for all future periods under the three RCP scenarios, except for RCP 2.6-P4, RCP 4.5-P1, and RCP

8.5-P1 for barley (Fig. 2.7 and Table 2.1). Barley and potato yields assume a decreasing trend under RCP 8.5, and no clear trend under the other RCP scenarios. Specifically, under RCP 8.5 there is a significant (p<0.05) reduction in both barley (P3: 13.2%, P4: 15.8%) and potato yields (P3: 14.1%, P4: 23.2%) relative to BL. Note that reductions in barley and potato yields for RCP 2.6 and 8.5 during P3, and for the three RCP scenarios during P4, are statistically significant (p<0.05).

Reductions in potato yields are greater than those of barley under all three RCP scenarios, possibly because of physiological differences between crops (Delazari et al., 2018). Reductions in yields of both crops mostly mirrored changes in average annual precipitation and atmospheric CO_2 concentration (Fig. 2.2). However, patterns differed under RCP 4.5. Yield reductions were greatest during P3 and P4 for barley and potatoes, respectively. Differences in average yield during all periods under the different RCP scenarios were mostly not statistically significant, except for P3 and P4 under RCP 8.5. This may be attributed to large year-to-year variations within the same periods and the large variation among GCM projections.

Overall, my results indicate crop yield reduction during the rest of the 21st century due to climate change. Under a moderately controlled emission scenario (i.e., RCP 4.5), the yield reduction is apparent, especially after 2040 (ranging from 3.8 to 4.5% for barley and from 4.6 to 7.5% for potatoes). The situation could improve under a strictly controlled emission scenario (i.e., RCP 2.6), where the percent yield reduction in P3 and P4 ranges from 1.4 to 2.4% for both crops. In contrast, the situation could worsen under an uncontrolled emission scenario (like RCP 8.5), where yield reductions for both crops during P3 and P4 are about three to several times more than those observed for RCP 4.5.

My results are consistent with other studies that report reductions in barley and potato crop yields under future climates in AC and southern Québec (Bootsma et al., 2005; Brassard and Singh, 2008).

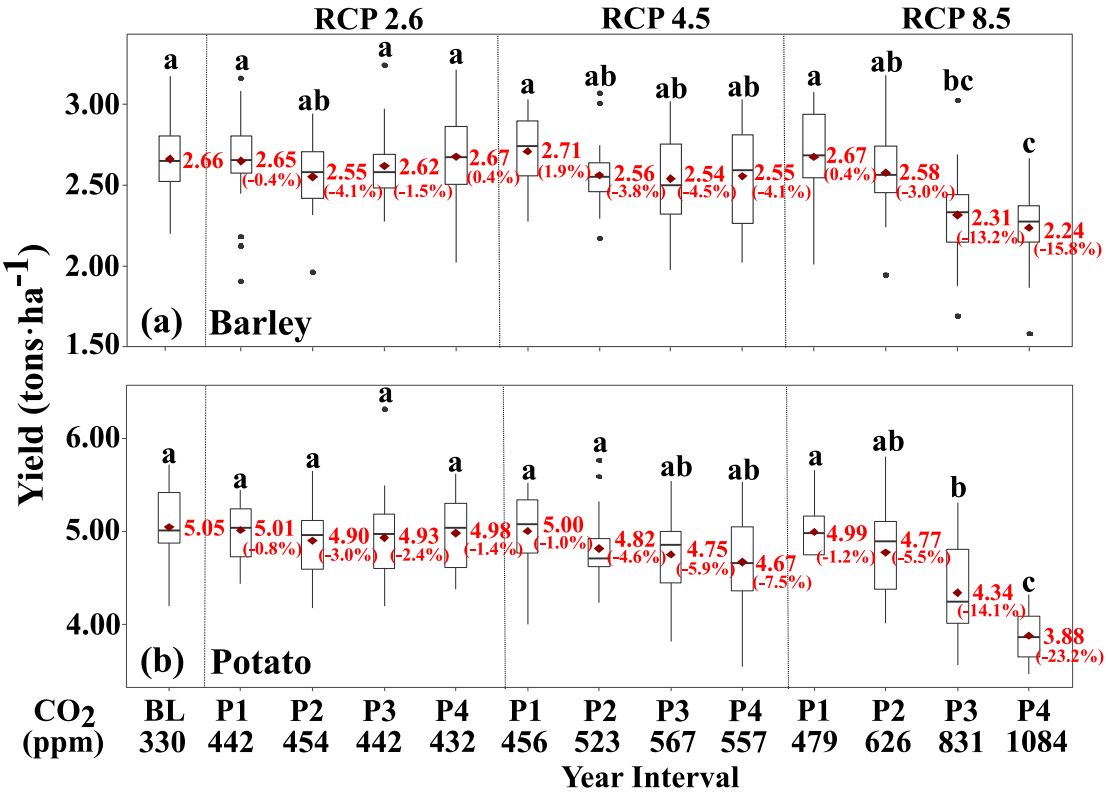

Fig. 2.7 Actual and percent change in crop yields for (a) barley and (b) potatoes under three RCP scenarios for four future 20-year periods relative to the baseline period (BL: 2000–2019). Values in parentheses under each average annual yield is the percent change in yield relative to BL. P1, P2, P3, and P4 represent the time periods of 2020–2039, 2040–2059, 2060–2079, and 2080–2099, respectively. Corresponding average ambient CO_2 concentrations are also given. The box in each box-and-whisker plot shows the interquartile range, and the horizontal line in the box marks the median. The red dot in the box is the mean value (specified in red to the right-hand-side of the box). The whiskers are lines extending from the top and bottom of each box, showing maximum and minimum values, respectively. The dots beyond the whiskers are outliners. Different letters on top of each box plot indicate that the means are statistically different (p<0.05) from other means based on Tukey's HSD tests.

2.3.4 Crop-yield-related hydrological parameters

Average annual ET is predicted to significantly increase (p<0.05) in the future relative to BL, except during P1 for all three RCP scenarios for barley and P1 for RCP 4.5 and 8.5 for potatoes (Fig. 2.8). Changes in average annual ET for both crops follow the trend observed in average annual air temperature (Fig. 2.2b). Evapotranspiration increases under RCP 8.5, with the greatest increase occurring in P4 for both barley and potatoes (19.7 *vs.* 19.5%). The greatest increase in average annual ET under RCP 2.6 amount to a 5.1% increase for both barley and potatoes, and 8.4 and 8.2% under RCP 4.5, respectively. There is a significant difference (p<0.05) in the increase in ET between RCP 4.5 and 8.5 in P3 and P4. No significant difference is detected between RCP 2.6 and 4.5. Annually, high variations in ET are found during all future periods under all RCP scenarios, with no clear temporal trend.

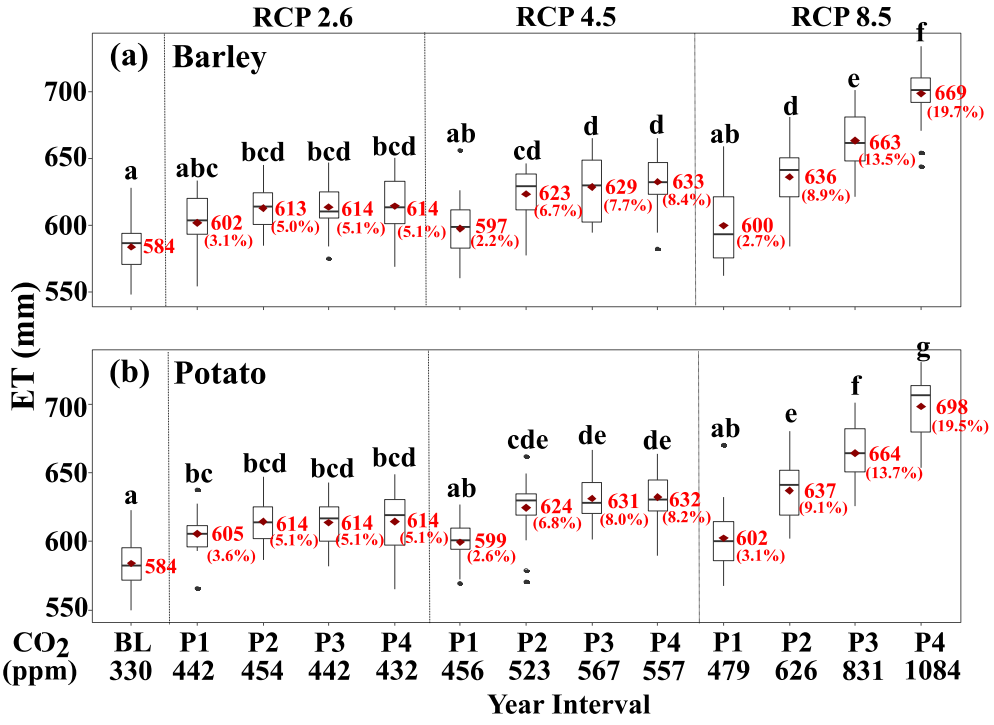

Fig. 2.8 Same as Fig. 2.7 but for evapotranspiration (ET).

Water use efficiency is an important indicator describing (i) trade-offs between water loss and carbon sequestration during plant photosynthesis, and (ii) crop-yield response to climate change. Table 2.1 shows that WUE will decrease in all future periods and under all RCP scenarios relative to BL. A decreasing trend in WUE is seen under both RCP 4.5 and 8.5, whereas under RCP 2.6, the decrease from P1 to P2 reverses from that observed for P3 to P4. The greatest percentage decrease in WUE for barley and potatoes are 8.7 and 7.0% under RCP 2.6-P2, 13.0 and 14.0% under RCP 4.5-P4, and 30.4 and 34.9% under RCP 8.5-P4, respectively. An increase in ET, along with a decrease in yield, was followed by a decrease in WUE (Eq. 2.5; Table 2.1).

Table 2.1 Simulated average annual evapotranspiration (ET), crop yield, and water use efficiency (WUE) for different periods and RCP scenarios.

Period	Barley			Potatoes		
	ET (mm)	Yield (tons ha^{-1})	WUE (kg ha^{-1} mm^{-1})	ET (mm)	Yield (tons ha^{-1})	WUE (kg ha^{-1} mm^{-1})
BL	584	2.66	4.6	584	5.05	8.6
RCP 2.6-P1	602 (3.1%)	2.65 (-0.4%)	4.4 (-4.3%)	605 (3.6%)	5.01 (-0.8%)	8.3 (-3.5%)
RCP 2.6-P2	613 (5.0%)	2.55 (-4.1%)	4.2 (-8.7%)	614 (5.1%)	4.90 (-3.0%)	8.0 (-7.0%)
RCP 2.6-P3	614 (5.1%)	2.62 (-1.5%)	4.3 (-6.5%)	614 (5.1%)	4.93 (-2.4%)	8.0 (-7.0%)
RCP 2.6-P4	614 (5.1%)	2.67 (0.4%)	4.3 (-6.5%)	614 (5.1%)	4.98 (-1.4%)	8.1 (-5.8%)
RCP 4.5-P1	597 (2.2%)	2.71 (1.9%)	4.5 (-2.2%)	599 (2.6%)	5.00 (-1.0%)	8.3 (-3.5%)
RCP 4.5-P2	623 (6.7%)	2.56 (-3.8%)	4.1 (-10.9%)	624 (6.8%)	4.82 (-4.6%)	7.7 (-10.5%)
RCP 4.5-P3	629 (7.7%)	2.54 (-4.5%)	4.0 (-13.0%)	631 (8.0%)	4.75 (-5.9%)	7.5 (-12.8%)
RCP 4.5-P4	633 (8.4%)	2.55 (-4.1%)	4.0 (-13.0%)	632 (8.2%)	4.67 (-7.5%)	7.4 (-14.0%)
RCP 8.5-P1	600 (2.7%)	2.67 (0.4%)	4.5 (-2.2%)	602 (3.1%)	4.99 (-1.2%)	8.3 (-3.5%)
RCP 8.5-P2	636 (8.9%)	2.58 (-3.0%)	4.1 (-10.9%)	637 (9.1%)	4.77 (-5.5%)	7.5 (-12.8%)
RCP 8.5-P3	663 (13.5%)	2.31 (-13.2%)	3.5 (-24.3%)	664 (13.7%)	4.34 (-14.1%)	6.5 (-24.4%)
RCP 8.5-P4	699 (19.7%)	2.24 (-15.8%)	3.2 (-30.4%)	698 (19.5%)	3.88 (-23.2%)	5.6 (-34.9%)

Note: Values in parentheses are percent changes in specific parameters compared to the baseline period (BL: 2000–2019); WUE: *WUE=1000*Yield/ET*.

To explore the reasons behind the future decline in crop yields, we analyzed trends in monthly ET and soil water content across BBW. Predicted variations in average monthly ET do not strictly follow those of monthly temperature for the different future periods under the three RCP scenarios (Fig. 2.9 *vs.* Fig. 2.4; also, Tables S2.5 and S2.6). The greatest ET appears in June and July (almost one month earlier than temperature) when crop water demand is least. Difference in average monthly ET across RCPs increases with time (from P1 to P4), especially for winter and early spring (from November to May of the following year; Fig. 2.9). This is consistent with patterns of monthly precipitation and temperature that yield warmer and wetter winters (Fig. 2.3 and 2.4). The greatest percentage increase in monthly ET occurs from winter into early spring (i.e., from December to May of the following year) for all RCP scenarios, with their corresponding maxima occurring in P4. In contrast, the average monthly ET from June to November does not vary much relative to BL from P1 to P4 under all RCP scenarios.

Compared to BL, predicted monthly soil water content increases during winter for all emission scenarios (Fig. 2.10). However, the predicted soil water content becomes much lower than that of BL as early as in March, which is more apparent from P2 to P4 for all RCP scenarios (Fig. 2.10; and Table S2.7 and S2.8 in SM). Note that a dramatic decrease occurs in monthly soil water content from March to October during P4 for RCP 8.5, separating this event from the other two scenarios. We speculate that increased early spring evaporation leads to spring drought, resulting in a long-lasting soil water deficit during the growing season. Precipitation does not increase during this time, but temperature increases greatly, particularly for RCP 8.5 (Fig. 2.3 and 2.4). The pronounced reduction in soil water during the growing season indicates that lower amounts of soil water would be used for

crop growth, resulting in reduced crop yields. Mitigating atmospheric CO_2 concentrations to at least within the range provided by RCP 4.5 may help avoid significant crop yield reductions.

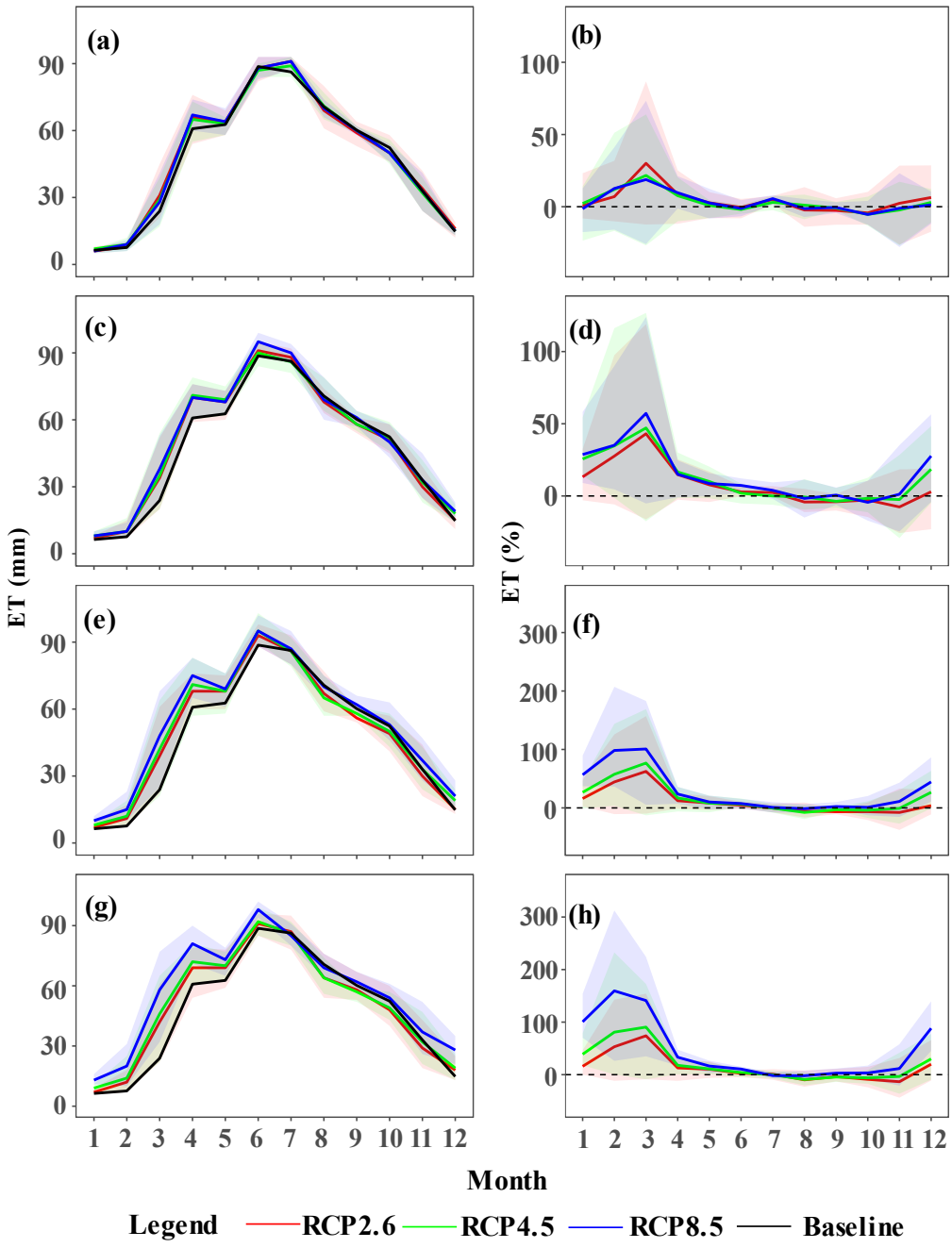

Fig. 2.9 Same as Fig. 2.3 but for evapotranspiration (ET).

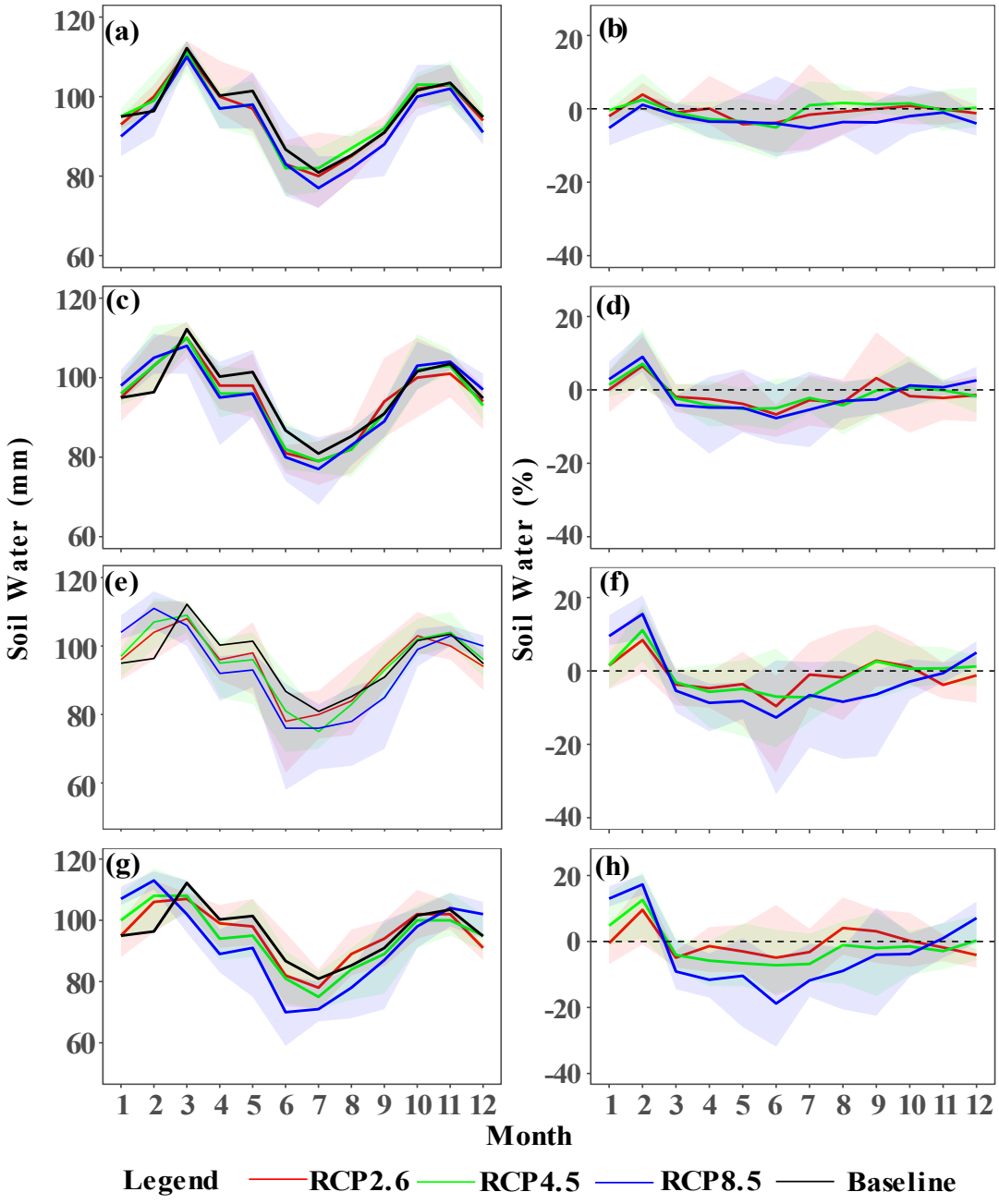

Fig. 2.10 Same as Fig. 2.3 but for soil water content.

2.4 Discussion

2.4.1 Climate change projections in AC

My results indicate increases in annual air temperature and precipitation in AC during the rest of the 21st century, consistent with the results of a study focused on crop-growing conditions in Ontario, Canada (Dong et al., 2021). Varying trends in temperature and precipitation over time appear to generally follow that of atmospheric CO_2 concentrations. For a moderately controlled CO_2 emission scenario (i.e., RCP 4.5), increases in annual air temperature and precipitation maxima towards the end of the century provide an overall increase of 2.1°C and 63 mm, respectively. Such increases can be reduced by strictly controlled CO_2 emissions, such as it is provided for RCP 2.6. Increases in annual temperature and precipitation for RCP 2.6 will be about half those for RCP 4.5. In contrast, increases in temperature and precipitation will be much greater under an uncontrolled emission scenario (RCP 8.5), with increases in annual temperature and precipitation about 2–3 times greater than those for RCP 4.5 by the end of the 21st-century. On a monthly basis, increases in temperature and precipitation appear greater during the winter than during the growing season. The projected precipitation increases in this study area would be favorable to spring crop growth. However, elevated temperatures would increase evaporation, possibly leading to spring drought. Elevated temperatures and unchanged or possibly lower precipitation during the growing season could lead to substantial water stress in crops.

2.4.2 Climate change impacts on potato yields and water stress

Climate change will have major impacts on agricultural food production in a complicated way with many regional differences. High temperatures during the growing season due to climate change may cause an array of physiological changes in potato plants

(e.g., height of plants, chlorophyll fluorescence in leaves, number of tubers, mass of individual tubers, tuber deformation, and sprouted tubers), affecting the development of potatoes and leading to a drastic reduction in yield (Rykaczewska, 2015). Studies have suggested that potato productivity can be greatly reduced at air temperatures greater than the optimum growing temperature of 20°C (Rykaczewska, 2015, 2017). Potato cultivar response to high temperatures during the growing season depends on the plant's growing stage (Rykaczewska, 2015, 2017). Heat stress at earlier stages of potato development may negatively affect its growth, exacerbating reduction in potato yield (Rykaczewska, 2015). In this study, average monthly temperatures during P1 and P2 are all below the optimal temperature for potato growth for all RCP scenarios, except for July in P2 for RCP 8.5. Concerning P3 and P4, temperatures are below 20°C under RCP 2.6, with temperatures greater than 20°C in July for RCP 4.5 and in July and August for RCP 8.5 (Fig. 2.4). Although we cannot rule out the possibility that temperatures on individual days could be sufficiently high to cause a drop in yield. Temperature increases are unlikely to cause potato yield reductions in a future warmer climate.

Warmer temperatures enhance evaporation, reducing surface water and drying out soils and vegetation. This makes periods with low precipitation drier than they would be under cooler conditions. The projected precipitation increases mainly occur in winter and early spring. The minor increase in precipitation during the growing season would not counterbalance the impact of high-temperature-induced water stress in potatoes. For example, the great reduction in soil water content during the growing season during P3 and P4 for RCP 8.5 is largely caused by rising temperatures. GCMs also predict a decrease in precipitation in August under all scenarios, especially in P2, P3, and P4 (Fig. 2.3). The

combined effects of rising temperature and decreased precipitation can potentially lead to a significant reduction in soil water content (P3: -8.4%; P4: -8.9%) in August for RCP 8.5 (Fig. 2.9 and 2.10). This reduced soil water content during the growing phase of potato is sufficiently harsh to limit ET rates (P3: -1.3%; P4: -2.0%). These results suggest that climate change could cause substantial reductions in potato yield. Others have also reported that water stress caused by elevated temperatures may be the main reason for crop yield reductions under future climate change (Asseng et al., 2015). Mitigation measures, such as supplementary irrigation may be needed to combat the negative effects of climate change.

2.4.3 The impact of atmospheric CO_2 fertilization

Previous studies have shown that elevated ambient CO_2 concentrations can promote crop growth through CO_2 fertilization (Ainsworth and Long, 2005). However, most experiments were conducted on a small scale or in laboratories. Due to their complex interactions, the actual impact of CO_2 fertilization on crops at the watershed scale has been largely uncertain (Walker and Schulze, 2008). In this study, we attempted to investigate CO_2 fertilization effects on crop yields for BBW using SWAT. Figure 2.11 shows crop yields before and after considering CO_2 fertilization effects in two future 40-year periods (i.e., 2020–2059 and 2060–2099) and BL period from 1980–2019 under the three RCP scenarios.

Overall, projected crop yields still tended to reduce, even when CO_2 fertilization effects were considered. Crop yield in response to CO_2 fertilization varies across different future periods and among the two crops. Yields of barley tend to be affected more by CO_2 fertilization (Fig. 2.11) than those of potato. CO_2 fertilization effects are visible in all future periods except for the 2020–2059 period under RCPs 2.6 and 8.5. However, significant

differences between the "with and without" CO_2 fertilization only occur in the period of 2060–2099 under RCP 8.5 for both crops. These results agree with prior studies on this subject. For example, Goswami et al. (2018) recorded a drastic reduction in tuber yield when neglecting CO_2 fertilization. Raymundo et al. (2018) reported a smaller tuber yield reduction after considering CO_2 fertilization. My results suggest that although elevated ambient CO_2 concentrations could potentially increase crop yields, a projected increase in water stress caused by increasing temperatures has the potential to offset any positive effect of fertilization, leading to an overall decrease in crop yields.

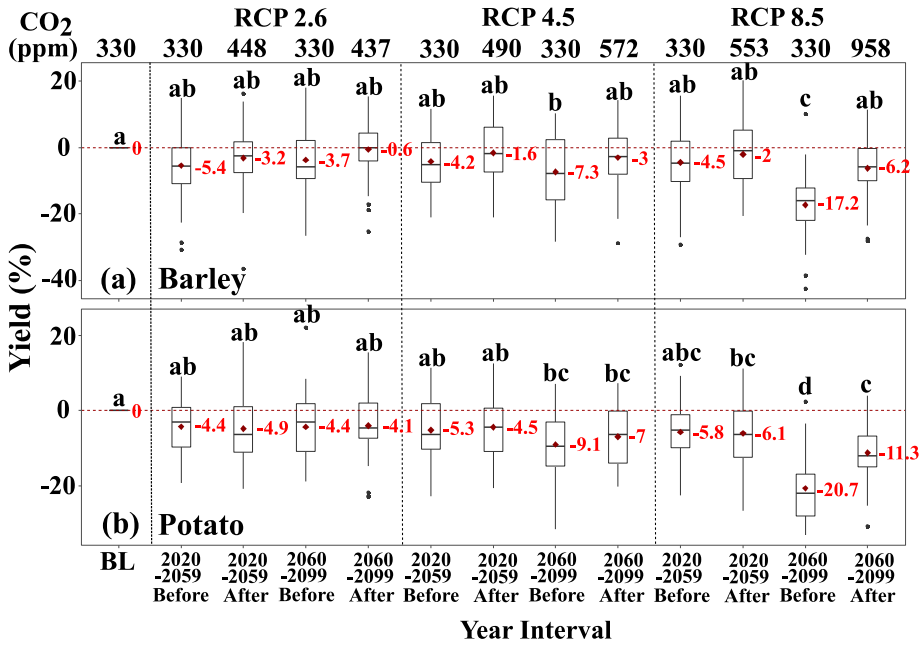

Fig. 2.11 Percent change in crop yields for (a) barley and (b) potatoes without and with CO_2 fertilization considered for two 40-year periods (i.e., 2020–2059 and 2060–2099) under three RCP scenarios. The baseline period is from 1980–2019. Corresponding average CO_2 concentrations are also given. The box in each box-and-whisker plot shows the interquartile range, and the horizontal line in the box marks the median. The red dot in the box is the mean, with its value shown in red to the right of the box. The whiskers are lines extending from the top and bottom of each box, showing maximum and minimum values, respectively. The dots beyond the whiskers are viewed as outliners. Different letters on top of each box plot indicate that the means are statistically different (p<0.05) from other means based on Tukey's HSD tests.

2.4.4 Mitigation of climate change impacts on crop yields

My study demonstrates that climate change under RCP 8.5 would lead to an economically significant crop yield reduction, consistent with results reported by others (e.g., Liu et al., 2021). At the global level, collective efforts are needed to limit CO_2 emissions below the RCP4.5 level to ensure sustainable crop yields. Locally, mitigating management practices are needed. For example, Sun and Ren (2014) suggested delaying the harvest time of summer maize in the Haihe Plain in China to reduce adverse effects associated with climate change. Hijmans (2003) concluded that the reduction in potato yields by climate change at high latitudes might be minimized by changing the planting time, using late-maturing cultivars, and shifting the location of potato production. Furthermore, Tatsumi et al. (2011) predicted that regions with cold weather under current climate conditions, such as in Canada, may become suitable for crop production under future climate scenarios. Considering changes in land management practices (Hijmans, 2003; Kim and Lee, 2020) to adapt to future climate change would be helpful to mitigate the reduction in crop yields, especially in AC. Based on my analysis, early-maturing cultivars may help avoid water stress in summer, minimizing harmful climate-related impacts on potato yields. Furthermore, optimizing cultivation practices (e.g., irrigation, fertilization) can conserve water resources, reducing water stress during the crop growing period (Brassard and Singh, 2008; Shahvari et al., 2019). However, prolonged irrigation could cause nutrient losses through surface runoff (Rykaczewska, 2015). Further studies are needed to examine this condition more thoroughly.

2.4.5 Limitations of the present study

The current version of SWAT cannot simulate stochastic events, such as disease outbreak and extreme weather events, based on discrepancies between predicted and measured annual yields for 1992, 1993, and 1994 (Fig. 2.6). Also, measured barley and potato yields in 2011 were lower than predicted, likely due to a severe hailstorm that occurred that year at BBW, causing serious crop damage. This was not accounted for in current model projections. This limitation would not have affected the performance of the model in estimating long-term average conditions brought on by climate change. However, we recognize that climate may also have impacts on disease and insect outbreaks, which were not addressed here.

Furthermore, rising atmospheric CO_2 concentrations can have direct impacts on the hydrological cycle (Ficklin et al., 2016). For example, elevated ambient CO_2 concentrations could cause stomatal aperture to contract in some plants (Morison, 1987; Field et al., 1995; Saxe et al., 1998; Wand et al., 1999; Medlyn et al., 2001), leading to a lower transpiration rate at the leaf level (Leakey et al., 2009; Sreeharsha et al., 2015; Xu et al., 2016). Also, in SWAT, the reduction in stomatal conductance by elevated CO_2 levels is assumed to be linear over the CO_2 concentration range from 330–660 ppm (Morison and Gifford, 1983; Neitsch et al., 2011). However, the average atmospheric CO_2 concentration for the 2060–2099 period under RCP 8.5 is 958 ppm, which is much greater than the current upper limit of 660 ppm. The reduction in stomatal conductance caused by these elevated ambient CO_2 concentrations is ~80% greater than SWAT's concentration range. This suggests that we may need to interpret the CO_2 fertilization effect on crop yields with caution and that further field and numerical experiments should be carried out under a

greater range of ambient CO_2 concentrations. We also recommend developing new algorithms for conditions with ambient CO_2 concentrations beyond 660 ppm.

In addition, a 'steady state' approach was taken in this study with respect to agricultural management practices. We assumed that crop rotation and management practices remain unchanged in future scenarios. However, farmers may implement climate mitigation practices, such as adjusting planting dates to earlier times in spring, switching to potato and barley cultivars that better tolerate climate change, and changing to more climate-tolerant crops, such as wheat or maize. Although modifying the configuration of SWAT to account for these mitigation practices is challenging, we attempted to simulate crop growth based on simplified heat units. However, the performance was admittedly unrealistic. We believe that this is one of the areas where SWAT can be improved. The results presented here can be considered conservative regarding crop yield projections.

2.5 Summary and conclusions

In this study, an enhanced version of SWAT was employed to estimate potential impacts of climate change on yields of two major crops (potatoes and barley) by considering three climate ensembles based on GHG emission scenarios, i.e., Representative Concentration Pathways 2.6, 4.5, and 8.5, provided by five GCMs. Changes in crop yields were evaluated based on four future 20-year periods (2020–2099) relative to a baseline period (BL: 2000–2019), including P1 (2020–2039), P2 (2040–2059), P3 (2060–2079), and P4 (2080–2099). Climate change impacts on hydrological variables associated with crop yields, including air temperature, precipitation, evapotranspiration (ET), soil water content, and water use efficiency (WUE), were investigated. Analyses of future climate projections in the study area indicate that annual temperatures will significantly

increase under all RCP scenarios and future periods with elevated atmospheric CO_2 concentrations in the 21st century. However, significant increases in annual precipitation are only found for RCP 4.5-P3 and 8.5-P2, -P3, and -P4. Seasonal analyses further demonstrated that projected increases in precipitation will largely occur in winter and early spring, with a minimal increase during the crop growing season and even a decrease in certain summer months under high GHG emission scenarios, such as RCP 4.5 and 8.5. My results indicate a significant crop yield reduction under RCP 8.5, with barley and potato yields reduced by 13.2 and 15.8% and 14.1 and 23.2% during P3 and P4, respectively, relative to BL. No significant trend was detected for the other RCP scenarios. The main reason for crop yield reduction is due to soil water stress during the growing season caused by rising temperatures and ET rates projected under emission scenario, RCP 8.5. Mitigating atmospheric CO_2 concentrations to at least within the range of RCP 4.5 would keep crop yields from decreasing.

We also found that future changes in SWAT-predicted annual ET for both crops followed the same pattern as annual air temperature. The WUEs of both food crops were predicted to decrease due to the combined effects of increased ET and reduced crop yields during the different future periods. Further analysis shows that most increases in ET occurred in winter and early spring and that changes in monthly ET were minimal from summer to fall due to low soil water content.

It was found that the response of crop yield to CO_2 fertilization varies across the different future periods and crops. In general, when CO_2 fertilization effects are considered, the predicted crop yield will still decrease relative to BL for both crops. Elevated ambient CO_2 concentrations can potentially increase crop yields. However, the projected increase

in water stress caused by warmer temperatures could potentially offset this effect, leading to an overall crop yield reduction under high GHG-emission scenarios. Supplementary irrigation or adjusting land management practices may help avoid crop yield reductions under future, high GHG-emission scenarios.

Acknowledgments

Funding: This work was supported by the province of New Brunswick under the aegis of the Enabling Agricultural Research and Innovation (EARI) project entitled "Modeling the effects of water stress and supplemental irrigation on potato production in New Brunswick under climate change" [project number J-002472] (PI: Li) and by Agriculture and Agri-Food Canada under the aegis of the project entitled "Landscape integrated soil and water conservation (LISWC) on sloping fields under potato production in Atlantic Canada" [project number J-001754] (PI: Li). The authors thank Sylvie Lavoie, Yulia Kupriyanovich, John Monteith, and Lionel Stevens for their technical support in data collection and sample analyses.

References

Ahiablame, L., Sinha, T., Paul, M., Ji, J.H., and Rajib, A. (2017). Streamflow response to potential landuse and climate changes in the James River watershed, Upper Midwest United States. Journal of Hydrology: Regional Studies, 14, 150–166. https://doi.org/10.1016/j.ejrh.2017.11.004

Ahmad, M.J., Iqbal, M.A., and Choi, K.S. (2020). Climate-driven constraints in sustaining future wheat yield and water productivity. Agricultural Water Management, 231, 105991. https://doi.org/10.1016/j.agwat.2019.105991

Ainsworth, E.A., and Long, S.P. (2005). What have I learned from 15 years of free-air CO_2 enrichment (FACE)? A meta-analytic review of the responses of photosynthesis, canopy properties and plant production to rising CO_2. New Phytologist, 165(2), 351–372. https://doi.org/10.1111/j.1469-8137.2004.01224.x

Arnold, J.G., Srinivasan, R., Muttiah, R.S., and Williams, J.R. (1998). Large area hydrologic modeling and assessment. Part I: Model development. Journal of the American Water Resources Association, 34(1), 73–89. https://doi.org/10.1111/j.1752-1688.1998.tb05961.x

Arnold, J.G., Kiniry, J.R., Srinivasan, R., Williams, J.R., Haney, E.B., and Neitsch, S.L. (2011). Soil and water assessment tool input/output file documentation version 2009. Texas Water Resources Institute. https://swat.tamu.edu/media/19754/swat-io-2009.pdf

Ashraf, V.S., Mousavi, S.J., Abbaspour, K.C., Srinivasan, R., and Yang, H. (2014). Analyses of the impact of climate change on water resources components, drought

and wheat yield in semiarid regions: Karkheh River Basin in Iran. Hydrological Processes, 28(4), 2018–2032. https://doi.org/10.1002/hyp.9747

Asseng, S., Ewert, F., Martre, P., Rötter, R.P., Lobell, D.B., Cammarano, D., Kimball, B.A., Ottman, M.J., Wall, G.W., White, J.W., Reynolds, M.P., Alderman, P.D., Prasad, P.V.V., Aggarwal, P.K., Anothai, J., Basso, B., Biernath, C., Challinor, A.J., De Sanctis, G., Doltra, J., Fereres, E., Garcia-Vila, M., Gayler, S., Hoogenboom, G., Hunt, L.A., Izaurralde, R.C., Jabloun, M., Jones, C.D., Kersebaum, K.C., Koehler, A.K., Müller, C., Naresh Kumar, S., Nendel, C., O'Leary, G., Olesen, J.E., Palosuo, T., Priesack, E., Eyshi Rezaei, E., Ruane, A.C., Semenov, M.A., Shcherbak, I., Stöckle, C., Stratonovitch, P., Streck, T., Supit, I., Tao, F., Thorburn, P.J., Waha, K., Wang, E., Wallach, D., Wolf, J., Zhao, Z., and Zhu, Y. (2015). Rising temperatures reduce global wheat production. Nature Climate Change, 5, 143–147. https://doi.org/10.1038/nclimate2470

Bootsma, A., Gameda, S., and McKenney, D.W. (2005). Potential impacts of climate change on corn, soybeans and barley yields in Atlantic Canada. Canadian Journal of Soil Science, 85(2), 345–357. https://doi.org/10.4141/S04-025

Boswell, V.G. (1926). The influence of temperature upon the growth and yield of garden peas. 162–168 ed, p. 26.

Brassard, J.P., and Singh, B. (2008). Impacts of climate change and CO_2 increase on agricultural production and adaptation options for Southern Québec, Canada. Mitigation and Adaptation Strategies for Global Change, 13, 241–265. https://doi.org/10.1007/s11027-007-9109-2

W. A. C. (1914). The Water Requirement of Plants [Review of The Water Requirement of Plants. I. Investigations in the Great Plains in 1910 and 1911. II. A Review of the Literature, by L. J. Briggs and H. L. Shantz]. The Plant World, 17(3), 76–78. http://www.jstor.org/stable/43477376

Cannon, A.J., Sobie, S.R., and Murdock, T.Q. (2015). Bias correction of GCM precipitation by quantile mapping: How well do methods preserve changes in quantiles and extremes? Journal of Climate, 28, 6938–6959. https://doi.org/10.1175/JCLI-D-14-00754.1

Chen, X., Qi, Z., Gui, D., Gu, Z., Ma, L., Zeng, F., and Li, L. (2019). Simulating impacts of climate change on cotton yield and water requirement using RZWQM2. Agricultural Water Management, 222, 231–241. https://doi.org/10.1016/j.agwat.2019.05.030

Chen, Y., Marek, G.W., Marek, T.H., Moorhead, J.E., Heflin, K.R., Brauer, D.K., Gowda, P.H., and Srinivasan, R. (2019). Simulating the impacts of climate change on hydrology and crop production in the Northern High Plains of Texas using an improved SWAT model. Agricultural Water Management, 221, 13–24. https://doi.org/10.1016/j.agwat.2019.04.021

Chow, L., Xing, Z., Benoy, G., Rees, H.W., Meng, F.-R., Jiang, Y., and Daigle, J.L. (2011). Hydrology and water quality across gradients of agricultural intensity in the Little River watershed area, New Brunswick, Canada. Journal of Soil and Water Conservation, 66(1), 71–84. https://doi.org/10.2489/jswc.66.1.71

Chow, T., and Rees, H. (2006). Impacts of intensive potato production on water yield and sediment load (Black Brook Experimental Watershed: 1992–2002 summary). Potato Research Centre, AAFC, Fredericton, NB, Canada

Cure, J.D., and Acock, B. (1986). Crop responses to carbon dioxide doubling: a literature survey. Agricultural and Forest Meteorology, 38(1–3), 127–145. https://doi.org/10.1016/0168-1923(86)90054-7

Delazari, F.T., Assis, I.R., Cabrera, D.F.V., Ferreira, M.G., Dias, L.E., Rueda, A., Zanuncio, J.C., and Silva, D.J.H. (2018). Morpho-physiological characteristics by sweet potato cultivars as function of irrigation depth. Anais da Academia Brasileira de Ciencias, 90(4), 3541–3549. https://doi.org/10.1590/0001-3765201820170687

Dong, F., Javed, A., Saber, A., Neumann, A., Alberto Arnillas, C., Kaltenecker, G., and Arhonditsis, G. (2021). A flow-weighted ensemble strategy to assess the impacts of climate change on watershed hydrology. Journal of Hydrology, 594, 125898. https://doi.org/10.1016/j.jhydrol.2020.125898

FAO, The State of Food and Agriculture 2019: Moving forward on food loss and waste reduction. (2021, April 20). https://reliefweb.int/report/world/state-food-and-agriculture-2019-moving-forward-food-loss-and-waste-reduction

Ficklin, D.L., Robeson, S.M., and Knouft, J.H. (2016). Impacts of recent climate change on trends in baseflow and stormflow in United States watersheds. Geophysical Research Letters, 43(10), 5079–5088. https://doi.org/10.1002/2016GL069121

Field, C.B., Jackson, R.B., and Mooney, H.A. (1995). Stomatal responses to increased CO_2: implications from the plant to the global scale. Plant, Cell and Environment, 18(10), 1214–1225. https://doi.org/10.1111/j.1365-3040.1995.tb00630.x

Gassman, P.W., Reyes, M.R., Green, C.H., and Arnold, J.G. (2005). SWAT peer-reviewed literature: a review. https://swat.tamu.edu/docs/swat/conferences/2005/PDF/Session_I/Gassman.pdf

Goswami, B., Hussain, R., Kumar, P.V., Saikia, U.S., and Banarjee, S. (2018). Impact assessment of climate change on potato productivity in Assam using SUBSTOR-Potato model. Journal of Agrometeorology, 20(2), 105–109. Retrieved from https://login.proxy.hil.unb.ca/login?url=https://www.proquest.com/scholarly-journals/impact-assessment-climate-change-on-potato/docview/2055190519/se-2

Hargreaves, G.H., and Samani, Z.A. (1985). Reference crop evapotranspiration from temperature. Applied Engineering in Agriculture, 1(2), 96–99. https://doi.org/10.13031/2013.26773

Harrison, M.T., Tardieu, F., Dong, Z., Messina, C.D., and Hammer, G.L. (2014). Characterizing drought stress and trait influence on maize yield under current and future conditions. Global Change Biology, 20(3), 867–878. https://doi.org/10.1111/gcb.12381

Hatfield, J.L., and Dold, C. (2019). Water-use efficiency: advances and challenges in a changing climate. Frontiers in Plant Science, 10, 103. https://doi.org/10.3389/fpls.2019.00103

He, W., Yang, J.Y., Qian, B., Drury, C.F., Hoogenboom, G., He, P., Lapen, D., and Zhou, W. (2018). Climate change impacts on crop yield, soil water balance and nitrate

leaching in the semiarid and humid regions of Canada. PLoS One, 13, e0207370. https://doi.org/10.1371/journal.pone.0207370

Hiebert, J., Cannon, A.J., Murdock, T., Sobie, S., and Werner, A. (2018). ClimDown: climate downscaling in R. Journal of Open Source Software, 3, 360. https://doi.org/10.21105/joss.00360

Hijmans, R.J. (2003). The effect of climate change on global potato production. American Journal of Potato Research, 80, 271–280. https://doi.org/10.1007/BF02855363

Idso, K.E., and Idso, S.B. (1994). Plant responses to atmospheric CO_2 enrichment in the face of environmental constraints: a review of the past 10 years' research. Agricultural and Forest Meteorology, 69(3–4), 153–203. https://doi.org/10.1016/0168-1923(94)90025-6

Kapoor, S., Mahajan, B.V.c., Sharma, S., and Gandhi, N. (2019). Storage behaviour of different potato varieties under ambient conditions. Agricultural Research Journal, 56(3), 576–578. https://doi.org/10.5958/2395-146X.2019.00090.5

Kim, Y.-U., and Lee, B.-W. (2020). Earlier planting offsets the adverse effect of global warming on spring potato in South Korea. Science of The Total Environment, 742, 140667. https://doi.org/10.1016/j.scitotenv.2020.140667

Leakey, A.D.B., Ainsworth, E.A., Bernacchi, C.J., Rogers, A., Long, S.P., and Ort, D.R. (2009). Elevated CO_2 effects on plant carbon, nitrogen, and water relations: six important lessons from FACE. Journal of Experimental Botany, 60(10), 2859–2876. https://doi.org/10.1093/jxb/erp096

Liang, K., Qi, J., Liu, E. Y., Jiang, Y., Li, S., and Meng, F.-R. (2019). Estimated potential impacts of soil and water conservation terraces on potato yields under different

climate conditions. Journal of Soil and Water Conservation, 74(3), 225–234. https://doi.org/10.2489/jswc.74.3.225.

Liu, Q., Niu, J., Sivakumar, B., Ding, R., and Li, S. (2021). Accessing future crop yield and crop water productivity over the Heihe River basin in northwest China under a changing climate. Geoscience Letters, 8, 2. https://doi.org/10.1186/s40562-020-00172-6

Lopes, T.R., Zolin, C.A., Mingoti, R., Vendrusculo, L.G., Almeida, F.T.D., Souza, A.P.D., Oliveira, R.F.D., Paulino, J., and Uliana, E.M. (2021). Hydrological regime, water availability and landuse/land cover change impact on the water balance in a large agriculture basin in the Southern Brazilian Amazon. Journal of South American Earth Sciences, 108, 103224. https://doi.org/10.1016/j.jsames.2021.103224

Magoon, C. A. and Culpepper, Charles W. (1932). "Response of Sweet Corn to Varying Temperatures from Time of Planting to Canning Maturity," Technical Bulletins 163380, United States Department of Agriculture, Economic Research Service. https://doi.org/10.22004/ag.econ.163380

Maurer, E.P., Hidalgo, H.G., Das, T., Dettinger, M.D., and Cayan, D.R. (2010). The utility of daily large-scale climate data in the assessment of climate change impacts on daily streamflow in California. Hydrology and Earth System Sciences, 14(6), 1125–1138. https://doi.org/10.5194/hess-14-1125-2010

Medlyn, B.E., Barton, C.V.M., Broadmeadow, M.S.J., Ceulemans, R., De Angelis, P., Forstreuter, M., Freeman, M., Jackson, S.B., Kellomäki, S., Laitat, E., Rey, A., Roberntz, P., Sigurdsson, B.D., Strassemeyer, J., Wang, K., Curtis, P.S., and Jarvis, P.G. (2001). Stomatal conductance of forest species after long-term

exposure to elevated CO_2 concentration: a synthesis. New Phytologist, 149(2), 247–264. https://doi.org/10.1046/j.1469-8137.2001.00028.x

Mellerowicz, K.T. (1993). Soils of Black Brook Watershed, St. Andre Parish, Madawaska County, New Brunswick. [Fredericton]: New Brunswick Department of Agriculture. https://sis.agr.gc.ca/cansis/publications/surveys/nb/nbbb/index.html

Mishra, S.K., and Singh, V.P. (2013). Soil conservation service curve number (SCS-CN) methodology. Springer Netherlands. https://citations.springernature.com/book?doi=10.1007/978-94-017-0147-1

Monteith, J. L. 1965. Evaporation and environment. Symposia of the Society for Experimental Biology. 19, pp. 205–234. https://repository.rothamsted.ac.uk/item/8v5v7

Moriasi, D.N., Arnold, J.G., Van Liew, M.W., Bingner, R.L., Harmel, R.D., and Veith, T.L. (2007). Model evaluation guidelines for systematic quantification of accuracy in watershed simulations. Transactions of the ASABE, 50(3), 885–900. https://doi.org/10.13031/2013.23153

Morison, J.I.L. (1987). Stomatal function, in: Zeiger, E.F., G.D.; Cowan, I.R. (Ed.), Intercellular CO_2 concentration and stomatal response to CO_2. Stanford Univiversity Press, pp. 229–251. https://books.google.com/books/about/Stomatal_Function.html?id=mp-aAAAAIAAJ

Morison, J.I.L. and Gifford, R.M. (1983). Stomatal sensitivity to carbon dioxide and humidity. Plant Physiology, 71(4), 789–796. https://doi.org/10.1104/pp.71.4.789

Motha, R.P., and Baier, W. (2005). Impacts of present and future climate change and climate variability on agriculture in the temperate regions: North America. Climate Change, 70, 137–164. https://doi.org/10.1007/s10584-005-5940-1

Mukezangango, J. (2017). Potato market information review 2015-2016, Agriculture and Agri-Food Canada. https://publications.gc.ca/collections/collection_2017/aac-aafc/A71-32-2016-eng.pdf

Neitsch, S.L., Arnold, J.G., Kiniry, J.R., and Williams, J.R. (2011). Soil and Water Assessment Tool Theoretical Documentation Version 2009. Texas Water Resources Institute. https://hdl.handle.net/1969.1/128050.

Ozturk, I., Sharif, B., Baby, S., Jabloun, M., and Olesen, J.E. (2017). The long-term effect of climate change on productivity of winter wheat in Denmark: a scenario analysis using three crop models. The Journal of Agricultural Science, 155(5), 733. https://doi.org/10.1017/S0021859616001040

Pathak, T.B., Maskey, M.L., Dahlberg, J.A., Kearns, F., Bali, K.M., and Zaccaria, D. (2018). Climate change trends and impacts on California agriculture: a detailed review. Agronomy, 8(3), 25. https://doi.org/10.3390/agronomy8030025

Paul, M. (2016). Impacts of landuse and climate changes on hydrological processes in South Dakota Watersheds. South Dakota State University. Theses and Dissertations. Paper 1018. https://openprairie.sdstate.edu/cgi/viewcontent.cgi?article=2018&context=etd

Paul, M., Dangol, S., Kholodovsky, V., Sapkota, A.R., Negahban-Azar, M., and Lansing, S. (2020). Modeling the impacts of climate change on crop yield and irrigation in

the Monocacy River watershed, USA. Climate, 8(12), 139. https://doi.org/10.3390/cli8120139

Potato, The Canadian Encyclopedia. (2021, December 13). https://www.thecanadianencyclopedia.ca/en/article/potato

PotatoPro, Potato Production in Canada. (2021, April 20). https://www.potatopro.com/canada/potato-statistics

Poulsen, H., Blaabjerg, K., Nørgaard, J., and Ton Nu, M.A. (2012). High-moisture air-tight storage of barley and wheat improves nutrient digestibility. Journal of Animal Science, 90, 242–244. https://doi.org/10.2527/jas.53985

Priestley, C.H.B., and Taylor, R.J. (1972). On the assessment of surface heat flux and evaporation using large-scale parameters. Monthly Weather Review, 100, 81–92. https://doi.org/10.1175/1520-0493(1972)100<0081:OTAOSH>2.3.CO;2

Qi, J., Li, S., Li, Q., Xing, Z., Bourque, C. P.-A., and Meng, F.-R. (2016a). Assessing an enhanced version of SWAT on water quantity and quality simulation in regions with seasonal snow cover. Water Resources Management, 30, 5021–5037. https://doi.org/10.1007/s11269-016-1466-8.

Qi, J., Li, S., Li, Q., Xing, Z., Bourque, C. P.-A., and Meng, F.-R. (2016b). A new soil-temperature module for SWAT application in regions with seasonal snow cover. Journal of Hydrology, 538, 863–877. https://doi.org/10.1016/j.jhydrol.2016.05.003.

Qi, J., Li, S., Yang, Q., Xing, Z., and Meng, F.-R. (2017). SWAT setup with long-term detailed landuse and management records and modification for a micro-watershed

influenced by freeze-thaw cycles. Water Resources Management, 31, 3953–3974. https://doi.org/10.1007/s11269-017-1718-2.

Qi, J., Liang, K., Li, S., Wang, L., and Meng, F.-R. (2018). Hydrological evaluation of flow diversion terraces using downhill-slope calculation method for high resolution and accuracy DEMs. Sustainability, 10(7), 2414. https://doi.org/10.3390/su10072414

Qi, J., Zhang, X., and Cosh, M. H. (2019a). Modeling soil temperature in a temperate region: A comparison between empirical and physically based methods in SWAT. Ecological Engineering, 129, 134–143. https://doi.org/10.1016/j.ecoleng.2019.01.017.

Qi, J., Zhang, X., and Wang, Q. (2019b). Improving hydrological simulation in the Upper Mississippi River Basin through enhanced freeze-thaw cycle representation. Journal of Hydrology, 571, 605–618. https://doi.org/10.1016/j.jhydrol.2019.02.020

Qi, J., Zhang, X., Yang, Q., Srinivasan, R., Arnold, J.G., Li, J., Waldholf, S.T., and Cole, J. (2020). SWAT ungauged: water quality modeling in the Upper Mississippi River Basin. Journal of Hydrology, 584, 124601. https://doi.org/10.1016/j.jhydrol.2020.124601

Rajib, M.A., Ahiablame, L., and Paul, M. (2016). Modeling the effects of future landuse change on water quality under multiple scenarios: a case study of low-input agriculture with hay/pasture production. Sustainability of Water Quality and Ecology, 8, 50–66. https://doi.org/10.1016/j.swaqe.2016.09.001

Rashid, M.A., Jabloun, M., Andersen, M.N., Zhang, X., and Olesen, J.E. (2019). Climate change is expected to increase yield and water use efficiency of wheat in the North China Plain. Agricultural Water Management, 222, 193–203. https://doi.org/10.1016/j.agwat.2019.06.004

Raymundo, R., Asseng, S., Robertson, R., Petsakos, A., Hoogenboom, G., Quiroz, R., Hareau, G., and Wolf, J. (2018). Climate change impact on global potato production. European Journal of Agronomy, 100, 87–98. https://doi.org/10.1016/j.eja.2017.11.008

Rykaczewska, K. (2015). The effect of high temperature occurring in subsequent stages of plant development on potato yield and tuber physiological defects. American Journal of Potato Research, 92, 339–349. https://doi.org/10.1007/s12230-015-9436-x

Rykaczewska, K. (2017). Impact of heat and drought stresses on size and quality of the potato yield. Plant, Soil and Environment, 63(1), 40–46. https://doi.org/10.17221/691/2016-PSE

Saxe, H., Ellsworth, D.S., and Heath, J. (1998). Tree and forest functioning in an enriched CO_2 atmosphere. New Phytologist, 139(3), 395–436. https://doi.org/10.1046/j.1469-8137.1998.00221.x

Shahvari, N., Khalilian, S., Mosavi, S.H., and Mortazavi, S.A. (2019). Assessing climate change impacts on water resources and crop yield: a case study of Varamin Plain Basin, Iran. Environmental Monitoring and Assessment, 191(3), 134. https://doi.org/10.1007/s10661-019-7266-x

Sharpley, A.N., and Williams, J.R. (1990). EPIC-erosion/productivity impact calculator: 1. Model documentation. https://agrilife.org/epicapex/files/2015/05/EpicModelDocumentation.pdf

Sinnathamby, S., Douglas-Mankin, K.R., and Craige, C. (2017). Field-scale calibration of crop-yield parameters in the Soil and Water Assessment Tool (SWAT). Agricultural Water Management, 180(A), 61–69. https://doi.org/10.1016/j.agwat.2016.10.024

Sloan, P.G., and Moore, I.D. (1984). Modeling subsurface stormflow on steeply sloping forested watersheds. Water Resources Research, 20(12), 1815–1822. https://doi.org/10.1029/WR020i012p01815

Smith, W.N., Grant, B.B., Desjardins, R.L., Kroebel, R., Li, C., Qian, B., Worth, D.E., McConkey, B.G., and Drury, C.F. (2013). Assessing the effects of climate change on crop production and GHG emissions in Canada. Agriculture, Ecosystems and Environment, 179, 139–150. https://doi.org/10.1016/j.agee.2013.08.015

Somura, H., Arnold, J.G., Hoffman, D., Takeda, I., Mori, Y., and Di Luzio, M. (2009). Impact of climate change on the Hii River basin and salinity in Lake Shinji: a case study using the SWAT model and a regression curve. Hydrological Processes, 23(13), 1887–1900. https://doi.org/10.1002/hyp.7321

Sreeharsha, R.V., Sekhar, K.M., and Reddy, A.R. (2015). Delayed flowering is associated with lack of photosynthetic acclimation in Pigeon pea (Cajanus cajan L.) grown under elevated CO_2. Plant Science, 231, 82–93. https://doi.org/10.1016/j.plantsci.2014.11.012

Srinivasan, R., Zhang, X., and Arnold, J.G. (2010). SWAT ungauged: hydrological budget and crop yield predictions in the Upper Mississippi River Basin. Transactions of the ASABE, 53(5), 1533–1546. https://doi.org/10.13031/2013.34903

Srivastava, A.K., Gaiser, T., Paeth, H., and Ewert, F. (2012). The impact of climate change on Yam (Dioscorea alata) yield in the savanna zone of West Africa. Agriculture. Ecosystems and Environment, 153, 57–64. https://doi.org/10.1016/j.agee.2012.03.004

Statistics Canada. (2021, April 20). Prince Edward Island has the largest potato crop in Canada. https://www150.statcan.gc.ca/n1/pub/95-640-x/2016001/article/14801-eng.htm

Sumathy, S., Kyle, R. D-M., and Collin, C. (2017). Field-scale calibration of crop-yield parameters in the Soil and Water Assessment Tool (SWAT). Agricultural Water Management, 180(A), 61–69. https://doi.org/10.1016/j.agwat.2016.10.024

Sun, C., and Ren, L. (2014). Assessing crop yield and crop water productivity and optimizing irrigation scheduling of winter wheat and summer maize in the Haihe plain using SWAT model. Hydrological Processes, 28(4), 2478–2498. https://doi.org/10.1002/hyp.9759

Tatsumi, K., Yamashiki, Y., Valmir da Silva, R., Takara, K., Matsuoka, Y., Takahashi, K., Maruyama, K., and Kawahara, N. (2011). Estimation of potential changes in cereals production under climate change scenarios. Hydrological Processes, 25(17), 2715–2725. https://doi.org/10.1002/hyp.8012

Taylor, K.E., Stouffer, R.J., and Meehl, G.A. (2012). An overview of CMIP5 and the experiment design. Bulletin of the American Meteorological Society, 93, 485–498. https://doi.org/10.1175/BAMS-D-11-00094.1

Tukey, J.W. (1949). Comparing individual means in the analysis of variance. Biometrics, 5(2), 99–114. https://doi.org/10.2307/3001913

Ullrich, A., and Volk, M. (2009). Application of the Soil and Water Assessment Tool (SWAT) to predict the impact of alternative management practices on water quality and quantity. Agricultural Water Management, 96(8), 1207–1217. https://doi.org/10.1016/j.agwat.2009.03.010

Walker, N.J., and Schulze, R.E. (2008). Climate change impacts on agro-ecosystem sustainability across three climate regions in the maize belt of South Africa. Agriculture, Ecosystems and Environment, 124(1–2), 114–124. https://doi.org/10.1016/j.agee.2007.09.001

Wand, S.J.E., Midgley, G.F., Jones, M.H., and Curtis, P.S. (1999). Responses of wild C4 and C3 grass (Poaceae) species to elevated atmospheric CO_2 concentration: a meta-analytic test of current theories and perceptions. Global Change Biology, 5(6), 723–741. https://doi.org/10.1046/j.1365-2486.1999.00265.x

Wang, Q., Qi, J., Li, J., Cole, J., Waldhoff, S.T., and Zhang, X. (2020a). Nitrate loading projection is sensitive to freeze-thaw cycle representation. Water Research, 186, 116355. https://doi.org/10.1016/j.watres.2020.116355

Wang, Q., Qi, J., Wu, H., Zeng, Y., Shui, W., Zeng, J., and Zhang, X. (2020b). Freeze-Thaw cycle representation alters response of watershed hydrology to future

climate change. Catena, 195, 104767. https://doi.org/10.1016/j.catena.2020.104767

Wang, Q., Qi, J., Qiu, H., Li, J., Cole, J., Waldhoff, S., and Zhang, X. (2021). Pronounced increases in future soil erosion and sediment deposition as influenced by Freeze–Thaw cycles in the Upper Mississippi River Basin. Environmental Science and Technology, 55(14), 9905–9915. https://doi.org/10.1021/acs.est.1c02692.

Werner, A.T., and Cannon, A.J. (2016). Hydrologic extremes: an intercomparison of multiple gridded statistical downscaling methods. Hydrology and Earth System Sciences, 20(4), 1483–1508. https://doi.org/10.5194/hess-20-1483-2016

Xu, Z., Jiang, Y., Jia, B., and Zhou, G. (2016). Elevated-CO_2 response of stomata and its dependence on environmental factors. Frontiers in Plant Science, 7, 657. https://doi.org/10.3389/fpls.2016.00657

Zhang, H., Xu, F., Wu, Y., Hu, H.-H., and Dai, X.-F. (2017). Progress of potato staple food research and industry development in China. Journal of Integrative Agriculture, 16(12), 2924–2932. https://doi.org/10.1016/S2095-3119(17)61736-2

Zhang, X., Vincent, L.A., Hogg, W.D., and Niitsoo, A. (2000). Temperature and precipitation trends in Canada during the 20th century. Atmosphere-Ocean, 38(3), 395–429. https://doi.org/10.1080/07055900.2000.9649654

SUPPLEMENTARY MATERIAL

Table S2.1 Actual monthly mean, maximum, and minimum precipitation (mm) during P1 (2020–2039), P2 (2040–2059), P3 (2060–2079), and P4 (2080–2099) under three emission scenarios (RCP 2.6, 4.5, and 8.5).

Month	RCP 2.6			RCP 4.5			RCP 8.5		
	Mean	Max	Min	Mean	Max	Min	Mean	Max	Min
P1 (2020–2039)									
1	92	107	84	93	102	85	85	91	81
2	77	87	67	78	88	70	78	84	70
3	79	86	71	78	88	71	79	91	64
4	80	86	72	88	112	74	81	93	72
5	96	111	84	84	91	76	88	99	65
6	95	102	87	92	96	89	92	97	84
7	112	119	103	108	117	95	109	119	100
8	102	125	85	113	137	98	109	125	100
9	93	127	79	96	109	88	89	100	74
10	97	107	85	99	105	94	91	101	83
11	112	120	96	101	108	96	100	123	89
12	95	100	90	104	120	81	100	105	96
P2 (2040–2059)									
1	90	94	82	90	95	86	95	105	87
2	82	89	71	84	94	73	87	112	76
3	85	101	71	82	98	64	86	114	70
4	84	94	68	85	94	70	88	100	80
5	97	104	87	93	100	84	95	112	82
6	100	105	96	99	108	85	100	114	93
7	115	130	91	116	120	113	113	131	102
8	106	118	85	104	128	86	105	121	88
9	93	98	81	91	94	87	91	105	80
10	99	135	81	98	120	79	97	112	86
11	103	110	100	103	118	87	109	127	96
12	102	108	95	97	108	85	106	115	96
P3 (2060–2079)									
1	95	102	88	95	103	92	105	107	104
2	80	87	75	86	94	78	93	112	86
3	81	90	72	86	90	80	95	114	84
4	82	91	69	83	94	74	91	112	78
5	94	109	84	94	109	79	97	126	79
6	95	106	76	102	114	93	98	113	84
7	114	129	97	107	116	96	103	118	82
8	98	122	76	98	104	94	107	127	93
9	97	118	82	97	114	85	94	107	76
10	97	112	82	101	115	80	101	123	82
11	104	117	90	110	136	99	108	115	96
12	100	114	85	116	127	109	114	122	110
P4 (2080–2099)									
1	92	112	76	97	115	86	106	124	94
2	77	87	68	84	93	77	99	114	90
3	79	100	68	88	96	77	101	114	89
4	86	96	73	91	118	70	103	116	90
5	95	107	83	96	103	87	105	115	89
6	102	120	80	99	102	95	96	117	82
7	108	115	95	108	115	99	112	127	103
8	106	119	94	104	121	90	105	116	97
9	96	104	83	94	123	72	101	116	75
10	91	103	82	96	108	77	100	140	77
11	106	114	92	104	120	92	104	120	94
12	94	111	80	106	114	102	122	141	99

Table S2.2 Percent changes (%) in monthly mean, maximum, and minimum precipitation during P1 (2020–2039), P2 (2040–2059), P3 (2060–2079), and P4 (2080–2099) under three emission scenarios (RCP 2.6, 4.5, and 8.5).

Month	RCP 2.6			RCP 4.5			RCP 8.5		
	Mean	Max	Min	Mean	Max	Min	Mean	Max	Min
P1 (2020–2039)									
1	2.0	18.8	-6.7	3.7	13.7	-5.1	-5.6	1.0	-9.7
2	3.4	17.4	-10.3	5.4	18.6	-5.7	4.8	12.7	-5.2
3	8.0	16.9	-3.7	5.9	19.7	-3.5	7.2	23.2	-13.1
4	-3.8	3.9	-13.1	6.2	35.4	-11.0	-2.1	12.7	-13.4
5	8.8	26.0	-5.0	-4.7	3.2	-14.2	-0.2	12.0	-26.6
6	-0.9	5.6	-9.3	-4.2	0.2	-7.5	-3.8	0.7	-12.5
7	8.6	15.1	-0.8	4.7	12.7	-7.8	5.8	14.7	-3.8
8	-7.8	13.5	-23.0	2.0	24.0	-11.2	-1.4	12.8	-9.7
9	-0.2	36.4	-15.1	3.6	17.7	-5.6	-3.8	8.0	-19.7
10	9.1	20.4	-4.2	11.8	18.9	5.6	2.4	13.8	-6.5
11	10.3	18.1	-5.3	-0.4	5.6	-6.1	-1.5	20.9	-12.7
12	-5.4	-0.7	-11.0	3.2	18.8	-19.3	-0.8	4.3	-4.3
P2 (2040–2059)									
1	-0.1	4.2	-8.6	0.5	5.3	-4.2	5.4	17.2	-2.7
2	10.6	19.3	-4.3	13.6	27.0	-2.1	17.9	50.7	2.8
3	16.2	37.3	-3.1	11.5	33.7	-12.2	17.5	55.0	-4.6
4	1.5	14.1	-17.5	2.6	13.3	-14.9	6.5	20.5	-3.6
5	10.1	17.4	-1.3	5.6	13.3	-4.5	7.2	26.7	-7.3
6	3.7	9.3	0.2	2.5	12.2	-11.9	3.5	18.5	-3.6
7	11.4	25.4	-11.7	12.4	15.7	9.1	9.2	26.4	-1.7
8	-4.4	6.8	-23.0	-5.8	16.0	-22.1	-4.7	9.7	-20.5
9	-0.2	5.2	-13.2	-2.1	1.6	-6.1	-1.6	12.7	-13.9
10	11.3	52.5	-8.1	11.0	35.8	-10.3	9.1	26.0	-3.3
11	1.4	8.0	-2.1	1.1	15.7	-14.3	7.0	24.3	-6.2
12	1.3	7.2	-5.5	-3.7	6.9	-15.7	5.0	14.2	-4.9
P3 (2060–2079)									
1	5.6	14.0	-1.9	5.9	15.0	2.0	17.4	19.1	15.6
2	8.3	17.0	1.1	15.8	27.2	4.8	26.0	50.4	15.7
3	9.6	22.0	-2.5	16.8	22.8	9.3	29.6	54.5	13.7
4	-1.1	10.5	-16.3	0.2	13.2	-10.6	10.3	35.2	-5.8
5	6.3	23.7	-5.1	6.1	23.1	-10.9	9.5	43.2	-10.2
6	-1.3	9.9	-20.7	5.8	18.3	-3.4	2.0	17.8	-12.2
7	10.2	24.5	-5.8	3.1	11.8	-7.6	0.0	14.5	-20.7
8	-11.3	10.9	-30.8	-11.2	-5.8	-14.9	-3.3	14.9	-16.2
9	4.8	27.0	-11.8	4.3	22.5	-8.4	1.0	15.6	-18.0
10	10.0	26.7	-7.7	13.8	29.7	-9.2	14.2	39.1	-7.2
11	2.4	14.6	-11.2	8.4	33.6	-2.4	5.6	12.7	-5.9
12	-1.0	13.4	-16.1	14.9	25.6	7.9	13.4	20.6	8.8
P4 (2080–2099)									
1	2.5	24.7	-15.6	8.5	28.3	-3.7	18.0	37.8	4.4
2	4.0	17.7	-8.3	13.6	25.0	3.6	33.5	54.3	21.8
3	7.8	35.9	-8.1	19.4	30.7	5.2	37.8	55.3	20.7
4	4.0	15.7	-11.5	10.3	43.1	-14.8	24.5	40.2	8.5
5	7.9	20.7	-5.5	8.5	16.9	-1.2	19.2	30.5	0.7
6	6.3	24.4	-16.4	2.5	6.5	-1.5	-0.1	21.5	-14.5
7	4.8	11.2	-8.0	4.4	11.2	-4.0	8.7	22.5	-0.7
8	-4.3	8.0	-14.6	-6.0	9.3	-18.9	-4.5	5.4	-12.0
9	3.6	11.9	-10.9	0.9	33.0	-22.0	8.4	25.2	-19.6
10	3.0	16.3	-7.9	8.6	21.5	-13.5	13.3	58.0	-13.3
11	3.6	12.1	-9.3	1.7	17.7	-9.3	2.2	17.6	-7.9
12	-6.3	10.5	-20.3	5.0	13.6	1.5	20.7	40.2	-2.0

Table S2.3 Actual monthly mean, maximum, and minimum temperature (°C) during P1 (2020–2039), P2 (2040–2059), P3 (2060–2079), and P4 (2080–2099) under three emission scenarios (RCP 2.6, 4.5, and 8.5).

Month	RCP 2.6			RCP 4.5			RCP 8.5		
	Mean	Max	Min	Mean	Max	Min	Mean	Max	Min
P1 (2020–2039)									
1	-10.7	-9.1	-12.1	-10.6	-9.7	-11.9	-10.3	-9.0	-11.9
2	-9.6	-8.1	-10.9	-9.4	-8.3	-9.8	-10.1	-8.8	-12.5
3	-3.6	-2.0	-4.8	-3.8	-2.4	-4.8	-4.8	-2.3	-8.9
4	3.7	4.9	2.3	3.4	4.1	3.0	2.7	4.5	-1.7
5	10.8	11.6	9.5	10.5	11.1	10.1	9.7	11.2	6.0
6	16.5	17.4	15.8	16.3	17.5	15.5	15.7	17.6	12.0
7	19.5	21.0	18.5	19.0	20.7	18.1	19.2	20.9	17.4
8	18.4	19.3	17.6	18.4	19.7	17.5	18.7	19.7	17.9
9	13.5	14.2	12.9	13.6	14.8	13.0	14.4	16.5	13.3
10	7.3	8.4	6.8	7.2	7.5	6.8	8.2	11.2	7.1
11	1.3	1.6	1.1	1.0	1.8	0.5	1.9	4.8	0.3
12	-6.5	-5.1	-7.3	-6.9	-5.7	-8.3	-5.9	-1.6	-7.6
P2 (2040–2059)									
1	-10.1	-7.9	-11.7	-8.9	-7.5	-10.6	-8.3	-5.7	-9.9
2	-9.1	-8.0	-9.7	-8.1	-6.2	-8.9	-8.1	-5.8	-9.1
3	-3.3	-1.5	-4.5	-3.0	-0.6	-4.2	-3.5	-1.3	-6.9
4	3.9	4.8	3.0	4.6	6.2	3.4	3.3	5.9	-1.8
5	11.2	11.9	10.6	11.4	12.6	10.6	10.5	12.8	4.8
6	16.8	17.4	15.8	17.2	18.3	16.5	16.6	19.3	12.0
7	19.8	21.2	18.8	19.9	21.6	19.0	20.1	22.7	17.1
8	18.5	19.6	17.3	19.1	20.8	18.2	19.7	21.2	18.8
9	13.8	14.4	13.1	14.2	15.1	13.3	15.8	17.9	14.7
10	7.8	8.7	6.8	7.7	8.1	7.4	9.4	12.8	8.1
11	1.3	2.1	0.7	1.7	2.4	1.0	2.9	7.1	1.2
12	-6.3	-5.4	-7.2	-5.5	-4.6	-6.2	-3.9	1.2	-5.5
P3 (2060–2079)									
1	-9.4	-7.5	-10.3	-8.5	-6.7	-9.8	-6.0	-3.9	-7.3
2	-8.5	-6.4	-9.9	-8.1	-6.3	-9.3	-6.2	-3.5	-7.9
3	-3.4	-1.1	-4.6	-2.3	-0.1	-3.5	-2.1	1.1	-6.3
4	3.7	5.1	2.8	4.5	6.2	3.5	4.4	7.1	-2.6
5	11.0	12.4	9.8	11.5	12.4	10.0	11.6	13.8	4.9
6	17.0	18.2	16.4	17.6	19.1	16.1	17.8	21.3	12.0
7	19.7	21.5	18.4	20.4	22.8	19.1	21.5	25.2	18.1
8	18.6	19.9	18.0	19.3	20.6	18.1	21.5	23.8	20.4
9	13.7	15.3	12.9	14.5	16.4	13.4	17.2	19.9	15.3
10	7.9	8.7	7.5	8.2	9.7	7.3	11.3	15.7	9.2
11	1.4	2.6	0.5	2.3	3.1	2.0	4.4	9.1	2.7
12	-6.4	-5.2	-7.0	-5.2	-4.7	-6.0	-2.2	3.6	-3.9
P4 (2080–2099)									
1	-9.3	-7.9	-10.1	-8.5	-6.2	-10.5	-3.7	-0.9	-5.1
2	-8.5	-7.0	-10.4	-7.4	-4.9	-9.5	-4.1	-1.9	-5.8
3	-3.3	-1.9	-4.0	-2.1	1.0	-3.6	-0.8	1.9	-5.5
4	4.0	5.5	3.0	5.1	6.3	4.0	6.0	9.1	-1.3
5	11.2	12.0	9.9	12.0	13.0	11.1	13.0	15.9	5.6
6	16.8	18.0	15.7	17.7	19.3	16.7	18.6	23.1	11.7
7	19.6	21.2	18.8	20.7	22.7	19.6	23.0	27.6	18.2
8	18.3	19.9	17.3	19.5	21.1	18.1	22.6	26.0	21.0
9	13.5	14.7	13.2	14.6	16.2	14.0	18.5	20.9	16.6
10	7.6	9.0	6.5	8.2	9.3	7.5	12.3	17.1	10.0
11	1.4	1.9	0.6	2.2	2.9	1.5	5.4	10.7	3.5
12	-6.1	-4.9	-6.7	-4.7	-4.1	-5.4	-1.3	5.2	-3.6

Table S2.4 Changes (°C) in monthly mean, maximum, and minimum temperature during P1 (2020–2039), P2 (2040–2059), P3 (2060–2079), and P4 (2080–2099) under three emission scenarios (RCP 2.6, 4.5, and 8.5).

Month	RCP 2.6			RCP 4.5			RCP 8.5		
	Mean	Max	Min	Mean	Max	Min	Mean	Max	Min
P1 (2020–2039)									
1	0.8	2.5	-0.6	0.9	1.8	-0.4	1.2	2.6	-0.3
2	0.5	2.0	-0.8	0.7	1.8	0.3	0.0	1.3	-2.5
3	0.6	2.3	-0.6	0.4	1.8	-0.6	-0.5	1.9	-4.7
4	0.8	2.0	-0.5	0.6	1.3	0.1	-0.2	1.7	-4.6
5	0.6	1.5	-0.7	0.4	0.9	0.0	-0.4	1.0	-4.1
6	0.4	1.4	-0.2	0.2	1.4	-0.6	-0.3	1.6	-4.1
7	1.0	2.5	-0.1	0.5	2.2	-0.4	0.6	2.3	-1.1
8	0.9	1.8	0.1	0.9	2.3	0.0	1.2	2.2	0.4
9	0.7	1.5	0.1	0.8	2.1	0.2	1.7	3.7	0.5
10	0.4	1.5	-0.1	0.2	0.5	-0.1	1.3	4.3	0.1
11	1.0	1.3	0.8	0.7	1.5	0.1	1.6	4.5	0.0
12	1.1	2.6	0.4	0.8	2.0	-0.6	1.8	6.1	0.0
P2 (2040–2059)									
1	1.5	3.6	-0.2	2.6	4.0	1.0	3.3	5.9	1.6
2	1.0	2.0	0.3	2.0	3.9	1.2	2.0	4.3	1.0
3	0.9	2.8	-0.2	1.2	3.6	0.0	0.8	2.9	-2.7
4	1.0	2.0	0.1	1.7	3.3	0.6	0.5	3.0	-4.7
5	1.0	1.7	0.5	1.3	2.4	0.5	0.4	2.7	-5.4
6	0.7	1.3	-0.3	1.1	2.2	0.4	0.6	3.3	-4.1
7	1.3	2.7	0.2	1.4	3.1	0.4	1.6	4.2	-1.4
8	1.0	2.1	-0.2	1.6	3.3	0.8	2.2	3.7	1.3
9	1.1	1.6	0.4	1.4	2.4	0.6	3.0	5.2	2.0
10	0.9	1.8	-0.1	0.8	1.1	0.5	2.5	5.9	1.2
11	0.9	1.8	0.4	1.4	2.1	0.7	2.6	6.8	0.9
12	1.4	2.3	0.4	2.1	3.1	1.4	3.7	8.8	2.2
P3 (2060–2079)									
1	2.1	4.0	1.2	3.0	4.8	1.7	5.5	7.6	4.3
2	1.6	3.7	0.1	2.0	3.8	0.8	3.9	6.6	2.1
3	0.9	3.1	-0.4	2.0	4.1	0.7	2.2	5.3	-2.1
4	0.9	2.2	0.0	1.7	3.4	0.7	1.5	4.3	-5.4
5	0.9	2.2	-0.4	1.4	2.2	-0.1	1.5	3.6	-5.3
6	1.0	2.1	0.3	1.5	3.1	0.0	1.7	5.3	-4.1
7	1.2	2.9	-0.1	1.9	4.2	0.6	3.0	6.7	-0.4
8	1.2	2.4	0.5	1.8	3.1	0.6	4.0	6.3	2.9
9	0.9	2.5	0.2	1.7	3.7	0.7	4.5	7.2	2.5
10	1.0	1.8	0.6	1.3	2.8	0.4	4.4	8.8	2.3
11	1.1	2.3	0.2	2.0	2.8	1.6	4.0	8.8	2.4
12	1.3	2.5	0.6	2.5	2.9	1.6	5.4	11.2	3.7
P4 (2080–2099)									
1	2.2	3.7	1.4	3.0	5.4	1.0	7.9	10.6	6.4
2	1.6	3.1	-0.4	2.7	5.2	0.6	6.0	8.2	4.2
3	0.9	2.4	0.2	2.1	5.2	0.6	3.4	6.1	-1.2
4	1.1	2.7	0.2	2.2	3.5	1.2	3.1	6.3	-4.2
5	1.1	1.8	-0.2	1.9	2.8	1.0	2.8	5.7	-4.5
6	0.8	1.9	-0.3	1.7	3.3	0.7	2.5	7.0	-4.3
7	1.1	2.6	0.2	2.2	4.2	1.1	4.5	9.0	-0.4
8	0.9	2.5	-0.2	2.0	3.6	0.6	5.2	8.5	3.5
9	0.8	1.9	0.4	1.9	3.4	1.3	5.8	8.2	3.8
10	0.7	2.1	-0.4	1.3	2.3	0.5	5.3	10.2	3.1
11	1.1	1.6	0.3	1.9	2.6	1.2	5.1	10.4	3.2
12	1.5	2.7	1.0	3.0	3.6	2.3	6.4	12.9	4.1

Table S2.5 Actual monthly mean, maximum, and minimum evapotranspiration (mm) during P1 (2020–2039), P2 (2040–2059), P3 (2060–2079), and P4 (2080–2099) under three emission scenarios (RCP 2.6, 4.5, and 8.5).

Month	RCP 2.6			RCP 4.5			RCP 8.5		
	Mean	Max	Min	Mean	Max	Min	Mean	Max	Min
P1 (2020–2039)									
1	6	8	6	7	7	5	6	7	5
2	8	10	7	9	12	6	9	11	6
3	31	45	21	29	39	17	28	41	18
4	66	76	54	65	73	55	67	74	60
5	64	69	58	63	66	58	64	70	58
6	88	93	82	87	90	84	88	93	83
7	91	93	88	89	93	84	91	93	87
8	69	80	61	71	77	65	70	74	66
9	59	64	53	60	62	59	60	62	58
10	50	58	46	50	56	45	50	54	46
11	34	42	24	32	39	24	33	41	24
12	16	19	12	15	17	13	15	16	13
P2 (2040–2059)									
1	7	8	6	8	10	7	8	10	7
2	10	15	7	10	16	8	10	14	8
3	34	52	20	35	54	20	38	53	23
4	70	76	59	71	79	60	70	76	60
5	68	73	60	69	75	62	68	73	63
6	91	95	88	90	96	84	95	99	91
7	88	92	86	86	89	81	90	94	85
8	68	74	63	70	79	64	69	79	60
9	58	61	54	58	64	55	61	64	57
10	51	58	45	52	59	46	50	58	43
11	30	39	25	32	42	23	33	45	25
12	15	18	11	18	22	14	19	23	14
P3 (2060–2079)									
1	7	10	7	8	9	6	10	12	9
2	11	17	7	12	19	8	15	23	10
3	39	61	22	42	64	21	48	68	25
4	68	76	60	71	83	57	75	83	65
5	68	75	60	68	76	58	69	76	61
6	93	98	88	95	103	90	95	102	88
7	86	93	80	86	92	79	87	95	80
8	67	77	59	65	75	57	70	75	65
9	56	60	54	58	61	57	62	66	59
10	49	57	41	50	58	43	53	63	46
11	30	44	21	33	43	24	37	47	28
12	15	19	13	19	24	15	21	28	16
P4 (2080–2099)									
1	7	9	6	9	11	7	13	16	11
2	12	18	7	14	25	8	20	31	10
3	42	61	22	46	65	22	58	77	32
4	69	79	54	72	81	61	81	90	71
5	69	78	59	70	77	63	73	79	65
6	91	96	85	92	99	85	98	102	94
7	87	95	78	86	92	80	85	91	80
8	64	76	54	64	74	56	69	76	64
9	58	67	53	57	59	52	62	67	58
10	48	60	40	49	57	43	54	61	48
11	29	43	19	32	47	21	37	52	26
12	18	25	13	19	26	13	28	35	21

Table S2.6 Percent changes (%) in monthly mean, maximum, and minimum evapotranspiration during P1 (2020–2039), P2 (2040–2059), P3 (2060–2079), and P4 (2080–2099) under three emission scenarios (RCP 2.6, 4.5, and 8.5).

Month	RCP 2.6			RCP 4.5			RCP 8.5		
	Mean	Max	Min	Mean	Max	Min	Mean	Max	Min
P1 (2020–2039)									
1	0.7	23.2	-8.1	2.2	14.1	-23.5	-1.4	12.7	-17.6
2	7.0	31.8	-10.1	11.9	51.2	-16.7	12.6	41.1	-15.9
3	30.1	86.8	-12.3	21.7	63.9	-26.8	18.8	73.3	-25.9
4	8.6	25.2	-11.8	7.6	20.4	-10.1	9.7	21.2	-1.3
5	2.7	10.1	-7.9	0.9	4.5	-7.9	2.6	12.4	-8.2
6	-0.5	5.4	-8.0	-1.9	1.3	-4.9	-1.2	4.5	-6.7
7	5.0	7.5	1.7	3.0	7.4	-2.4	5.6	8.0	1.3
8	-2.3	13.6	-13.9	1.1	8.4	-8.7	-1.3	5.3	-7.2
9	-2.6	5.9	-12.5	-0.9	3.4	-2.6	-0.5	3.1	-4.4
10	-4.3	10.3	-12.4	-5.3	7.0	-13.1	-5.4	4.0	-12.5
11	2.4	28.5	-26.2	-2.3	17.3	-26.8	-1.1	23.2	-27.9
12	6.4	28.6	-17.3	3.0	12.2	-10.9	1.2	10.4	-11.8
P2 (2040–2059)									
1	13.2	32.5	-3.0	25.6	54.4	14.4	28.7	58.2	9.0
2	27.6	97.5	-5.9	34.7	116.2	-1.3	35.1	90.0	4.6
3	43.1	119.0	-16.2	47.1	126.8	-17.5	57.2	123.9	-5.2
4	14.8	25.4	-2.6	16.6	30.1	-1.4	15.0	24.6	-0.9
5	7.7	16.9	-4.2	10.0	20.3	-1.6	8.6	15.8	0.0
6	2.8	6.9	-0.3	1.9	8.6	-5.2	7.3	12.2	2.2
7	2.4	6.8	-0.4	0.0	3.7	-6.1	3.9	9.4	-2.0
8	-4.2	4.9	-11.2	-0.7	11.6	-9.5	-1.7	11.3	-15.0
9	-4.0	1.2	-10.1	-3.7	5.6	-8.1	0.6	5.9	-6.1
10	-2.8	10.6	-14.6	-1.6	12.6	-11.3	-4.4	10.5	-17.1
11	-7.6	18.4	-25.7	-2.5	28.4	-29.2	1.2	35.2	-24.6
12	2.9	18.9	-23.0	18.5	48.4	-4.7	27.7	56.6	-4.1
P3 (2060–2079)									
1	16.0	50.4	2.5	26.6	46.4	-1.1	56.6	89.5	37.0
2	44.4	125.7	-10.7	57.5	143.8	3.6	98.3	207.2	36.6
3	62.5	157.0	-9.8	76.7	169.0	-12.8	100.8	183.0	5.4
4	12.3	24.9	-1.5	17.0	36.0	-6.1	23.7	36.1	7.1
5	8.3	20.0	-3.9	8.0	20.9	-7.6	10.1	21.1	-2.6
6	4.6	10.7	-1.3	6.7	16.1	1.3	7.5	15.5	-1.1
7	-0.3	7.3	-7.4	-0.4	6.9	-8.1	0.9	9.9	-7.8
8	-5.4	9.2	-16.5	-7.7	5.6	-19.2	-1.3	6.6	-8.0
9	-6.5	-1.1	-10.9	-3.1	1.7	-5.3	2.3	10.0	-1.7
10	-6.5	9.2	-20.8	-3.9	11.4	-17.2	1.0	20.4	-12.6
11	-7.8	33.0	-37.7	-0.8	30.6	-27.0	11.1	43.3	-15.5
12	3.9	30.7	-11.0	26.7	63.5	-0.9	44.5	86.6	10.8
P4 (2080–2099)									
1	15.9	46.5	-0.1	38.9	78.9	17.8	100.6	154.0	70.2
2	53.1	142.8	-11.7	80.9	232.6	0.3	159.5	312.6	26.3
3	74.0	154.1	-8.8	90.5	172.6	-8.8	141.1	224.2	34.9
4	12.8	29.1	-11.8	17.8	33.2	0.5	33.2	47.6	17.1
5	10.4	25.1	-6.2	11.0	23.3	0.7	16.4	26.7	3.4
6	2.5	7.8	-4.7	4.1	11.3	-4.2	10.7	15.2	5.8
7	1.0	10.6	-9.7	-0.2	6.9	-7.7	-1.7	5.1	-6.7
8	-9.9	8.1	-23.1	-9.1	4.5	-20.3	-2.0	7.7	-9.1
9	-3.7	11.2	-12.7	-4.5	-1.6	-13.8	2.9	11.7	-4.1
10	-8.9	14.9	-24.1	-6.0	9.0	-17.4	3.3	17.3	-8.1
11	-13.4	31.7	-43.8	-3.4	41.8	-36.3	11.7	58.0	-20.9
12	19.9	65.8	-11.1	30.0	77.4	-9.5	88.2	139.7	45.1

Table S2.7 Actual monthly mean, maximum, and minimum soil water (mm) during P1 (2020–2039), P2 (2040–2059), P3 (2060–2079), and P4 (2080–2099) under three emission scenarios (RCP 2.6, 4.5, and 8.5).

Month	RCP 2.6			RCP 4.5			RCP 8.5		
	Mean	Max	Min	Mean	Max	Min	Mean	Max	Min
P1 (2020–2039)									
1	93	95	92	95	97	91	90	93	85
2	100	103	96	99	106	96	97	100	90
3	111	114	108	111	114	106	110	114	108
4	100	109	96	97	102	92	97	100	92
5	97	106	91	98	104	90	98	106	92
6	83	89	76	82	88	75	83	94	75
7	80	91	72	82	87	76	77	85	72
8	85	90	79	87	91	83	82	85	79
9	91	95	88	92	93	90	88	93	80
10	102	105	97	103	106	99	100	108	95
11	103	108	99	103	109	97	102	108	98
12	94	96	92	95	100	90	91	93	88
P2 (2040–2059)									
1	95	100	89	96	100	93	98	102	94
2	103	110	97	103	113	97	105	111	101
3	110	114	105	110	114	107	108	110	101
4	98	102	92	96	103	90	95	104	83
5	98	106	90	96	102	92	96	107	90
6	81	83	76	82	89	77	80	88	74
7	79	84	73	79	84	76	77	85	68
8	82	88	76	82	87	75	83	87	78
9	94	105	85	91	94	84	89	94	85
10	100	110	90	102	111	97	103	109	97
11	101	106	95	103	107	101	104	106	102
12	94	98	87	93	95	89	97	101	93
P3 (2060–2079)									
1	96	103	90	97	99	91	104	109	102
2	104	113	96	107	114	99	111	116	105
3	108	113	102	109	113	104	106	112	100
4	96	100	90	95	102	85	92	97	84
5	98	107	86	96	104	83	93	98	88
6	78	86	63	81	92	69	76	89	58
7	80	87	73	75	80	70	76	83	64
8	84	95	74	83	90	79	78	88	65
9	94	102	87	93	101	84	85	91	70
10	103	110	98	102	108	97	99	105	94
11	100	106	96	104	110	100	103	106	100
12	94	98	87	96	99	91	100	103	96
P4 (2080–2099)									
1	95	100	88	100	109	94	107	111	105
2	106	113	96	108	117	97	113	116	110
3	107	109	103	108	113	102	102	113	96
4	99	105	91	94	100	87	89	97	83
5	98	107	92	95	107	88	91	102	75
6	82	96	72	81	90	73	70	82	59
7	78	84	71	75	83	71	71	80	67
8	89	97	82	84	91	74	78	84	68
9	94	100	85	89	99	76	87	100	71
10	102	110	94	100	105	91	98	104	91
11	102	106	97	100	109	95	104	109	98
12	91	92	87	95	102	90	102	106	94

Table S2.8 Percent changes (%) in monthly mean, maximum, and minimum soil water during P1 (2020–2039), P2 (2040–2059), P3 (2060–2079), and P4 (2080–2099) under three emission scenarios (RCP 2.6, 4.5, and 8.5).

Month	RCP 2.6			RCP 4.5			RCP 8.5		
	Mean	Max	Min	Mean	Max	Min	Mean	Max	Min
P1 (2020–2039)									
1	-2.0	-0.5	-3.4	-0.4	2.6	-4.2	-5.2	-1.6	-10.0
2	3.9	7.1	-0.3	2.5	9.8	-0.4	1.1	3.7	-6.4
3	-1.0	1.2	-3.8	-1.0	1.9	-5.1	-1.8	1.5	-3.8
4	0.1	9.0	-4.2	-2.8	1.9	-8.1	-3.5	0.1	-7.9
5	-4.2	4.4	-9.8	-3.4	2.7	-10.8	-3.6	4.1	-9.4
6	-3.8	2.3	-11.9	-5.1	1.0	-13.8	-4.0	8.9	-13.0
7	-1.6	12.2	-11.0	1.0	7.5	-5.6	-5.3	5.0	-11.4
8	-0.8	5.0	-6.9	1.6	6.7	-3.1	-3.6	-0.7	-7.2
9	0.0	4.7	-3.5	1.2	2.5	-1.0	-3.7	2.2	-12.6
10	0.8	3.2	-4.2	1.5	3.9	-2.4	-2.0	6.3	-6.9
11	-0.1	4.8	-4.3	-0.4	5.2	-6.0	-1.0	4.5	-4.8
12	-1.2	1.0	-3.0	0.3	5.9	-5.0	-4.0	-1.5	-7.3
P2 (2040–2059)									
1	0.1	5.2	-6.1	1.4	5.2	-1.9	2.9	7.7	-0.8
2	6.5	14.5	1.2	7.1	16.8	0.4	9.0	15.7	4.9
3	-1.9	1.6	-6.0	-2.3	1.4	-4.7	-4.1	-1.6	-10.2
4	-2.5	1.3	-7.7	-4.2	2.4	-10.0	-4.8	3.6	-17.4
5	-3.8	4.8	-11.3	-5.2	0.4	-9.5	-4.9	5.6	-11.6
6	-6.7	-4.0	-12.8	-5.0	3.0	-10.9	-7.7	1.4	-14.5
7	-2.8	4.0	-9.7	-2.2	3.5	-6.1	-5.4	4.9	-15.6
8	-3.4	2.9	-10.9	-4.2	1.7	-12.2	-3.0	2.3	-7.9
9	3.2	15.7	-6.4	-0.2	3.9	-7.2	-2.6	3.1	-6.5
10	-1.7	8.7	-11.7	0.6	9.4	-4.6	1.2	7.7	-4.6
11	-2.2	2.0	-8.2	-0.1	3.1	-2.8	0.7	2.6	-1.5
12	-1.4	3.8	-8.7	-1.7	0.4	-6.3	2.6	6.3	-2.4
P3 (2060–2079)									
1	1.5	8.9	-5.0	1.6	4.6	-4.7	9.5	15.2	7.0
2	8.4	17.0	-0.7	11.1	18.2	2.5	15.5	20.6	8.7
3	-3.7	0.4	-9.4	-3.1	0.8	-7.6	-5.4	-0.1	-11.3
4	-4.7	-0.2	-10.0	-5.7	1.7	-15.4	-8.7	-3.5	-16.5
5	-3.6	5.2	-15.0	-4.9	2.9	-17.7	-8.2	-3.1	-13.1
6	-9.6	-1.3	-27.8	-7.0	6.1	-20.9	-12.7	2.9	-33.6
7	-1.0	7.8	-9.8	-7.2	-1.4	-13.8	-6.6	2.4	-20.9
8	-1.8	11.4	-13.4	-2.3	5.5	-7.8	-8.4	2.7	-24.0
9	2.8	12.6	-4.3	2.6	11.2	-7.6	-6.4	0.1	-23.3
10	1.2	8.4	-3.6	0.6	6.8	-4.6	-2.9	3.2	-7.9
11	-3.8	2.3	-7.5	0.7	6.5	-3.4	-0.6	2.4	-3.1
12	-1.2	3.8	-8.7	1.2	4.1	-4.2	5.0	8.1	1.6
P4 (2080–2099)									
1	-0.5	5.0	-6.9	4.8	14.8	-1.2	13.0	16.8	10.6
2	9.6	17.5	-0.9	12.6	21.1	1.1	17.3	20.2	14.1
3	-4.9	-2.8	-7.9	-4.1	0.9	-8.9	-9.1	0.4	-14.5
4	-1.4	4.4	-9.2	-5.8	0.0	-13.5	-11.6	-3.6	-17.0
5	-3.0	5.1	-9.2	-6.6	5.5	-13.6	-10.4	1.0	-25.9
6	-4.9	11.1	-16.5	-7.2	3.6	-15.9	-18.8	-5.6	-31.9
7	-3.2	3.9	-12.4	-6.8	2.4	-12.2	-11.8	-0.7	-16.8
8	4.1	13.4	-4.0	-1.1	6.2	-12.8	-8.9	-1.9	-20.6
9	3.1	9.7	-6.5	-2.0	8.8	-16.5	-4.0	10.3	-22.5
10	0.2	8.7	-7.7	-1.5	3.3	-10.2	-3.8	2.5	-10.8
11	-1.8	2.1	-6.0	-2.9	5.4	-8.4	1.0	5.7	-4.9
12	-4.1	-2.5	-7.9	0.3	7.9	-5.6	7.1	12.1	-0.6

CHAPTER 3

ASSESSING WATERSHED-SCALE IMPACTS OF BEST MANAGEMENT PRACTICES AND ELEVATED ATMOSPHERIC CARBON DIOXIDE CONCENTRATIONS ON WATER YIELD

Kang, X., Qi, J., Bourque, C. P.-A., Li, S., Jin, C., and Meng, F.-R. (2024). Assessing watershed-scale impacts of best management practices and elevated atmospheric carbon dioxide concentrations on water yield: a case study. Science of the Total Environment, 926, 171629. https://doi.org/10.1016/j.scitotenv.2024.171629.

Abstract

Changes in water yield are influenced by many intersecting biophysical elements, including climate, on-land best management practices, and landcover. Large-scale reductions in water yield may present a significant threat to water supplies globally. Many of these intersecting factors are intercorrelated and confounded, making it challenging to separate the factors' individual contributions to shape local streamflow dynamics. Comprehensive hydrological models constructed based on a well-established understanding of biophysical processes are often employed to address these matters. However, these models rarely incorporate all relevant factors influencing local hydrological processes, due to the reliance of these models on the latest, albeit limited, state-of-the-art research. For instance, complexities inherent in watershed hydrology, which involve multilayered interactions among potentially many biophysical factors, leave the direct analysis of subtle impacts on water yields measured *in-situ* largely challenging. Therefore, we propose an innovative approach to assess impacts of elevated atmospheric CO_2 concentrations and flow diversion terraces (FDTs) on stream discharge rates at the watershed scale. Initially, we use a comprehensive hydrological model to account for the impacts of major climatic and landuse/landcover factors on changes in field-acquired measurements of water yield. Next, we employ conventional and advanced statistical methods to decompose the residuals of model predictions to facilitate the identification of subtle influences promoted by increases in atmospheric CO_2 concentrations and the application of FDTs in an agriculture-dominated watershed. Through this innovative approach, we find that FDTs contributed to a watershed-wide, net water-yield reduction of 188.0 mm (or 28.9%) from 1992–2014. Ongoing increases in ambient CO_2 concentrations,

which are responsible for an overall reduction in a watershed-level assessment of stomatal conductance, have led to a minor increase in stream discharge rates during the same 23-year period, i.e., 0.45 mm of water yield per year, or 1.6% overall. Streamflow reductions explicitly caused by regional warming in the area alone, on account of increased evapotranspiration, may be overestimated due to the opposing, synergistic effects on water yield associated with CO_2-enrichment of the lower atmosphere and the annual application of FDTs.

Keywords: ambient CO_2 concentration; flow diversion terraces; residuals; stomatal conductance; watersheds

3.1 Introduction

Stream water yields are particularly important in sustaining terrestrial and aquatic ecosystems and domestic water supplies (Rozas-Vásquez et al., 2019). Therefore, having a good understanding of water yield dynamics and its influencing factors are particularly important in informing water-management policy (Yin et al., 2021). Water supply is affected by many intercorrelated, confounding factors, including those associated with rapid changes in regional climatology and land-management practices (Li et al., 2021; Yin et al., 2022). Most recent studies relating climatic factors to water yields focus on assessing impacts associated with changes in precipitation and temperature (Shukla et al., 2021; Yifru et al., 2021; Yin et al., 2022; Kang et al., 2022). For instance, it has been reported that increases in precipitation can lead to increases in water yield. Whereas, rising air temperatures are projected to increase evapotranspiration (ET), leading to an increase in atmospheric water-vapor demand and consumption. In addition, increases in atmospheric concentrations of greenhouse gases (GHGs) have caused global temperatures to rise, invoking many other changes in the global-to-regional climate system (IPCC, 2021). Of the many species of GHGs, increases in atmospheric CO_2 may not only cause mean air temperatures to increase, but may also cause the spatiotemporal distribution of precipitation to change, increasing the risk of heavy rainfall events, flooding, and drought, resulting with corresponding changes in water yield (Eckhardt and Ulbrich, 2003). Many of these climatic factors are correlated with each other, making it difficult to evaluate their individual contribution to variations in water yield with traditional statistical methods alone, especially when the effects of landcover change and best management practices (BMPs) contribute to this complexity at the watershed level.

As a substitute for direct statistical analysis, comprehensive hydrological models, as an integration of the latest, though limited, state-of-the-art scientific understanding of hydrological processes, are widely used in hydrological research (Cao et al., 2021; Liang et al., 2020; Qi et al., 2016a, 2020b; Wang et al., 2020a, 2020b). Among these models, the Soil and Water Assessment Tool (SWAT) is designed to simulate hydrological processes and predict water quantity and quality as affected by BMPs, which govern field-level variation in crop cover, as well as in the level of strip cropping, conservation tillage, terracing, and nutrient management employed by farmers (D'Arcy and Frost, 2001). In recent years, SWAT has been successfully used to estimate climate impacts on large and small river basins, with aspects of model application appearing in over 600 peer-reviewed journal articles (e.g., Arnold et al., 1998; Bhatta et al., 2019; Liang et al., 2020; Qi et al., 2020a; Wang et al., 2020a). In the current working-version of SWAT, the major hydrological processes consist of surface runoff, soil and root zone infiltration, ET, soil water evaporation, snow sublimation, and baseflow (Arnold et al., 1998). Precipitation can be either intercepted or infiltrated into the soil, with the remaining water participating in surface runoff. The amount of precipitation can be lost to the atmosphere because of ET, which varies throughout the year. When simulating the impact of precipitation on water yield, a water balance equation consisting of the components of precipitation, surface runoff, ET, percolation, and return lateral flow is used. Furthermore, with a well-established energy balance model, SWAT can also be used to simulate the impact of air and soil temperatures, along with other climatic factors, such as solar radiation, relative humidity, and wind speed, on ET and streamflow dynamics (Arnold et al., 1998, 2012; Neitsch et al., 2011).

However, SWAT does not incorporate all conceivable factors that influence hydrological processes due to its reliance on the latest research results concerning the underlying mechanisms. Recent research has indicated that rising atmospheric CO_2 concentrations associated with the anthropogenic release of carbon dioxide to the atmosphere may lead to a reduction in stomatal conductance and, thus, decrease rates of transpiration in plants (Ficklin et al., 2009; Wu et al., 2012a). This scenario will likely cause terrestrial water yields and stream discharge rates to increase, partially in compensation for the effects associated with the augmentation of potential ET (i.e., PET; Liao et al., 2021; Pan et al., 2015). However, ambient CO_2 concentration impacts on streamflow dynamics due to changes in stomatal conductance have yet to be incorporated in SWAT in any meaningful manner, due to the lack of field data demonstrating this relationship at the watershed level.

Land management practices can affect hydrological processes, altering the release of water from watersheds. Best management practices are developed to reduce the downgradient movement of sediments, nutrients, and pesticide residues from agricultural lands to aquatic ecosystems (D'Arcy and Frost, 2001). One of these BMPs includes the application of flow diversion terraces (FDTs), originally designed as a landuse management control of water quantity and quality and soil erosion in agricultural fields (Chow et al., 1999; Al et al., 2008). On FDT-protected lands, long slopes are characteristically reduced into shorter segments, using spacings suitable for both erosion control and ease of farming. A typical FDT consists of earth embankments and grassed channel ways (Yang et al., 2009). Flow diversion terraces can improve soil water accessibility by reducing surface waterflow velocities and increasing the infiltration rate of

pooled surface water and retention along the frontal channels of terraces (Anna and Pierzgalski, 2008), causing surface runoff and contaminant transfer to decrease. The effectiveness of FDTs can be determined by various methods, including benchmarking or paired-watershed experiments, upstream and downstream monitoring, and edge-of-field testing (Zheng et al., 2021). However, the impact of FDTs on water yield is affected by many factors and its effectiveness may vary from watershed-to-watershed depending on local topography, soil characteristics, climatic conditions, and landuse practices (Fernandez et al., 2003). Direct assessments of FDTs' capabilities to impact water yields are generally considered statistically insignificant, due to the large year-to-year variations and low response-signal-to-noise ratios involved. Currently, SWAT does not fully address the impact of FDTs on water yields, possibly due to the lack of dependable interpretations acquired from direct analysis of *in-situ* hydrological data.

Although the effects of atmospheric CO_2 concentrations and FDTs on water yield are not integrated in the current version of SWAT, their influences should still be present in model residuals. Moreover, as SWAT accounts for most other significant factors affecting water yield and stream discharge rates, the residuals should exhibit fewer variations, potentially making the identification of impacts associated with the two unaccounted variables more apparent in the systematic divergence in residuals. The objective of this study is to estimate the potential impacts of a standard BMP and environmental factors on water yield at the watershed scale. Specifically, we focus on separating the individual effects of atmospheric CO_2 concentrations, FDTs, and monthly weather variables on water yield in an experimental watershed in Atlantic Canada. The analysis is facilitated by

merging model simulations with historical hydrometeorological, and land-surface records acquired from 1992–2014.

3.2 Materials and methods

3.2.1 Study sites and relevant data

Black Brook Watershed (BBW) is in northwestern New Brunswick (NB), Atlantic Canada (47°5′ to 47°9′N and 67°44′ to 67°48′W), with elevations ranging from 150–242 m above mean sea level (ASL, Fig. 3.1). It is a typical agricultural watershed in the potato belt of NB. The climate is strongly influenced by marine weather, with an average annual temperature of 3.7 ℃ (Chow et al., 2011). The annual precipitation is 1,037.4 mm, with about one third of the amount occurring in the form of melting snow in spring, a major source of surface runoff and groundwater replenishment (Chow and Rees, 2006). The drainage area of the watershed is 13.1 km^2, with agricultural, forests, and residential land accounting for 65, 21, and 14% of the total watershed area, respectively (Chow et al., 2011). Soils in BBW are classified into six mineral soil classes, namely Grand Falls, Holmesville, Interval, Muniac, Siegas, and Undine, and one organic soil, Saint-Quentin (Mellerowicz, 1993). These soils are developed from glacial till and are generally very stony. Soil texture ranges from sandy loam, loam, to clay loam.

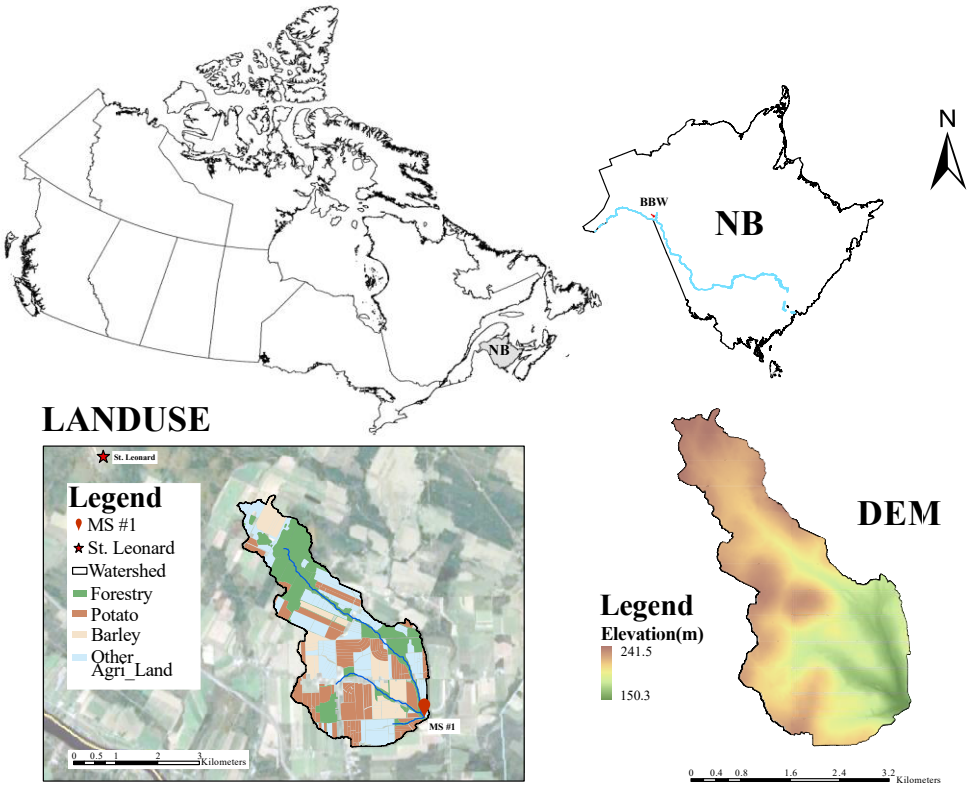

Fig. 3.1 Location of the study area.

Black Brook Watershed was founded by Agricultural and Agri-Food Canada (AAFC) as a national benchmark watershed. A water-monitoring station at the outlet of BBW has been in operation since 1992 (MS#1, Fig. 3.1). Discharge rates at the outlet were recorded from 1992–2014 (Chow et al., 2011). Weather data, i.e., daily precipitation, air temperature, relative humidity, solar radiation, and wind speed were acquired for the same 23-year period from the Saint Leonard, Environment and Climate Change Canada weather station, 5-km from BBW (Fig. 3.1). Multiple soil conservation BMPs have been used to prevent soil erosion and reduce the movement of contaminants from agricultural lands to water courses downslope. As one BMP employed in the area, FDTs have been constructed on more than 50% of cultivated lands in BBW (Yang et al., 2009). A timeseries of cumulative,

annual construction of FDTs and their % footprint area in BBW (1992–2014) is provided in Fig. 3.2. Global monthly atmospheric CO_2 concentrations in Fig. S3.1 were based on measurements acquired from the NOAA Earth System Research Laboratory at Mauna Loa, Hawaii, USA (GML, 2021). During the 23 years of the study atmospheric CO_2 concentrations have increased from 356.1 to 397.3 ppm (Fig. S3.1).

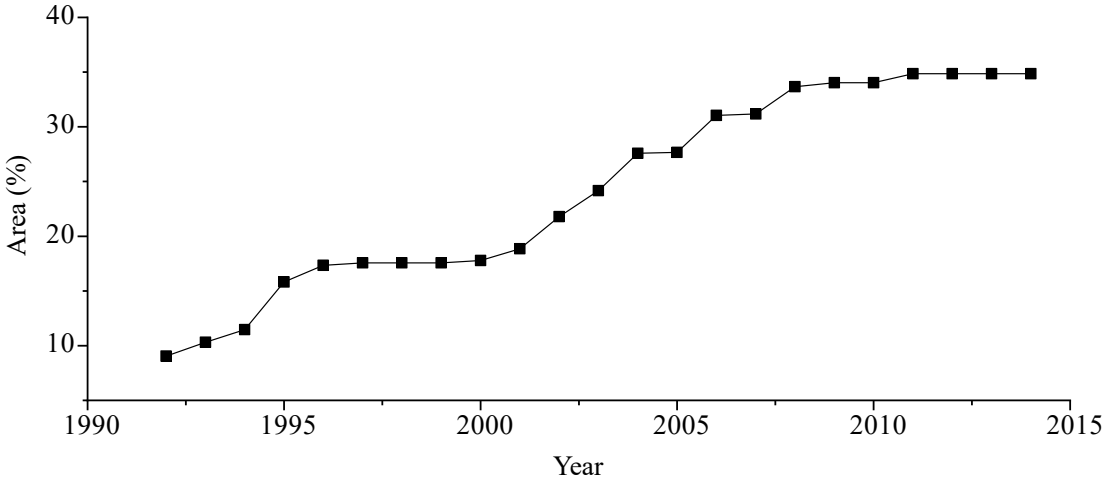

Fig. 3.2 Cumulative change in % area protected with FDTs in BBW from 1992–2014.

3.2.2 Implementation of SWAT

As a widely used comprehensive hydrological model, SWAT was selected to simulate stream discharge rates (water yields) for this study. The model is a semi-distributed and process-based watershed hydrology model providing a flexible framework for simulating the effectiveness of a broad range of BMPs (Arnold et al., 2012; Qi et al., 2018). SWAT has an ability to predict hydrological outcomes associated with water quantity/quality, plant biomass growth, crop yields, and other outcomes associated with the assessment of agricultural lands' environmental integrity as affected by climate, landuse, and landcover change (Arnold et al., 1998, 2012). Major model components include a weather simulator

and several modules focusing on the hydrological processes, waterflow dynamics, crop-growing response, land-management effects, as well as stream water-contaminant loadings and fluxes. Neitsch et al. (2011) provides a detailed description of the model.

An enhanced version of SWAT was established in previous studies to incorporate a physically-based soil temperature module that accounts for the insulating properties of snow and latent heat exchanges resulting from soil freeze-thaw cycles commonly in Atlantic Canada (see Qi et al., 2016a, 2016b). These model enhancements significantly improved the accuracy of monthly streamflow and timing of peak predictions on discharge rates and water quality parameters for BBW (Qi et al., 2016a, 2016b; Wang et al., 2020b). This is the version of SWAT used here.

3.2.3 Model setup, calibration, and validation

A high-resolution light detection and ranging (LiDAR)-based DEM (digital elevation model) of 1-m resolution was used to delineate the watershed and derive corresponding topographical attributes (Zhao et al., 2010; Qi et al., 2018). Soil data were derived from a detailed soil survey map of high spatial resolution (Mellerowicz, 1993) developed by AAFC personnel. Landuse data, including % watershed area protected with FDTs, were incorporated in SWAT through its management files and a field-based assessment of hydrological response units (HRUs) created in a previous study (Qi et al., 2017b, 2022). Model calibration and validation of monthly discharge rates were carried out for the period of 1992–2001 and 2002–2014, respectively. Snowfall and melting processes play a significant role in governing the hydrological dynamics within the watershed of the study area. We followed established practices for calibrating and validating snowfall and melt simulations, paying particular attention to the nuances of snow processes (Qi et al., 2017a).

Model performance was assessed based on commonly used statistical criteria in hydrological studies, namely % bias (*PBIAS*) and Nash-Sutcliffe model efficiency (NS), i.e.,

$$PBIAS = 100\frac{\sum_{i=1}^{N}(P_i - O_i)}{\sum_{i=1}^{N} O_i}, \text{ and} \quad (3.1)$$

$$NS = 1 - \frac{\sum_{i=1}^{n}(O_i - P_i)^2}{\sum_{i=1}^{n}(O_i - O_{avg})^2}, \quad (3.2)$$

where O_i (O_{avg}) and P_i (P_{avg}) are the observed and predicted values and their corresponding averages.

3.2.4 Residual analysis and Bayesian multiple linear regression

3.2.4.1 Residual analysis

Multiple factors, such as model formulation, input and validation data, and parameter calibration can lead to uncertainty in model simulations (Abbaspour, 2013). Residual analysis is often used to reveal the main model components that introduce uncertainty in predicted outcomes (Semadeni-Davies et al., 2021). Residuals are defined as the difference between observed and predicted quantities of a response variable. When plotted against the data from an influencing factor, like precipitation or temperature, residuals created with a properly calibrated model should be randomly distributed about the abscissa (residuals ~ zero). The presence of structure in plotted residuals is a clear indication of methodical bias (error) in models. The motivation of the current study is the statistical decomposition of model residuals for greater explanation and insight into selected drivers of streamflow discharge rates, particularly those difficult to characterize by any other means. Additionally, we examined residuals of ET for further validation of the methods and findings, given their strong association with streamflow. Due to the lack of field-based measurements of ET

across the watershed, corresponding estimates of ET were derived by deducting streamflow at the watershed outlet from recorded annual precipitation. Akin to the calculation of residuals of streamflow, residuals of ET were determined by subtracting the field-based estimates of ET (addressed above) from corresponding estimates generated with SWAT.

3.2.4.2 Bayesian multiple linear regression

Bayesian inference is widely used in situations (i) with limited observations, and (ii) with an expectation of exploiting available expert judgement in the examination of associated data. Bayesian multiple linear regression (BMLR) is an expansion of multiple linear regression (MLR), where data are supplemented with *a priori* distributions for coefficients $\beta_0, \beta_1, \dots, \beta_n$, and the error term, ε, in

$$Y = \beta_0 + \beta_1 X_1 + \beta_2 X_2 + \cdots + \beta_p X_p + \varepsilon, \quad (3.3)$$

where X_p represents the p^{th} explanatory variable, and β_p formulizes the association between predictors to the response variable Y. Here, we assume that ε is independent and distributed as a normal random variable, with a mean of zero and a uniform standard deviation of σ. The posterior distributions for $\beta_0, \beta_1, \dots, \beta_n$, and ε in BMLR are predicted based on *a priori* and likelihood distributions, rather than relying on the least squares regression to minimize the sum of residuals squared as it is normally done with MLR. The Student t-test is commonly used to determine the statistical significance between various estimates of equation parameters and zero (James et al., 2014). The *rstan* package for R *v.* 4.1.0 was employed in a provision of full Bayesian inference associated with Markov chain, Monte Carlo (MCMC)-based sampling (Reinert, 2007; Stan Development, 2019).

Residual analysis combined with BMLR can separate the individual effects of FDTs and in-air CO_2-enrichment on water yields and ET by specifying the probability of the two

variables *a priori*. The *a priori* probability of CO_2 was restricted as being greater (less) than zero for water yield (ET), which can reduce overall uncertainty based on our understanding that elevated CO_2 concentrations can lead to reductions in stomatal conductance (Herrick et al., 2004), and as a result cause water yields at the outlet of the watershed to increase (Wu et al., 2012a, 2012b). We set the *a priori* probability of FDTs to be less (greater) than zero for water yield (ET), reflecting our belief that an increase in FDTs is likely to result in a reduction in waterflow downstream.

3.2.5 Parametric tests

In this study, we applied Student t-tests to detect the significance of parameters under several circumstances. The t-test is a statistical method used to determine whether there is a significant difference between the means of two groups, making it one of the most used hypotheses testing techniques in statistics. This test is particularly useful when dealing with small sample sizes or when the population standard deviation is unknown. The t-test is based on the t-distribution, a type of probability distribution that is symmetrical and bell-shaped, like the normal distribution but with thicker tails. The t-distribution allows for the estimation of population means from small sample sizes, with some level of variation among samples.

3.3 Results

3.3.1 Model calibration and validation

The monthly timeseries of observed and predicted discharge rates for the 1992–2014 period is shown in Fig. 3.3. The performance of SWAT was generally satisfactory for both the calibration and validation periods (based on performance criteria in Moriasi et al., 2007), yielding *PBIAS* (%) and NS (non-dimensional) of 1.1%, 0.61, 13.3%, and 0.76,

respectively. The current model was revealed to be sufficiently robust to address issues of attribution regarding the influencing variables not accounted for in SWAT. It should be noted that *PBIAS* rose from the calibration to the validation phase, highlighting the challenges in accurately simulating the impacts of FDTs on streamflow, despite our efforts to incorporate FDT-data into the management files using observed landuse information (Qi et al., 2018). FDTs' role in reducing water yields will be further investigated in subsequent analyses.

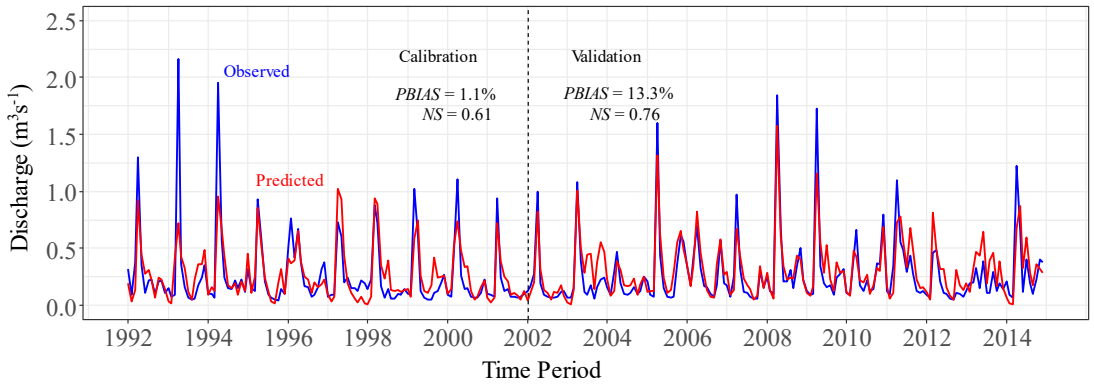

Fig. 3.3 BBW-specific observed and predicted discharge rates (m^3/s) from 1992–2014. The dotted vertical line subdivides the timeseries relative to model calibration and validation.

3.3.2 Residuals Analyses

Initially, we examined the connection between time (year) and the residuals of streamflow and ET, along with various influencing factors, which include precipitation, temperature, ambient CO_2 concentrations, and % watershed area protected with FDTs (Table 3.1, Fig. 3.4, and Fig. S3.1). Residuals of streamflow exhibited a significant downward trend ($p<0.05$) over the 23 years. No statistically significant trend could be detected in the residuals of ET ($p>0.05$). Influencing factors, including precipitation, temperature ($p<0.05$), and ambient CO_2 concentrations ($p<0.001$) all exhibited clear

upward trends. Land management practices with respect to the use of FDTs also disclosed a significant increasing trend (p<0.001).

Correlation analyses were carried out to assess the relationship between residuals of stream discharge rate and ancillary variables, such as precipitation, temperature, ambient CO_2 concentrations, and the % area protected with FDTs (Fig. 3.4). Here, we transformed the % area of FDTs to ln [FDT (%) +1], ensuring the data assumed a near-normal distribution. Downward trends in residuals of streamflow were not only detectible annually, but also exhibited trends when compared with some of the influencing factors (Fig. 3.4). Residuals of streamflow were not evident when plotted against precipitation and temperature, suggesting that the two climatic variables were reasonably dealt with in current model formulation. Ambient CO_2 concentrations and %-watershed-area with FDTs showed a significant correlation with residuals of streamflow, which was anticipated given that the model does not account for the effects of these two variables in its current design.

Table 3.1 Trending (slopes) in hydrology-related variables and their statistical significance.

Variable	Slope	Significance
Residuals of streamflow (mm·year^{-1})	-8.58	*
Residuals of ET (mm·year^{-1})	7.40	-
Precipitation (mm·year^{-1})	6.57	-
Temperature (°C·year^{-1})	0.07	*
CO_2 (ppm·year^{-1})	1.91	***
FDTs (%·year^{-1}) (ln [FDT (%) +1])	0.06	***

Note: Residuals = observed – predicted quantities; significance levels identified are p<0.001 (denoted as ***), 0.01 (**), 0.05 (*), and p>0.05 (-). The unit of FDTs is % watershed area protected.

Correlation analyses were also performed to evaluate the connection between residuals of ET and factors such as precipitation, temperature, ambient CO_2 concentrations,

and % area covered with FDTs (see Fig. 3.5). Mirroring the findings for streamflow, residuals of ET did not display a significant correlation with either precipitation or temperature. However, a notable correlation was observed between residuals of ET and both ambient CO_2 concentrations and % area with FDTs. It is important to note that the correlation coefficients for ambient CO_2 concentrations and FDTs with residuals of ET were inversely related, compared to correlations with residuals of streamflow.

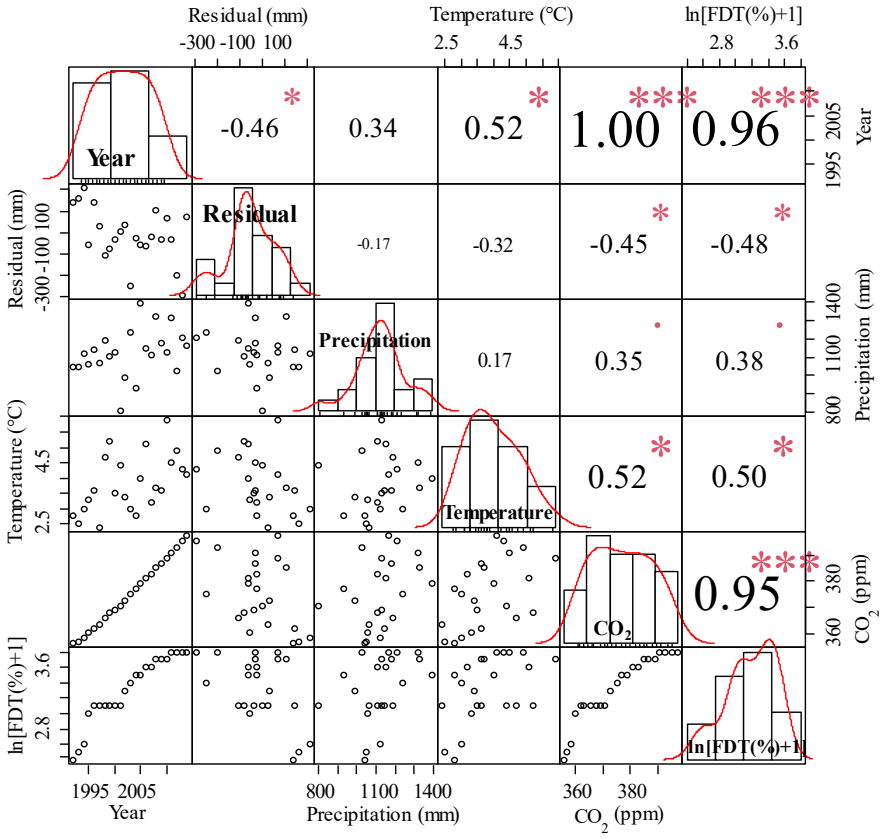

Fig. 3.4 Annual trends and coefficient matrix with respect to **residuals of streamflow** (mm), precipitation (mm), temperature (°C), ambient CO_2 concentrations (ppm) and $\log_e$-transformed % watershed area protected with FDTs, or ln [FDT (%) +1]. The first column shows the annual trend of all variables. The value in the upper-right half of the matrix represents the correlation coefficient between two variables; asterisks in the upper-right corner give the significance level of correlation. The histograms along the diagonal of the series of graphs represent the distributions of the suite of variables considered in this study. The dots in the lower-left section of the matrix represent the correlation between the paired datasets. The significance levels considered here are p<0.001 (denoted by ***), 0.01 (**), and 0.05 (*).

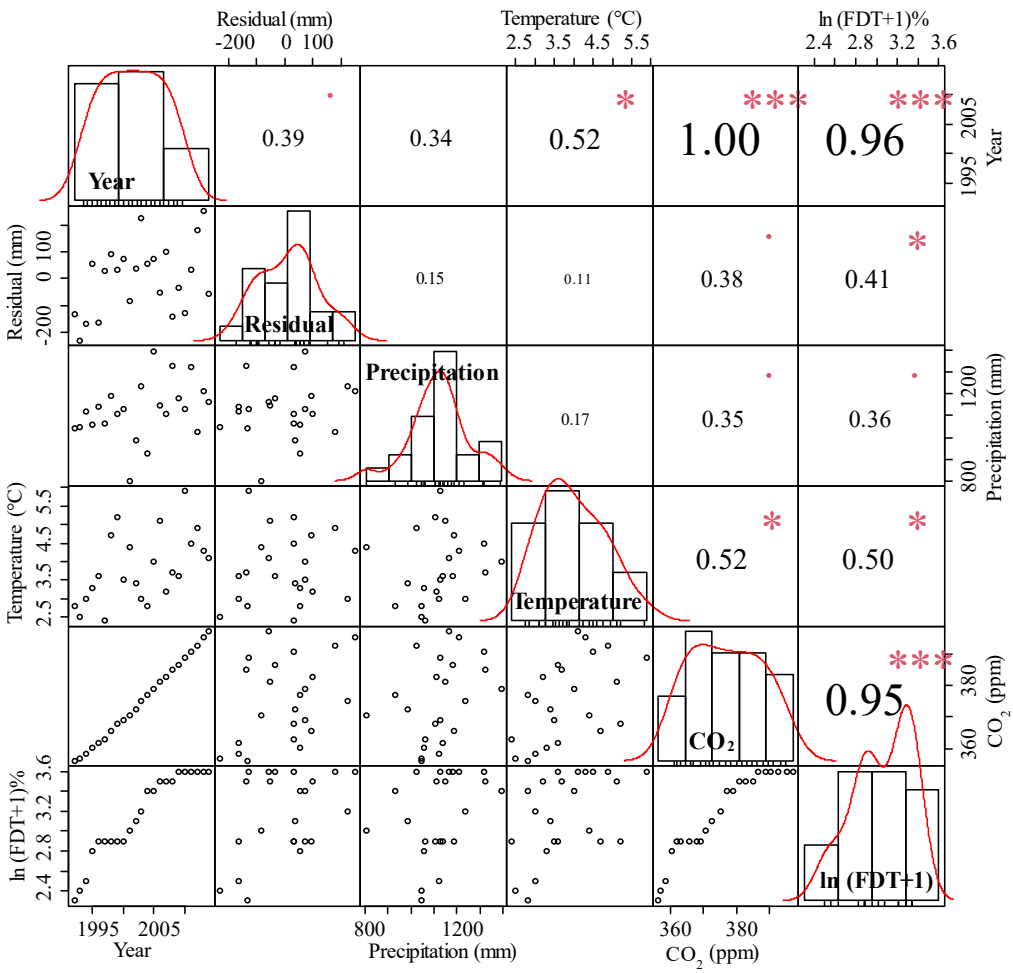

Fig. 3.5 Coefficient matrix for **residuals of ET (mm)**, precipitation (mm), temperature (°C), ambient CO_2 concentration (ppm), and $\log_e$-transformed % watershed area protected with FDTs, or ln [FDT (%) +1]. The first column shows the annual trend of all variables. Values in the upper-right half of the matrix represent the correlation coefficient between two variables; asterisks in the upper-right corner give the significance level of correlation. The histograms along the diagonal of the series of graphs represent the distributions of the suite of variables considered. The dots in the lower-left section of the matrix represent the correlation between the paired datasets. The significance levels considered are p<0.001 (denoted by ***), 0.01 (**), and 0.05 (*).

3.3.3 Disentangling the effects of FDTs and CO_2 with BMLR

The impact of various influencing factors on the residuals of streamflow (Table 3.2) and ET (Table 3.3) was analyzed using BMLR. For comparative reasons, ordinary MLR was also employed to highlight the benefits of BMLR in clarifying the effects of processes

not accounted for in SWAT (the results are presented in Supplementary Material, SM). Drawing from prior analyses of residuals of streamflow and ET, temperature and precipitation were omitted from subsequent analyses because they were adequately administered in SWAT.

The impact of ambient CO_2 concentrations on streamflow was successfully detected by BMLR, while it was not with MLR (as indicated by $p>0.05$ associated with Eq. (a) in Table S3.1). The MLR tended to overlook the importance of ambient CO_2 concentrations in the control of streamflow, under-evaluating the reduction in water yields associated with the application of FDTs. According to Table 3.2, increases in water yield caused by increases in ambient CO_2 concentrations were 0.4–20.2 mm from 1992–2014, suggesting an overall minor increase of about 0.1–3.1%. Whereas, % watershed area treated with FDTs contributed to a net reduction in water yields from 115.2–247.4 mm, representing a decline of about 17.7–38.0% over the same time period. Across all years of the study period, elevated ambient CO_2 concentrations increased water yields by 10.3 mm or 1.6%, with a corresponding net mean change of +0.45 mm $year^{-1}$, whereas FDTs reduced water yields by about 188.0 mm (or 28.9%), with a corresponding mean change of -8.2 mm $year^{-1}$. It is worth noting that BMLR-based estimates of water-yield reductions caused by the implementation of FDTs over the 23 years were slightly greater than those projected with MLR without accounting for the effects of in-air CO_2 [see Eq. (b) in Table S1], i.e., 188.0 mm *vs*. 183.5 mm (28.2%).

Table 3.2 Coefficients of Bayesian multiple linear regression (BMLR) as derived from pairwise comparisons of **residuals of streamflow** and selected explanatory variables (identified in column one).

Variables	Mean	Standard Deviation	Credible Interval	
			2.50%	97.50%
CO_2	0.25	0.14	0.01	0.49
FDTs	-147.74	27.15	-194.42	-90.52

Note: Residuals = observed streamflow – SWAT-predicted streamflow; explanatory variables include atmospheric CO_2 concentration, and $\log_e$-transformed % watershed area protected with FDTs or ln [FDT (%) +1].

Like streamflow, the impact of ambient CO_2 concentrations on ET was successfully detected with BMLR, and not with MLR [p>0.05 based on Eq. (a) in Table S3.2]. The MLR tended to overlook the importance of CO_2 concentrations in the control of ET, underestimating the increase in ET associated with the application of FDTs. According to Table 3.3, decreases in ET caused by increases in ambient CO_2 concentrations were 0.4–20.2 mm from 1992–2014, suggesting a decrease of about 0.08–4.3%. Whereas, % watershed area treated with FDTs contributed to a net increase in ET from 91.1–238.9 mm, representing an a 19.2–50.4% increase over the same time period. Across all years of the study period, elevated CO_2 concentrations reduced ET by 10.3 mm or 2.2%, with a corresponding net mean change in water yield of +0.45 mm year^{-1}, whereas FDTs increase ET by about 168.2 mm (or 35.5%), providing a corresponding mean change in water yield of -7.3 mm year^{-1}. Results based on BMLR showed ET to have increased by 168.2 mm (Table 3.3) with the implementation of FDTs, compared to 160.4 mm as assessed with MLR (33.9%; Eq. (b); Table S3.2). Findings related to the residuals of ET are consistent with those for streamflow, although changes in modeled streamflow and ET (i.e., decreases and increases, respectively) did not precisely match in terms of average values.

Nonetheless, the broad overlap in their ranges provides compelling evidence for a water balance at the watershed scale.

Table 3.3 Coefficients of Bayesian Multiple Linear Regression (BMLR) as derived from pairwise comparisons of **residuals of ET** and selected explanatory variables (column one).

Variable	Mean	Standard Deviation	Credible Interval	
			2.50%	97.50%
CO_2	-0.25	0.14	-0.49	-0.01
FDTs	132.2	29.82	71.63	187.79

Note: Residuals = observed ET – SWAT-predicted ET; explanatory variables include atmospheric CO_2 concentration (CO_2), and $\log_e$-transformed % watershed area protected with FDTs (or ln [FDT (%) +1]).

3.4 Discussion

3.4.1 State-of-the-art and contribution

Assigning attribution as to the influence a controlling factor may have on a system's response is crucial in many scientific fields (Guerrieri et al., 2019). A recent example involves determining the extent to which human activity, such as burning of fossil fuels or causing large-scale landcover change, contributes to changes in weather patterns and ecosystems observed globally (IPCC, 2021). In many studies, assigning attribution relies on application of computer models to quantify the roles of model processes on various modeled projections. However, the effort to assign attribution can be challenging because many of the variables affiliated with the system may be confounded with each other. In such cases, the direct application of limited models may lead to improperly modeled outcomes, producing deviations (structure) in model residuals. In this study, we show that results from a limited model along with associated field measurements can be used to facilitate the assessment of attribution by statistical means.

3.4.2 Previous studies

Attribution of various BMPs on peak waterflows has been previously assessed with a fully parameterized version of SWAT for the Lower Pearl River Watershed (12,500 km^2) in southern Mississippi, USA, based on a calibration and validation of the model with streamflow data from four gauging stations (Dakhlalla and Parajuli, 2016). For a baseline climate scenario, the modeling study found that grass waterways and detention ponds helped to reduce peak flows by 8.4 and 6.0%, respectively. Likewise, parallel terraces were shown to be responsible for another 3.1% reduction in average peak flow. Combined, the three BMPs produced greater reductions in average peak flow than when applied individually. Increases in ambient CO_2 concentrations were also shown to lower the effectiveness of BMPs in reducing peak flows. This finding is consistent with my own study-based conclusions, regarding the role of in-air CO_2-enrichment, stomatal conductance (Stockle et al., 1992), and streamflow dynamics at the watershed level. The quality of attribution based on a direct application of SWAT relies heavily on the quality of the BMP-based process modules that were added to SWAT. However, there are questions about the accuracy of some of these attributions, given that the associated hydrological processes are very difficult to characterize without the required data representing conditions across entire watersheds.

In another modeling study, Yang et al. (2009) uncovered a systematic divergence between SWAT-generated predictions and field measurements of water yields in BBW after the construction of FDTs. It was estimated that a constant level of FDTs (covering 24% of BBW, representing % area coverage at the end of the implementation phase in 2005) reduced water yield by 20% at the end of the study period. This attribution was seen to be

high, most likely as a result of the assumed, constant coverage applied in model simulation, notwithstanding actual modifications having been applied from 1995–2005 (see Fig. 3.2).

3.4.3 Model Limitations

Owing to the lack of meaningful landscape-level characterization of relationships between FDTs, in-air changes in CO_2 concentrations, and streamflow dynamics in SWAT (or other hydrological models, for that matter), the direct use of such models in attribution studies is at times challenged by complications. This is reflected in the lack of literature addressing these specific relationships at the watershed scale. To avoid these problems, we have developed this new method to decompose model residuals based on outputs from a well-established, calibrated hydrological model that addresses most important hydrological processes and actual field measurements. The decomposition of model residuals helps to isolate the effects of ancillary processes that are missing or improperly addressed in models. This decomposition has shown that variations in ambient CO_2 concentrations and FDTs at the levels described earlier are responsible for causing streamflow discharge rates to vary. The total impact of ambient CO_2 concentrations on streamflow for BBW is small, i.e., within 0.1–3.1% over 23 years, given a 41.2-ppm increase in 1992 baseline ambient concentrations estimated here. In effect, a 11.6% increase in ambient CO_2 concentration from 1992–2014 (Fig. S3.1) meant a 5% decrease in stomatal conductance at the watershed scale [based on Eq. (1) in a paper by Ficklin et al. (2009)]. Other studies have shown that for similar changes in stomatal conductance, in response to a 11.6% increase in ambient CO_2 concentration, net reductions in ET amounted to 0.9–2.6% at the watershed scale and a corresponding increase in surface runoff of 1.5–2.7% (Arias and Spain, 2014; Desai et al., 2020). The function of FDTs at BBW is to cause water yields to decrease, leaving an

appreciable amount of water to infiltrate the soils, improving growing conditions for crops while restricting the downgradient transfer of contaminants. A recent literature search revealed a lack of experimental data directly linking the effects of FDTs to changes in water yield. The lack of literature on this matter may be attributed to the significant variation caused by the many factors involved in natural agricultural watersheds, such as annual changes in precipitation, temperature, and land management practices that tend to obscure the effects of FDTs at a broader scale. With the decomposition of residuals, we found that FDTs could lead to a 28.9% reduction in water yield over the 23 years (Table 3.2 and Fig. 3.2). This result was seen to be greater than the initial estimate provided by Yang et al. (2009) for the same watershed, as usage of FDTs was observed to increase substantially after 2005 (Fig. 3.2).

3.5 Conclusions

In this study, we introduced an innovative approach to discern the subtle roles of atmospheric CO_2 concentrations and flow diversion terraces (FDTs) share in modifying surface waterflow dynamics. The approach is based on an application of (i) a recent version of SWAT to eliminate the effects of most modeled factors; and (ii) a subsequent decomposition of residuals (i.e., field observations – model predictions) in isolating the effects of the unaccounted variables. The feasibility of the method is based on the premise that SWAT can effectively address the impacts of most major climatic, soil, and landuse factors on water yield. Systematic errors in model predictions associated with the effects of unaccounted variables are expected to persist throughout all model simulations and residuals, providing a means to isolate the contribution of the unaccounted variables to observed streamflow dynamics. With residual decomposition, we are able to identify

significant impact due to the implementation of FDTs, with the level of effectiveness increasing with increase FDT density. To better simulate the impact of ambient CO_2 concentrations on water yield, further data are needed from watersheds, where FDTs are not used.

As global warming and climate change progresses, escalating temperatures are projected to augment ET and reduce water yields at the watershed scale — an impact that most existing hydrological models can address fairly well. Our findings indicate that elevated levels of atmospheric CO_2 are likely to decrease stomatal conductance and ET. Consequently, this annual reduction can contribute to an increase in streamflow, effectively offsetting a portion of the decline in streamflow due to rising temperatures. Furthermore, soil conservation BMPs, such as constructing FDTs, are anticipated to bolster surface flow retention rates and enhance in-field soil water content. This land management practice can ultimately lead to a watershed-level reduction in surface waterflow.

Acknowledgements

The authors would like to acknowledge (i) the Natural and Science and Engineering Council (NSERC), New Brunswick Environmental Trust Fund (NBETF) and Environment and Climate Change Canada (ECCC) for funding this project; (ii) the Faculty of Forestry and Environmental Management, University of New Brunswick, for license and computer support for ESRI ArcGIS™ and other software employed in this study. Authors are thankful to Sylvie Lavoie, Yulia Kupriyanovich, John Monteith, and Lionel Stevens for their technical support in data collection and sample analyses.

References

Abbaspour, K.C. (2013). SWAT-CUP: SWAT Calibration and Uncertainty Program - A User Manual. https://swat.tamu.edu/media/114860/usermanual_swatcup.pdf/

Al, A.Y., Touma, J., Zante, P., Nasri, S., and Albergel, J. (2008). Water and sediment balances of a contour bench terracing system in a semi-arid cultivated zone (El Gouazine, central Tunisia). Hydrological Sciences Journal, 53, 883–892. https://doi.org/10.1623/hysj.53.4.883

Anna, B., and Pierzgalski, E. (2008). Ridged terraces - functions, construction and use. Journal of Environmental Engineering and Landscape Management, 16 (2), 1–6. https://doi.org/10.3846/1648-6897.2008.16.104-109

Arias, R., Rodríguez-Blanco, M. L., Taboada-Castro, M. M., Nunes, J. P., Keizer, J. J., and Taboada-Castro, M. T. (2014). Water resources response to changes in temperature, rainfall and CO_2 concentration: A first approach in NW Spain. Water, 6(10), 3049–3067. https://doi.org/10.3390/w6103049

Arnold, J.G., Moriasi, D.N., Gassman, P.W., Abbaspour, K.C., White, M.J., Srinivasan, R., Santhi, C., Harmel, R., Van Griensven, A., and Van Liew, M.W. (2012). SWAT: Model use, calibration, and validation. Transactions of the ASABE, 55(4), 1491–1508. https://doi.org/10.13031/2013.42256

Arnold, J. G., Srinivasan, R., Muttiah, R. S., and Williams, J. R. (2007). Large area hydrologic modeling and assessment part I: Model Development. Journal of the American Water Resources Association, 34 (1), 73–89. https://doi.org/10.1111/j.1752-1688.1998.tb05961.x

Bhatta, B., Shrestha, S., Shrestha, P. K., and Talchabhadel, R. (2019). Evaluation and application of a SWAT model to assess the climate change impact on the hydrology of the Himalayan River Basin. Catena, 181, 104082. https://doi.org/10.1016/j.catena.2019.104082

Cao, W., Zhang, Z., Liu, Y., Band, L.E., Wang, S., and Xu, H. (2021). Seasonal differences in future climate and streamflow variation in a watershed of Northern China. Journal of Hydrology: Regional Studies, 38, 100959. https://doi.org/10.1016/j.ejrh.2021.100959

Chow, L., Xing, Z., Benoy, G., Rees, H.W., Meng, F.-R., Jiang, Y., and Daigle, J.L. (2011). Hydrology and water quality across gradients of agricultural intensity in the Little River watershed area, New Brunswick, Canada. Journal of Soil and Water Conservation, 66(1), 71–84. https://doi.org/10.2489/jswc.66.1.71

Chow, T., and Rees, H. (2006). Impacts of intensive potato production on water yield and sediment load (Black Brook Experimental Watershed: 1992–2002 summary). Potato Research Centre, AAFC, Fredericton, NB, Canada

Chow, T.L., Rees, H.W., and Daigle, J.L. (1999). Effectiveness of terraces/grassed waterway systems for soil and water conservation: A field evaluation. Journal of Soil and Water Conservation, 54(3), 577–583.

D'Arcy, B., and Frost, A. (2001). The role of best management practices in alleviating water quality problems associated with diffuse pollution. Science of The Total Environment, 265(1–3), 359–367. https://doi.org/10.1016/S0048-9697(00)00676-8

Dakhlalla, A.O., and Parajuli, P.B. (2016). Evaluation of the best management practices at the watershed scale to attenuate peak streamflow under climate change scenarios. Water Resources Management, 30, 963–982. https://doi.org/10.1007/s11269-015-1202-9

Desai, S., Singh, D.K., Islam, A., and Sarangi, A. (2020). Impact of climate change on the hydrology of a semi-arid river basin of India under hypothetical and projected climate change scenarios. Journal of Water and Climate Change, 12(3), 969–996. https://doi.org/10.2166/wcc.2020.287

Eckhardt, K., and Ulbrich, U. (2003). Potential impacts of climate change on groundwater recharge and streamflow in a central European low mountain range. Journal of Hydrology, 284(1–4), 244–252. https://doi.org/10.1016/j.jhydrol.2003.08.005

Fernandez, C., Wu, J.Q., McCool, D.K., and Stöckle, C.O. (2003). Estimating water erosion and sediment yield with GIS, RUSLE, and SEDD. Journal of Soil and Water Conservation, 58(3), 128–136.

Ficklin, D.L., Luo, Y., Luedeling, E., and Zhang, M. (2009). Climate change sensitivity assessment of a highly agricultural watershed using SWAT. Journal of Hydrology, 374(1–2), 16–29. https://doi.org/10.1016/j.jhydrol.2009.05.016

Guerrieri, R., Belmecheri, S., Ollinger, S.V., Asbjornsen, H., Jennings, K., Xiao, J.F., Stocker, B.D., Martin, M., Hollinger, D.Y., Bracho-Garrillo, R., Clark, K., Dore, S., Kolb, T., Munger, J.W., Novick, K., and Richardson, A.D. (2019). Disentangling the role of photosynthesis and stomatal conductance on rising

forest water-use efficiency. Proceedings of the National Academy of Sciences, 116(34), 16909–16914. https://doi.org/10.1073/pnas.1905912116

GML. (2021, October 15). Global Monitoring Laboratory. Trends in Atmospheric Carbon Dioxide. https://gml.noaa.gov/ccgg/trends/

Herrick, J.D., Maherali, H., and Thomas, R.B. (2004). Reduced stomatal conductance in sweetgum (Liquidambar styraciflua) sustained over long-term CO_2 enrichment. New Phytologist, 162(2), 387–396. https://doi.org/10.1111/j.1469-8137.2004.01045.x

IPCC, 2021: Summary for Policymakers. In: Climate Change 2021: The Physical Science Basis. Contribution of Working Group I to the Sixth Assessment Report of the Intergovernmental Panel on Climate Change [Masson-Delmotte, V., P. Zhai, A. Pirani, S.L. Connors, C. Péan, S. Berger, N. Caud, Y. Chen, L. Goldfarb, M.I. Gomis, M. Huang, K. Leitzell, E. Lonnoy, J.B.R. Matthews, T.K. Maycock, T. Waterfield, O. Yelekçi, R. Yu, and B. Zhou (eds.)]. In Press.

James, G., Witten, D., Hastie, T., and Tibshirani, R. (2014). An Introduction to Statistical Learning: with Applications in R. Springer, New York. https://citations.springernature.com/book?doi=10.1007/978-1-4614-7138-7

Kang, X., Qi, J., Li, S., and Meng, F.-R. (2022). A watershed-scale assessment of climate change impacts on crop yields in Atlantic Canada. Agricultural Water Management, 269, 107680. https://doi.org/10.1016/j.agwat.2022.107680.

Li, H., Liu, L., Koppa, A., Shan, B., Liu, X., Li, X., Niu, Q., Cheng, L., and Miralles, D. (2021). Vegetation greening concurs with increases in dry season water yield over

the Upper Brahmaputra River basin. Journal of Hydrology, 603, 126981. https://doi.org/10.1016/j.jhydrol.2021.126981

Liang, K., Jiang, Y., Qi, J., Fuller, K., Nyiraneza, J., and Meng, F.-R. (2020). Characterizing the impacts of landuse on nitrate load and water yield in an agricultural watershed in Atlantic Canada. Science of The Total Environment, 729, 138793. https://doi.org/10.1016/j.scitotenv.2020.138793

Liao, D., Niu, J., Kang, S., Singh, S.K., and Du, T. (2021). Effects of elevated CO_2 on the evapotranspiration over the agricultural land in Northwest China. Journal of Hydrology, 593, 125858. https://doi.org/10.1016/j.jhydrol.2020.125858

Lu, H., Yan, Y., Zhu, J., Jin, T., Liu, G., Wu, G., Stringer, L.C., and Dallimer, M. (2020). Spatiotemporal water yield variations and influencing factors in the Lhasa River Basin, Tibetan Plateau. Water, 12(5), 1498. https://doi.org/10.3390/w12051498

Mellerowicz, K.T. (1993). Soils of Black Brook Watershed St. Andre Parish, Madawaska County, New Brunswick. [Fredericton]: New Brunswick Department of Agriculture. https://sis.agr.gc.ca/cansis/publications/surveys/nb/nbbb/index.html

Moriasi, D.N., Arnold, J.G., Van Liew, M.W., Bingner, R.L., Harmel, R.D., and Veith, T.L. (2007). Model evaluation guidelines for systematic quantification of accuracy in watershed simulations. Transactions of the ASABE, 50(3), 885–900. https://doi.org/10.13031/2013.23153

Neitsch, S.L., Arnold, J.G., Kiniry, J.R., and Williams, J.R. (2011). Soil and Water Assessment Tool Theoretical Documentation Version 2009. Texas Water Resources Institute. https://hdl.handle.net/1969.1/128050

Pan, S., Tian, H., Dangal, S.R.S., Yang, Q., Yang, J., Lu, C., Tao, B., Ren, W., and Ouyang, Z. (2015). Responses of global terrestrial evapotranspiration to climate change and increasing atmospheric CO_2 in the 21st century. Earth's Future, 3(1), 15–35. https://doi.org/10.1002/2014EF000263

Qi, J., Li, S., Li, Q., Xing, Z., Bourque, C. P.-A., and Meng, F.-R. (2016a). Assessing an enhanced version of SWAT on water quantity and quality simulation in regions with seasonal snow cover. Water Resources Management, 30, 5021–5037. https://doi.org/10.1007/s11269-016-1466-8.

Qi, J., Li, S., Li, Q., Xing, Z., Bourque, C. P.-A., and Meng, F.-R. (2016b). A new soil-temperature module for SWAT application in regions with seasonal snow cover. Journal of Hydrology, 538, 863–877. https://doi.org/10.1016/j.jhydrol.2016.05.003.

Qi, J., Li, S., Jamieson, R., Hebb, D., Xing, Z., and Meng, F.-R. (2017a). Modifying SWAT with an energy balance module to simulate snowmelt for maritime regions. Environmental Modelling and Software, 93, 146–160. https://doi.org/10.1016/j.envsoft.2017.03.007.

Qi, J., Li, S., Yang, Q., Xing, Z., and Meng, F.-R. (2017b). SWAT setup with long-term detailed landuse and management records and modification for a micro-watershed influenced by freeze-thaw cycles. Water Resources Management, 31, 3953–3974. https://doi.org/10.1007/s11269-017-1718-2.

Qi, J., Liang, K., Li, S., Wang, L., and Meng, F.-R. (2018). Hydrological evaluation of flow diversion terraces using downhill-slope calculation method for high

resolution and accuracy DEMs. Sustainability, 10(7), 2414. https://doi.org/10.3390/su10072414

Qi, J., Du, X., Zhang, X., Lee, S., Wu, Y., Deng, J., Moglen,G., Sadeghi, A., and McCarty, G. (2020a). Modeling riverine dissolved and particulate organic carbon fluxes from two small watersheds in the northeastern United States. Environmental Modelling and Software, 124, 104601. https://doi.org/10.1016/j.envsoft.2019.104601

Qi, J., Lee, S., Zhang, X., Yang, Q., McCarty,G., and Moglen,G. (2020b). Effects of surface runoff and infiltration partition methods on hydrological modeling: a comparison of four schemes in two watersheds in the Northeastern US. Journal of Hydrology, 581, 124415. https://doi.org/10.1016/j.jhydrol.2019.124415

Qi, J., Kang, X., Li, S., and Meng, F.-R. (2022). Evaluating impacts of detailed land use and management inputs on the accuracy and resolution of swat predictions in an experimental watershed. Water, 14(15), 23–52. https://doi.org/10.3390/w14152352.

Reinert, G. (2007). Markov Chain Monte Carlo and Applied Bayesian Statistics. https://www.stats.ox.ac.uk/~reinert/mcmc/mcmc.pdf

Rozas-Vásquez, D., Fürst, C., and Geneletti, D. (2019). Integrating ecosystem services in spatial planning and strategic environmental assessment: the role of the cascade model. Environmental Impact Assessment Review, 78, 106291. https://doi.org/10.1016/j.eiar.2019.106291.

Semadeni-Davies, A.F., Jones-Todd, C.M., Srinivasan, M.S., Muirhead, R.W., Elliott, A.H., Shankar, U., and Tanner, C.C. (2021). CLUES model calibration: residual

analysis to investigate potential sources of model error. Agricultural Research, 64(3), 320–343. https://doi.org/10.1080/00288233.2019.1697708

Shao, S., and Yang, Y. (2021). Effects of precipitation and landuse/cover changes on the spatio-temporal distribution of the water yield in the Huang-Huai-Hai basin, China. Environmental Earth Sciences, 80(24), 812. https://doi.org/10.1007/s12665-021-10119-5

Shukla, S., Jain, S.K., and Kansal, M.L. (2021). Hydrological modelling of a snow/glacier-fed western Himalayan basin to simulate the current and future streamflows under changing climate scenarios. Science of The Total Environment, 795, 148871. https://doi.org/10.1016/j.scitotenv.2021.148871

Stan Development Team. (2019). Stan User's Guide, Version 2.34. https://mc-stan.org/docs/stan-users-guide/index.html

Stockle, C.O., Williams, J.R., Rosenberg, N.J., and Jones, C.A. (1992). A method for estimating the direct and climatic effects of rising atmospheric carbon dioxide on growth and yield of crops: Part I—Modification of the EPIC model for climate change analysis. Agricultural Systems, 38(3), 225–238. https://doi.org/10.1016/0308-521X(92)90067-X

Wang, Q., Qi, J., Li, J., Cole, J., Waldhoff, S., and Zhang, X. (2020a). Sensitivity of nitrate loading projection to freeze-thaw cycle representation. Water Resources, 186, 116355. https://doi.org/10.1016/j.watres.2020.116355

Wang, Q., Qi, J., Wu, H., Zeng, Y., Shui, W., Zeng, J., and Zhang, X. (2020b). Freeze-Thaw cycle representation alters response of watershed hydrology to future

climate change. Catena, 195, 104767. https://doi.org/10.1016/j.catena.2020.104767

Wu, Y., Liu, S., and Abdul-Aziz, O. I. (2012a). Hydrological effects of the increased CO_2 and climate change in the Upper Mississippi River Basin using a modified SWAT. Climatic Change, 110, 977–1003. https://doi.org/10.1007/s10584-011-0087-8.

Wu, Y., Liu, S., and Gallant, A. L. (2012b). Predicting impacts of increased CO_2 and climate change on the water cycle and water quality in the semiarid James River Basin of the Midwestern USA. Science of The Total Environment, 430, 150–160. https://doi.org/10.1016/j.scitotenv.2012.04.058.

Yang, Q., Meng, F.-R., Zhao, Z., Chow, T. L., Benoy, G., Rees, H. W., and Bourque, C. P.-A. (2009b). Assessing the impacts of flow diversion terraces on stream water and sediment yields at a watershed level using SWAT model. Agriculture, Ecosystems and Environment, 132(1–2), 23–31. https://doi.org/10.1016/j.agee.2009.02.012.

Yifru, B.A., Chung, I.-M., Kim, M.-G., and Chang, S.W. (2021). Assessing the effect of land use/land cover and climate change on water yield and groundwater recharge in East African rift valley using integrated model. Journal of Hydrology: Regional Studies, 37, 100926. https://doi.org/10.1016/j.ejrh.2021.100926

Yin, G., Wang, G., Zhang, X., Wang, X., Hu, Q., Shrestha, S., and Hao, F. (2022). Multi-scale assessment of water security under climate change in North China in the past two decades. Science of The Total Environment, 805(20), 150103. https://doi.org/10.1016/j.scitotenv.2021.150103

Yin, L., Feng, X., Fu, B., Wang, S., Wang, X., Chen, Y., Tao, F., and Hu, J. (2021). A coupled human-natural system analysis of water yield in the Yellow River basin, China. Science of The Total Environment, 762(25), 143141. https://doi.org/10.1016/j.scitotenv.2020.143141

Zhao, Z., Benoy, G., Chow, T.L., Rees, H.W., Daigle, J.-L., and Meng, F.-R. (2010). Impacts of accuracy and resolution of conventional and LiDAR-based DEMs on parameters used in hydrologic modeling. Water Resources Management, 24, 1363–1380. https://doi.org/10.1007/s11269-009-9503-5

Zheng, F., Lobb, D. and Li, S. (2021). A plot study on the effects of water eroded channels on tillage translocation. Soil and Tillage Research, 213, 105118. https://doi.org/10.1016/j.still.2021.105118

SUPPLEMENTARY MATERIAL

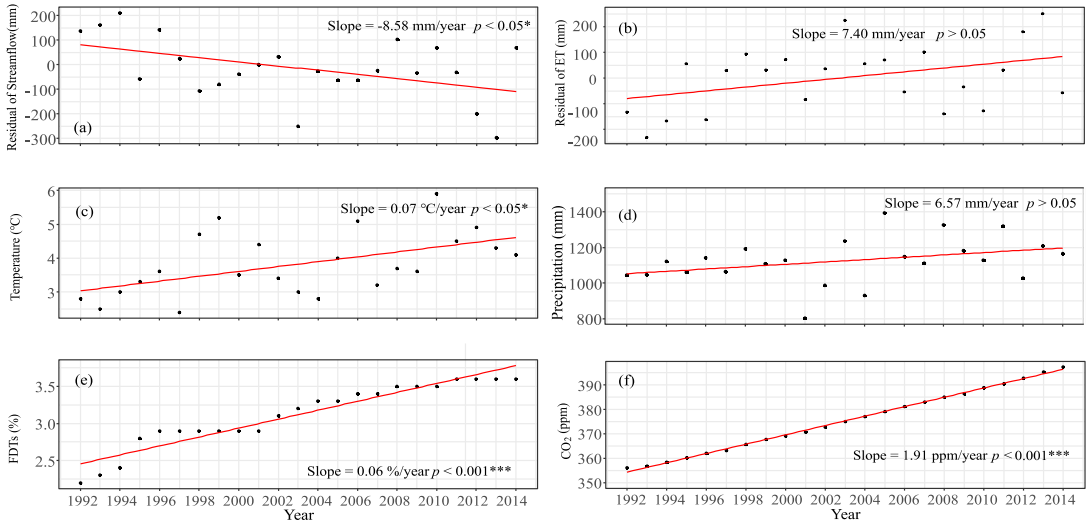

Fig. S3.1 Time trends in variables, including (a) residual of streamflow (mm), (b) residual of ET (mm), (c) temperature (°C), (d) precipitation (mm), (e) $\log_e$-transformed % watershed area protected with FDTs, or ln [FDT (%) +1], and (f) CO_2 concentration (ppm). The slope of the trend and its significance level accounted being p<0.001 (denoted by ***), 0.01 (**), and 0.05 (*) were attached on the corner of each plot.

Table S3.1 Coefficients of multiple linear regression as derived from pairwise relationships between the **residuals of streamflow** and selected explanatory variables (1992–2014).

Variable	Mean	Std. Error	t-value	Pr (> |t|)	Pr (> F)
Eq. (a) Residuals ~ *f* (CO_2, FDTs)					
Intercept	424.64	1727.82	0.246	0.808	
CO_2	0.06	6.08	0.010	0.992	0.074
FDTs	-146.01	188.06	-0.776	0.447	
Eq. (b) Residuals ~ *f* (FDTs)					
Intercept	441.97	183.76	2.405	0.026*	0.021*
FDTs	-144.21	57.65	-2.501	0.021*	

Note: The response variable is the residual (residual = measured - predicted streamflow determined with SWAT); Explanatory variables include ambient CO_2 concentrations, $\log_e$-transformed % watershed area protected with FDTs, or ln [FDT (%) +1]. Student t-tests were performed on the means of estimates. The significance levels are $p<0.001$ (denoted as ***), 0.01 (**), and 0.05 (*).

Table S3.2 Coefficients of multiple linear regression as derived from pairwise relationships between the **residuals of ET** and selected explanatory variables (1992–2014).

Variable	Mean	Std. Error	t-value	Pr (> |t|)	Pr (> F)
Eq. (a) Residuals ~ *f* (CO_2, FDTs)					
Intercept	-143.26	1815.05	-0.079	0.938	
CO_2	-0.90	6.39	-0.140	0.890	0.152
FDTs	152.42	197.56	0.772	0.449	
Eq. (b) Residuals ~ *f* (FDTs)					
Intercept	-396.41	193.13	-2.052	0.053.	0.0499*
FDTs	126.10	60.59	2.081	0.0498*	

Note: The response variable is the residual (residual = measured - predicted ET determined with SWAT); explanatory variables include ambient CO_2 concentrations, $\log_e$-transformed % watershed area protected with FDTs, or ln [FDT (%) +1]. Student t-tests were performed on the means of estimates. The significance levels are $p<0.001$ (denoted as ***), 0.01 (**), and 0.05 (*).

CHAPTER 4

AN INTER-WATERSHED COMPARISON OF HYDROLOGICAL RESPONSE IN AGRICULTURE- AND FOREST-DOMINATED WATERSHEDS IN ATLANTIC CANADA

Kang, X., Qi, J., Bourque, C. P.-A., Li, S., Jin, C., Hao, S., Meng, F.-R. (2024). An inter-watershed comparison of hydrological response in agriculture- and forest-dominated watersheds in Atlantic Canada. *Under Revision*.

Abstract

It is a common belief that large, canopy trees consume greater amounts of water than short-statured vegetation because of their increased rates of transpiration. In general, raised evapotranspiration rates within forested watersheds usually translates into an overall reduction in streamflow and groundwater recharging potential. These relationships have raised concern that large-scale reforestation projects may lessen local-to-regional water supplies. However, field experiments meant to compare streamflow patterns in agricultural and forested watersheds have produced inconclusive results, largely because of the extreme variability in regional weather and complex interactions amongst the biophysical factors that influence the hydrological characteristics of watersheds. In this study, we used an integrated hydrological model, i.e., the Soil and Water Assessment Tool (SWAT), to disentangle the complex interactions of biophysical factors that influence streamflow discharge rates by analyzing the hydrological responses in three neighboring watersheds in the upper Saint John River basin in northwestern New Brunswick, Atlantic Canada, with two of the watersheds being predominantly forested and one dominated by agriculture. In contrast to common belief, we found that the two forested watersheds consistently produced higher water yields compared to the agricultural watershed. With the application of SWAT, we found that the forested watersheds had lower peak flow during the snowmelt seasons, with peak flow delayed by at least 7–17 days compared to the incidence of peak flow in the agricultural watershed. Reduction in peak and enhanced accumulated flow in the two forested watersheds (+2.8–15.6% more) occurred mostly as a function of the prolonged snowmelt season associated with increased sublimation and shading provided by forests. Additionally, low waterflow during the warm seasons was consistently greater

in the forested watersheds, most likely due to increased infiltration rates and shallow groundwater recharging. The findings have profound implications for landcover conversion, especially as they concern flood-control and water-resources planning.

Keywords: agriculture- and forest-dominated watersheds; landcover conversion; streamflow modeling; water yields

4.1 Introduction

Large-scale landuse changes can lead to significant changes in the hydrological cycle (Jin et al., 2023), including the severity and frequency of flooding, and decline in accessible water resources (Xia et al., 2017; Yang et al., 2021). This is because landcover change can affect water yields by altering surface runoff, soil infiltration capacity, groundwater recharge and discharge, as well as other hydrological flows, further influencing water quality and river/stream flow dynamics (Hurkmans et al., 2009; Kiptala et al., 2013; Yu and Bourque, 2022). It is commonly believed that large canopy trees consume immense amounts of water because of their increased rates of transpiration. Enhanced transpiration at the watershed scale can lead to reductions in available water for both streamflow and groundwater recharging (Zhang et al., 2017; Zhang and Wei, 2021). These trends have raised concerns that large-scale reforestation projects may augment water losses at the landscape level (Lu et al., 2018; Ricciardi et al., 2022). Conventional experiments meant to compare streamflow in agricultural and forested watersheds have produced inconclusive results (Zhang et al., 2017; Zhang and Wei, 2021; Teo et al., 2022). This is because different vegetation-cover types can result in varied watershed responses due to their differences in the interception of rain and snow (Crockford and Richardson, 2000; Carlyle-Moses and Gash, 2011), rates of evapotranspiration (ET; Bearup et al., 2014), and shading (Yaseef et al., 2010; Johnson and Wilby, 2015), which can naturally lead to differences in surface runoff, groundwater discharge, and irrigation diversion, even when subjected to similar climatic conditions (Truong et al., 2022). In addition, this effect varies across regions (Zhou et al., 2015; Wang et al., 2018), being more pronounced in tropical areas (Randow et al., 2004) than in mid- or high-latitude positions (Duveiller et al., 2018). For example, some

studies have shown that ET in forests was generally lower (Williams et al., 2012; Breil et al., 2021) than in watersheds dominated by other types of vegetation, causing streamflow to increase. Given differences in forcing variables and watershed response globally, addressing water-yield production under different landcover types is an important scientific undertaking. However, such studies have been seldom applied to watersheds in Atlantic Canada, a region known for its maritime climate of ample seasonal precipitation, long snow-accumulation and snowmelt seasons, and moderate temperatures.

Recent studies have mostly focused on addressing the impact of vegetation change on hydrological processes in single watersheds at variable timescales (Brown et al., 2005). These results are not comparable because of divergent weather conditions that normally occur over large geographic areas. To address this problem, paired-watershed studies are often used to determine the magnitude of water yield changes resulting from changes in vegetation cover in one of the watersheds. The second watershed is typically used as an experimental control. These types of experiments can be extended to study the role of land management practices in their impact on water yields. However, watersheds selected for these studies may vary in other hydrological drivers unfamiliar to the researchers, such as routing pathways, soil characteristics, and other influencing factors (Robbie and Younes, 2023). The variations in biophysical conditions that affect hydrological processes are significant, making it difficult to obtain sufficient field measurements, because acquiring such measurements is time-consuming and expensive. Additionally, differences in hydrological responses, if any, can only be assessed over short time intervals (Schmidt et al., 1998).

Integrated hydrological models are often used to evaluate the effects of diverse landuse management practices on streamflow and water quality (Viney et al., 2009; Dwarakish and Ganasri, 2015; Gunacti et al., 2023). A properly calibrated hydrological model can facilitate the evaluation of landuse change on water resources, effectively functioning as a decision-support tool (Qi et al., 2018, 2022). When field measurements are missing or scarce, regionalization of model parameters, based on physical similarity, can be used in model calibration and subsequent validation (Mengistu et al., 2019; Qi et al., 2022). Regionalization assumes that watersheds with similar physiographic and climatic conditions and vegetation cover should have near-similar hydrological response (Mengistu et al., 2019). From an opposing viewpoint, when watersheds share similar physiographic and climatic conditions, excluding vegetation-cover effects, the approach can be used to evaluate differences in watershed hydrological response as a function of vegetation type and extent of cover. Along this line of thinking, an innovative approach is presented for investigating differences in hydrological responses in agricultural and forested watersheds. This method takes advantage of an integrated hydrological model to account for natural variations in biophysical factors, other than vegetation, that can affect the hydrological response of watersheds. While the impacts of physiographic, soil, and climatic conditions are being accounted for by these integrated models, the remaining variances in hydrological responses (regarding changes in water yield) can be attributed to differences in forest and agricultural cover. The Soil Water Assessment Tool (SWAT; Arnold et al., 1998) is applied in my assessment of hydrological control provided by vegetation cover. Here, SWAT is validated with regionalized parameters particular to

northwestern New Brunswick (Atlantic Canada) established with the automatic calibration of the model.

The main objective of this research is to analyze the disparities in hydrological response between agricultural and forested watersheds in Atlantic Canada. Specifically, we developed an innovative calibration approach to compare hydrological responses in three neighboring watersheds in the upper Saint John River (Wolastoq) basin, with two of the watersheds being predominantly forested and one dominated by agriculture. In this study we also tried to identify potential problems encountered in the use of SWAT in analyzing the hydrological response in the three watersheds.

4.2 Materials and Method

4.2.1 Study Area

The upper Saint John River (USJR, Wolastoq) basin upstream from the capital city of New Brunswick (NB), Fredericton (45.96° N, 66.64° W), covers a large land area of approximately 41,179 km^2 and spans the jurisdictions of NB, Quebec, and Maine, USA (Fig. 4.1). The USJR basin falls within the Atlantic Maritime Ecozone of Canada and the New England-Acadian Forests Zone of the USA. Three gauged watersheds in the USJR basin were selected for this study, including (i) Black Brook (BBW; Fig. 4.1a; with its outlet at 47.2° N, 67.8° W), (ii) Grande Rivière (GRW, Fig. 4.1b, 47.2° N, 67.9° W), and (iii) Iroquois River watersheds (IRW, Fig. 4.1c, 47.5° N, 68.4° W).

Black Brook Watershed is in the northwestern section of NB, with elevations ranging from 150–242 m above mean sea level (ASL). The land is dominated by agricultural fields associated with the production of potatoes (Fig. 4.1a). The annual precipitation is 1,132.7

mm, with about one third falling in the form of snow. Most snowmelt occurs in spring (typically from early March to mid-May) and is a major source of surface runoff and groundwater recharge in the area (Chow and Rees, 2006; Qi et al., 2017a). The annual mean temperature in the area is about 3.8 °C. The drainage area covers about 13.1 km^2, with agricultural fields, forests, and wetlands accounting for 72.7, 16.5, and 1.7% of the total watershed area (Chow et al., 2011; Table 4.1). Soils in BBW are classified as Podzol, Regosol, or Luvisol based on the Canadian soil classification system (Mellerowicz, 1993). These soils are developed from glacial till and are generally very stony. Soil texture ranges from sandy loam, loam, to clay loam.

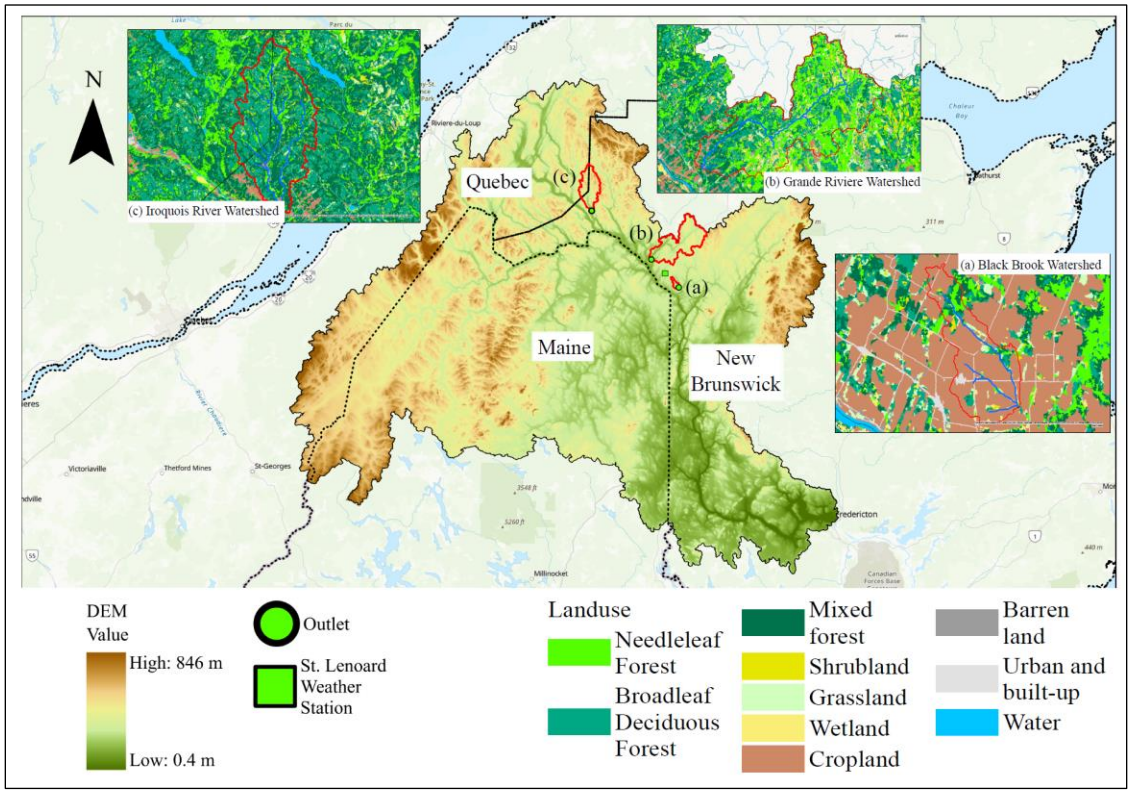

Fig. 4.1 Study area with the three gauged watersheds outlined. The watersheds include (a) Black Brook (BBW), (b) Grande Rivière (GRW), and (c) Iroquois River watersheds (IRW), including their respective outlets, landcover, and a nearby weather station.

Grande Rivière Watershed is north of BBW, with elevations ranging from 140–475 m ASL (Fig. 4.1b). The watershed is dominated by forests, which account for more than 75% of the total drainage area (i.e., 370.1 km^2; Table 4.1). Forest cover in GRW is mostly associated with needleleaf forest species (Fig. 4.1, Table S4.1 in Supplementary Material). Local climatic conditions are very close to that of BBW, with very similar annual total precipitation and mean temperature.

Iroquois River Watershed is in the northern-most part of the USJR basin with elevations ranging from 160–515 m ASL (Fig. 4.1c). The dominant landcover in IRW is deciduous and mixedwood forests, with the total forested area accounting for about 90% of the drainage area (i.e., 183 km^2; Table 4.1 and S4.1). Annual total precipitation and mean air temperature in IRW is about 1,032.1 mm and 3.7 ℃, respectively.

Table 4.1 Attributes of the three gauged watersheds in the USJR basin for an average hydrological year based on data from 1993–2014. Precipitation values in parentheses are based on Daymet *v.* 4.0 data (Thornton et al., 2022) averaged over the same time period. Longitude and latitude give the geographic location of hydrometric stations at each watershed outlet.

Watershed	Long.	Lat.	Elevation Range	Area	Forest	Agriculture	Mean Precipitation	Mean Temperature	Mean Streamflow
	°	°	m ASL	km^2	%	%	mm	℃	mm
BBW	-67.8	47.2	150–242	13.1	16.5	72.7	1132.8 (1139.6)	3.8	642.5
GRW	-67.9	47.2	140–475	370.1	76.8	2	1132.8 (1139.6)	3.8	701.1
IRW	-68.4	47.5	160–515	183.4	90.6	1.3	(1031.5)	3.7	677.0

4.2.2 Model development and setup

Among the many hydrological models available, SWAT is widely used to simulate hydrological processes as affected by landuse and landcover change (e.g., Wang et al., 2020; Saravanan et al., 2022; Chen et al., 2023). SWAT is a semi-distributed model used to simulate hydrological processes at the watershed scale (Neitsch et al., 2011). Recently,

SWAT was extended to evaluate climate change impact on forested watersheds (Yang and Zhang, 2016). SWAT segments target watersheds into hydrological response units (HRUs), based on intersecting digital elevations extracted from a digital elevation model (DEM) of the area, variation in landuse and landcover, and soil-type data in formulating zones of hydrological similarity. SWAT uses the HRU as a fundamental unit in which waterflow is predicted and aggregated at the watershed level by means of DEM-identified routing channel ways. Amounts of surface runoff and infiltration are calculated based on the Soil Conservation Service curve number (CN). The CN-numbers are updated based on soil permeability, landuse type, and antecedent soil water conditions. Water infiltrated into the soils is either delivered to water courses through lateral, shallow subsurface flow or is allowed to percolate to groundwater pools when soil water content exceeds field capacity. The groundwater portion is then (i) transported to streams and rivers through groundwater discharge (baseflow), (ii) percolated deeper underground to groundwater aquifers, or (iii) discharged to the soil profile.

Table 4.2 SWAT-specific input data and their sources.

Dataset	BBW	GRW and IRW
DEM	LiDAR	Dias et al. (2015), 20-m (https://apps.nationalmap.gov/downloader/)
Landcover	Landuse survey, BBW	2015 Landcover of Canada map, 30-m (https://open.canada.ca/data/en/dataset/)
Soil	NB-created soil map (Mellerowicz, 1993)	GeoNB-based forest soils (http://www.snb.ca/geonb1/e/dc/forestsoils.asp) Soil Landscape of Canada *v.* 2.2 map (https://sis.agr.gc.ca/cansis/nsdb/slc/v2.2/index.html)
Weather	St. Leonard Airport (ID: 8104928) and Agriculture and Agri-Food Canada Archives	St. Leonard Airport (ID: 8104928) and Agriculture and Agri-Food Canada Archives + Daymet data (https://daymet.ornl.gov/)
Discharge	Agriculture and Agri-Food Canada Archives	Natural Resources Canada (https://wateroffice.ec.gc.ca/)

The original version of SWAT (Neitsch et al., 2011) calculated soil temperature with an empirical equation based on warm climate conditions, and it was found to severely underestimate soil temperatures during winter in regions with substantial snow cover (Qi et al., 2016a, 2016b). Based on this, a physically-based soil temperature module was recently developed and subsequently integrated into the model to account for snow-related effects and soil freeze-thaw cycles (Qi et al., 2016a, 2016b, 2019). The enhanced version of SWAT has dramatically improved the prediction of hydrological processes in snow-dominated areas, including areas in Atlantic Canada (Wang et al., 2021). For additional detail concerning improvements to SWAT, refer to Neitsch et al. (2011) and Qi et al. (2016b).

Individual SWAT projects were developed for each of the three watersheds, i.e., BBW, GRW, and IRW. Model initialization was based on data provided in Table 4.2. The model

project for BBW was initialized with individual HRUs explicitly representing farms and best management practices (BMPs) defined from long-term records reported in Qi et al. (2017b). Since BBW is an agriculture-dominated watershed, field-level landuse information on crop rotation, fertilizer usage, management practices, planting and harvesting dates, and crop yields for individual farms had been collected by means of annual surveys conducted since 1992 (Liang et al., 2019). For the two remaining watersheds, a 2015 landcover map of Canada (Table 4.2) was used to characterize the vegetation cover within individual HRUs. High-resolution DEMs were used to describe the topography (i.e., at 1-m resolution for BBW and 20-m for both GRW and IRW), based on elevations collected with airborne light detection and ranging technology (LiDAR; Qi et al., 2016a, 2016b) for BBW and Dias et al. (2015) for the other two watersheds. Soil data were extracted from a detailed soil survey map created for BBW (Mellerowicz, 1993), as well as data available from GeoNB (provincial government data portal) and a Soil Landscape map of Canada *v.* 2.2 for GRW and IRW (Table 4.2). Discharge data from 1992–2014 were acquired for all three watershed outlets (i.e., hydrometric stations) by accessing data from Agriculture and Agri-Food Canada for BBW and Natural Resources Canada for the other two watersheds (Table 4.2). Weather data for both BBW and GRW, particularly daily precipitation, air temperature, relative humidity, solar radiation, and wind speed, were acquired for the 1992–2014 period from the Saint Leonard Airport weather station (47.2° N, 67.8° W) located approximately 5-km from BBW (Fig. 4.1). Additional weather data were acquired from Agriculture and Agri-Food Canada data archives. Due to the remoteness of the third watershed, the model project for IRW was based on daily surface weather data acquired as point extractions of Daymet *v.* 4.0 data (Thornton et al., 2022),

provided at 1-km resolution (Table 4.2). A field-based calculation of ET (i.e., Calculated-ET) was obtained as a direct comparison to SWAT-generated estimates of ET (see below). We also acquired products of ET at 1-km resolution from the Global LAnd Surface Satellite (GLASS) data archive, found at http://www.glass.umd.edu/Download.html, for additional comparisons. The final ET-based products were derived from multi-model ensembles for the 2000–2018 period, including products based on Bayesian Model Averaging (BMA; Yao et al., 2014), merging five ET-products associated with (i) the MODIS-sensor (i.e., MOD16; Mu et al., 2011), (ii) a version of ET-calculated from a remote-sensing-based-application of the Penman-Monteith equation (i.e., RRS-PM; Yuan et al., 2010), (iii) Priestley-Taylor-equation-based application (i.e., PT-JPL; Fisher et al., 2008), (iv) modified satellite-based application of the Priestley-Taylor equation (i.e., MS-PT; Yao et al. 2013), and (v) an application of a semi-empirical version of the Penman equation embraced by the University of Maryland (i.e., UMD-SEMI; Wang et al., 2010).

4.2.3 Parameter regionalization and manual recalibration

Streamflow discharge at an outlet can vary according to variations in topography (T), soil type (S), climate (C), landuse and landcover (L), and other environmental factors (ε). We grouped the parameters in a hydrological model in corresponding sets of parameters, e.g., a for topography, b for soil, c for climate, and d for landuse and landcover. Here, ε stands for the other and not so well-defined governing variables in SWAT, i.e.,

$$Streamflow = f(aT, bS, cC, dL, \varepsilon). \quad (4.1)$$

For a gauged agricultural watershed, we calibrated multiple parameters to reduce bias between measured and predicted streamflow, such that,

$$Streamflow^{A} = f(a^{A}T^{A}, b^{A}S^{A}, c^{A}C^{A}, d^{A}L^{A}, \varepsilon), \quad (4.2)$$

where superscript A pertains to the "agricultural watershed". The principle of parameter regionalization is that the calibrated parameters for a designated, gauged watershed (in this case, BBW) can be directly used in the simulation of hydrological processes in neighboring watersheds (i.e., GRW and IRW; Garna et al., 2023). Consequently, streamflow for the forested watersheds can be simulated as

$$Streamflow^{F} = f(a^{A}T^{F}, b^{A}S^{F}, c^{A}C^{F}, d^{A}L^{F}, \varepsilon), \quad (4.3)$$

where superscript F pertains to the "forested watersheds". Based on the parameter regionalization principle, we can assert that $T^{F} = T^{A}$, $S^{F} = S^{A}$, and $C^{F} = C^{A}$. As a result, the differences in modeled and observed streamflow in the forested watersheds can be ascribed largely to differences in landuse and landcover, and as such $L^{F} \neq L^{A}$. To reduce streamflow bias for the forested watersheds, we need to recalibrate the model parameters, such that,

$$Streamflow^{F'} = f(a^{F}T^{F}, b^{F}S^{F}, c^{F}C^{F}, d^{F}L^{F}, \varepsilon), \quad (4.4)$$

where $Streamflow^{F'}$ stands for the prediction of streamflow after manual recalibration. Contrasting model simulations forced with the agriculture-based set of parameters (i.e., AP, as emphasized in Eq. 4.3) with those for the forest-based parameters (i.e., FP, in Eq. 4.4), we can uncover disparities between watershed-level streamflow response associated with differences in landcover. This approach is innovative as it enhances our comprehension of hydrological mechanisms across varied ecosystems by means of a systematic calibration of SWAT (Arnold et al., 2012).

4.2.4 SWAT calibration and validation specific to BBW

All streamflow-related parameters in SWAT (Table S4.2) were estimated by conducting the following steps, namely (i) theoretical analysis (Arnold et al., 2012), (ii) literature review (Tang et al., 2012; Qi et al., 2016a, 2016b, 2017a; Aloui et al., 2023; Rocha et al., 2023), and (iii) model sensitivity analysis. For calibration of the model project for BBW, automatic methods were employed based on an application of Calibration and Uncertainty Procedures (SWAT-CUP) and Sequential Uncertainty Fitting algorithm *v.* 2 (SUFI-2). SUFI-2 is seen as an inverse modeling algorithm noted for its enhanced computational efficiency (Yang et al., 2008; Abbaspour et al., 2015). With the SUFI-2 algorithm, the parameter value ranges were narrowed with every successive iteration, always centered on finding the parameter set that minimized the objective function (Abbaspour et al., 2004 and 2015). After several iterations, the parameter set found was then used in the validation of SWAT. The calibrated parameter set from this calibration (referred to later as the agriculture-based parameters, AP; Table S4.2) was subsequently applied to the two forested watersheds (Section 4.3). These same parameter sets were later manually changed according to the parameters' specific roles in governing modeled watershed processes, including the processes of ET, snowmelt, and groundwater discharge (designated as ET-, SNO-, and GW-parameters, abbreviated here as EP, SP, and GP; Table S4.3). Finally, all these manually changed parameters were grouped together and treated as the forest-based parameters (designated here as FP).

In this study, model calibration was carried out from 1992–2001, whereas data from 2002–2014 were used in model validation. A 3-year model warm-up phase from 1989–1991 was used. When exploring the hydrological response of watersheds, the observed and

simulated hydrological simulations were divided into two distinctive periods according to the calendar year, namely: (i) the **snowmelt season,** defined from March–May [i.e., day of year (DOY) = 60–151], and (ii) the **dry, warm season**, from July–September (i.e., DOY = 182–273). When evaluating the annual hydrological response, the **hydrological year**, defined as the period from October of the previous year to September of the current year for 1993–2014, was used. Additionally, we obtained a field-based calculation of ET directly by taking the difference between total precipitation and streamflow measurements.

4.2.5 Model performance evaluation and statistical analysis

Model performance pertaining to streamflow simulations was assessed according to percent bias ($PBIAS$), coefficient of determination (R^2), and Nash-Sutcliffe (NSE) and Kling-Gupta modeling efficiencies (KGE; Knoben et al., 2019). For NSE and $PBIAS$, model performance criteria were based on those reported in Moriasi et al. (2007) and reproduced in Table 4.3. When greater than 0.5, both R^2 and KGE pointed to adequate model performance. All model-performance statistics were evaluated with the R-package, *hydroGOF*. Their evaluation was based on the following expressions,

$$PBIAS = 100 \times \frac{\sum_{i=1}^{N}(P_i - O_i)}{\sum_{i=1}^{N} O_i} \tag{4.5}$$

$$R^2 = \left(\frac{\sum_{i=1}^{n}(O_{i-}O_{avg})\cdot(P_i - P_{avg})}{[\sum_{i=1}^{n}(O_{i-}O_{avg})^2 \cdot \sum_{i=1}^{n}(P_i - P_{avg})^2]^{0.5}}\right)^2 \tag{4.6}$$

$$NSE = 1 - \frac{\sum_{i=1}^{n}(O_i - P_i)^2}{\sum_{i=1}^{n}(O_{i-}O_{avg})^2}, \text{ and} \tag{4.7}$$

$$KGE = 1 - \sqrt{(r-1)^2 + (\alpha - 1)^2 + (\beta - 1)^2} \tag{4.8}$$

where O_i and P_i are the observed and modeled data, O_{avg} and P_{avg} their corresponding averages, r the linear correlation between observed and modeled data, α the flow variability error, and β the bias term.

Table 4.3 Model performance criteria following Moriasi et al. (2007).

Performance Rating	*PBIAS*	NSE
Very good	$\lvert PBIAS \rvert < 10$	0.75 < NSE < 1.00
Good	$10 < \lvert PBIAS \rvert < 15$	0.65 < NSE < 0.75
Satisfactory	$15 < \lvert PBIAS \rvert < 25$	0.50 < NSE < 0.65
Unsatisfactory	$\lvert PBIAS \rvert > 25$	NSE < 0.5

The Wilcoxon Signed Rank Test, as a nonparametric equivalent of the paired t-test, was used here to evaluate the hydrological differences between agricultural and forested watersheds (Scheff, 2016). The procedure was performed directly in Origin 2023b with the strength of statistical significance characterized according to critical p-values of 0.001 (designated by ***), 0.01 (**), and 0.05 (*).

4.3 Results

4.3.1 BBW-model project performance

Figure 4.2 gives the measured and SWAT-based predictions of monthly streamflow for BBW during the calibration and validation periods. Best-fitting model parameters are given in Table S4.3. SWAT-based predictions of streamflow generally agreed with the measurements at a monthly scale for both periods. Measured and predicted accumulated streamflow were generally in agreement for most of the 23 years (1992–2014). Overall, model predictions during calibration and validation were largely satisfactory, yielding *PBIAS* = 1.1 and 13.3%, NSE = 0.61 and 0.76, R^2 = 0.62 and 0.78, and KGE = 0.64 and 0.77, respectively (Fig. 4.2 and Table 4.3).

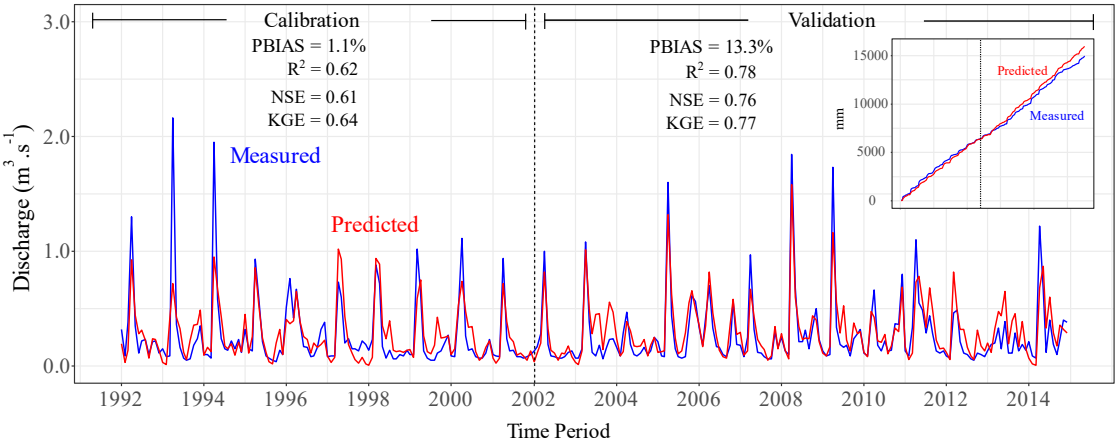

Fig. 4.2 Measured and SWAT-based predictions of monthly streamflow for BBW for both model project calibration (with data from 1992–2001) and validation (2002–2014). Accumulated streamflow for both periods is depicted in the inset. The dash vertical line defines the point of transition between the calibration and validation phases of the research.

4.3.2 Model-project performance with stepwise calibration

Figures 4.3 and 4.4 provide timeseries of measured and SWAT-based predictions of monthly streamflow for the two forested watersheds, as well as their accumulated streamflow, with different model parameters adjusted according to various hydrological processes (Table S4.3). When applying the agriculture-based parameters (i.e., AP) in the simulation of streamflow, model predictions for both forested watersheds were substantially lower than those measured in the field (Fig. 4.3 and 4.4). These underestimations became more evident when viewing the accumulated streamflow for each watershed. These underestimations were reflected in *PBIAS* of -15.0 and -34.7% for GRW and IRW, respectively (Fig. 4.3 and 4.4). Modeled monthly fluctuations in streamflow were generally poorly simulated, yielding inferior performance scores.

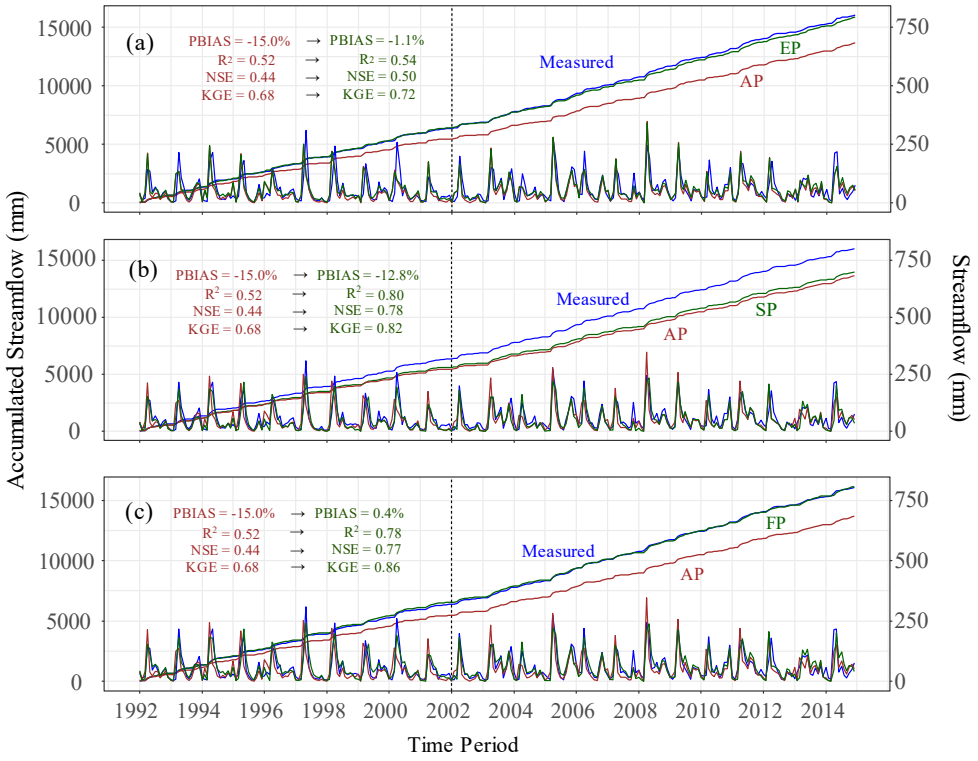

Fig. 4.3 Measured and SWAT-based predictions of accumulated streamflow (mm, y-axis to the left) and unit area streamflow (mm, y-axis to the right) for GRW governed by variations in process-based groupings of parameters (identified above) during the 1992–2014 period. Model performance was evaluated for each modification of the GRW-based model project with stepwise manual calibration. The dash vertical lines define the point of transition between the calibration and validation phases of the research. ET-, SNO-, agriculture-, and forest-based parameters are abbreviated as EP, SP, AP, and FP.

While conducting stepwise manual calibration of the model projects for GRW and IRW, we observed that overestimations in ET led to underestimation of streamflow. After manually adjusting the ET-based parameters (Table S4.3), *PBIAS* reduced from -15.0 to -1.1% for GRW and -34.7 to -5.4% for IRW (Fig. 4.3a and 4.4a). Model performance indices R^2, NSE, and KGE also improved for both simulations (Fig. 4.3a and 4.4a). Adjusting the SNO-based parameters (Table S4.3) highlighted the discrepancies in snowmelt processes between agriculture- and forest-dominated watersheds, having significant effects on the

calculations of R^2, NSE, and KGE, while only marginally influencing *PBIAS* (Fig. 4.3b and 4.4b). The prior mismatch between measured and predicted peak flows was reduced with the adjustment of the SNO-based parameters (Fig. 4.3b and 4.4b). Finally, a joint adjustment in both ET- and SNO-based parameters (yielding the forest-based parameters, FP, in Fig. 4.3c and 4.4c) improved model-project performances from unacceptable to satisfactory for both GRW and IRW. Improvements in model performance were reflected in all statistical criteria associated with both watersheds (Table 4.3).

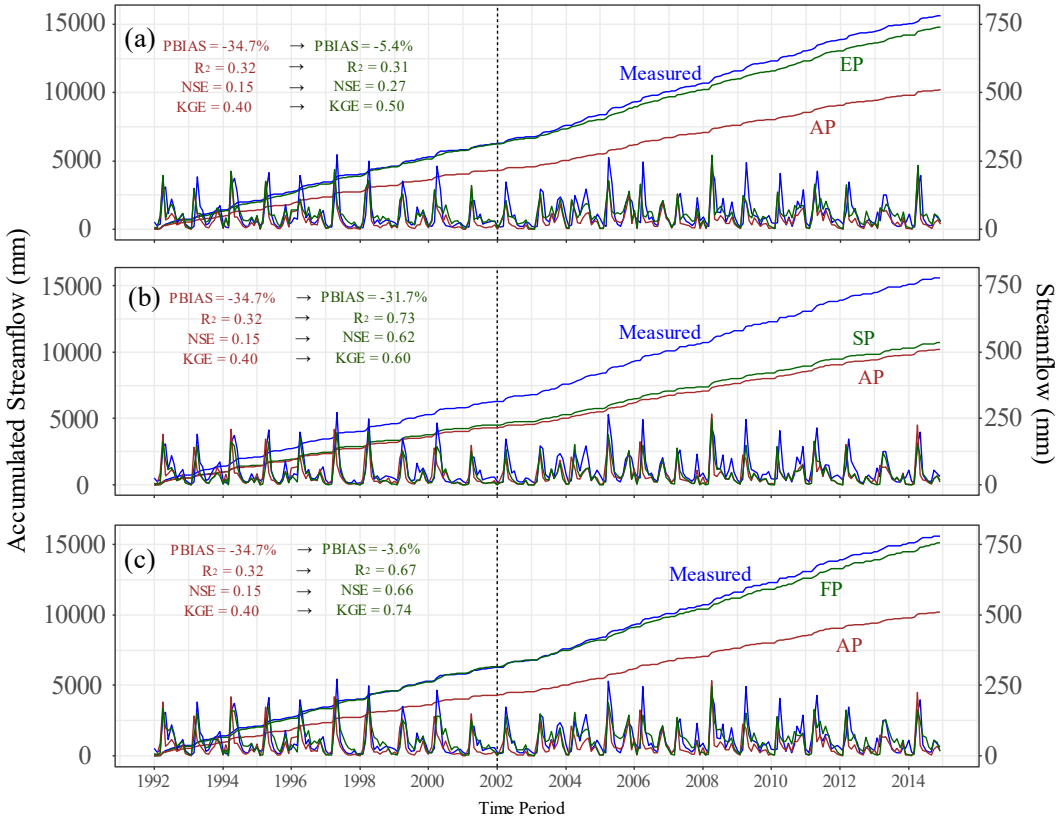

Fig. 4.4 Measured and SWAT-based predictions of accumulated streamflow (mm, y-axis to the left) and unit area streamflow (mm, y-axis to the right) for IRW governed by variations in process-based groupings of parameters (identified above) during the 1992–2014 period. Model performance was evaluated for each modification of the IRW-based model project with stepwise manual calibration. The dash vertical lines define the point of transition between the calibration and validation phases of the research. ET-, SNO-, agriculture-, and forest-based parameters are abbreviated as EP, SP, AP, and FP.

4.3.3 Differences in streamflow

4.3.3.1 Hydrological-year differences

Watershed-outlet measured and predicted streamflow are illustrated in Fig. 4.5a, 4.5b, and 4.5c for all hydrological years (1993–2014). Two simulations of streamflow were driven by different sets of parameters for the model projects for GRW and IRW, i.e., agriculture- and forest-based parameters (AP and predicted; Fig. 4.5). Significant differences (p<0.01) were found between simulation-scenarios governed by AP and 'predicted' for both forested watersheds. When comparing the measured streamflow only, the forested watersheds generally provided elevated streamflow rates than those produced by BBW. Likewise, predicted streamflow rates were generally greater when governed by the array of FP. Predictions in accumulated streamflow for GRW and IRW were 107.5±22.7 and 212.8±22.7 mm, respectively.

4.3.3.2 Differences in accumulated low flow during the dry, warm season

Figures 4.5g, 4.5h, and 4.5i provide both measured and predicted accumulated low flow rates during the dry, warm seasons from 1993–2014 for the three watersheds. Predicted accumulated low flow, separately governed by the array of parameters for both AP and FP groupings are in Fig. 4.5h and 4.5i. SWAT did not predict accumulated low flow very well for all three watersheds. Measured accumulated low flow was greatest in the two forested watersheds. This feature was captured by SWAT when based on the input of FP. Significant difference in accumulated low flow was found to occur between simulations for both forested watersheds (p<0.01), with GRW and IRW yielding rates of 58.1±12.7 and 93.6±14.8 mm per dry season.

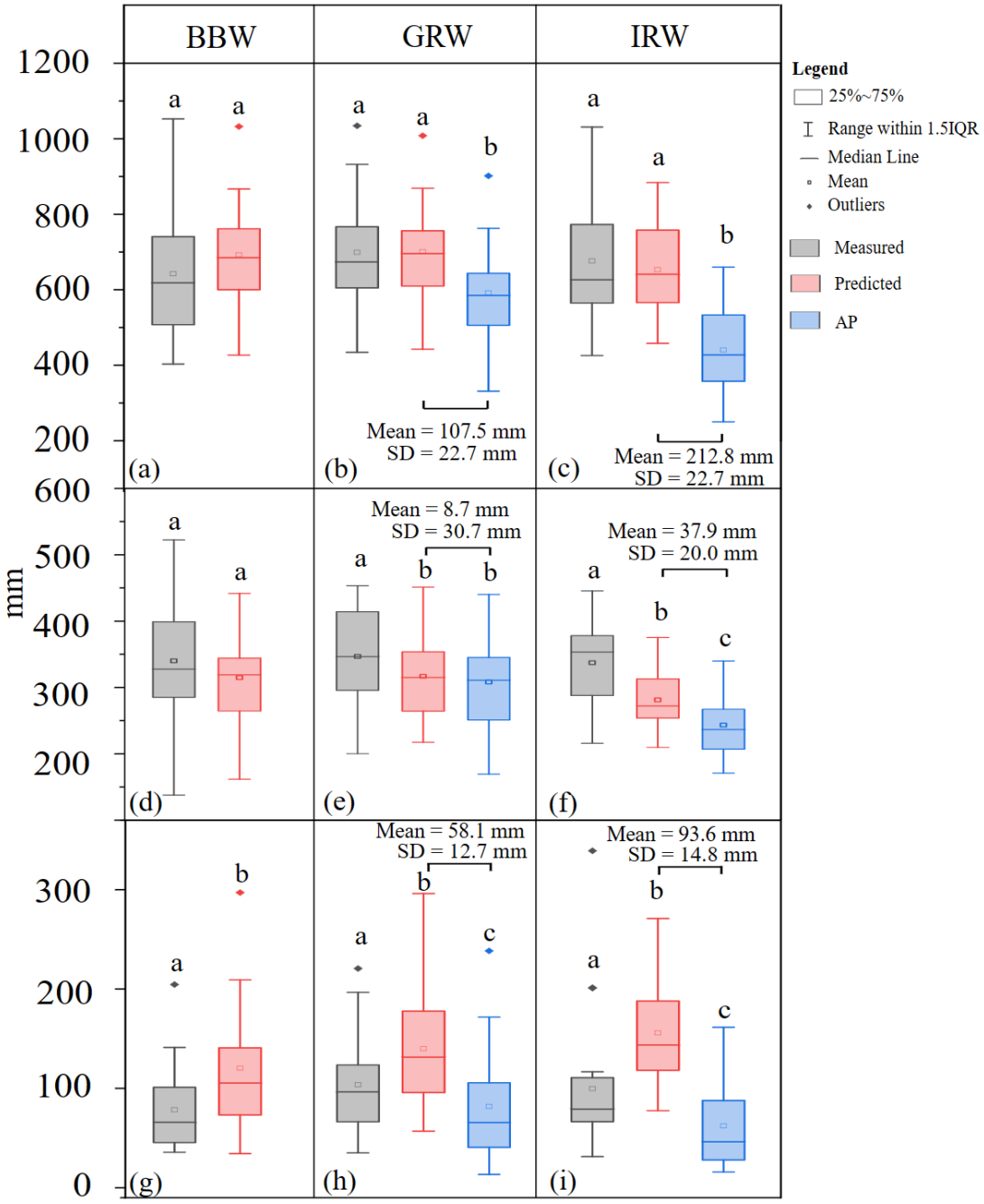

Fig. 4.5 Measured and predicted annual mean streamflow for all hydrological years (a–c), accumulated flow during the snowmelt seasons (d–f), and accumulated low flow during the dry, warm seasons (g–i) for the three watersheds. Predicted flows were governed by specific calibrations of model projects for BBW, GRW, and IRW (represented as 'predicted' in the figure) and agriculture-based parameters (AP), separately. Different letters above each boxplot represent the statistical significance at a critical *p*-level of 0.01; IQR stands for the interquartile range. Differences in mean and standard deviation (SD) for the different streamflow simulations for both GRW and IRW were also provided.

4.3.3.3 Differences in peak flow and accumulated streamflow during the snowmelt season

Figures 4.5d, 4.5e and 4.5f give the measured and predicted accumulated flow during the snowmelt seasons of 1993–2014 for all three watersheds based on simulations governed by both AP- and FP-grouping of parameters for GRW and IRW. SWAT using the AP-set of parameters was unable to predict accumulated flow very well during the snowmelt season. Measured and predicted accumulated flow rates were greatest for the forested watersheds. Accumulated peak flow for the two simulation-scenarios were 8.7±30.7 and 37.9±20.0 mm for GRW and IRW, respectively. When examining predicted volume and timing of peak flow based on the two sets of parameters (Table 4.4), simulations governed by AP for both GRW and IRW produced larger and earlier peak flows. Significant difference in peak flow occurrence (p<0.01) between simulations governed by the different sets of parameters was found in both watersheds. Peak flow tended to occur 7–17 days earlier for BBW than for the neighboring forested watersheds, GRW and IRW.

Table 4.4 SWAT-based predictions of volume (mm) and timing of peak flow (DOY) for GRW and IRW governed by either agriculture- or forest-based parameter sets (i.e., AP and FP) during the snowmelt season (i.e., March–May) of each hydrological year from 1993–2014.

Variables	GRW					IRW				
	AP		FP		*Sig.*	AP		FP		*Sig.*
	Mean	SD	Mean	SD		Mean	SD	Mean	SD	
Peak Flow (mm)	35.4	11.5	30.8	10.6	-	32.1	10.2	28.4	9.8	-
Timing of Peak Flow (DOY)	96.6	13	107.4	14.4	***	94.3	6.6	106	11.4	**

Note: Significance levels identified are p<0.001 (denoted as ***), 0.01 (**), and p>0.01 (nonsignificant, -).

4.3.4 Differences in evapotranspiration

Figure 4.6 gives the field-based calculation of ET (i.e., Calculated-ET) and SWAT-based predictions of annual mean ET governed by both AP and FP ('predicted', Fig. 4.6) for all three watersheds and individual hydrological years from 1993–2014. As expected, there were no significant differences between SWAT-based predictions and field-based calculations of average ET for all three watersheds. However, significant difference in ET was observed for GRW and IRW when governed by AP- and FP-set of parameters (p<0.01). Simulated ET-rates for both forested watersheds were greatest when based on the AP-set of parameters. Likewise, the field-based calculations of ET provided near-similar tendencies, with ET always being greatest for BBW. Significant differences were found to occur between BBW (+ GRW) and IRW for the field-based calculation of ET. SWAT-based predictions of ET mirrored this trend. Predictions of ET governed by AP and FP were 109.0±16.6 mm for GRW and 212.7±18.1 mm for IRW. Annual and monthly ET-based GLASS-products corroborated our findings throughout this study (Fig. S4.1). The related data in conjunction with field-based calculations of ET support the fact that agricultural watersheds consume more water by elevated ET compared to forested watersheds (Fig. S4.2; explanation provided in supplementary documents).

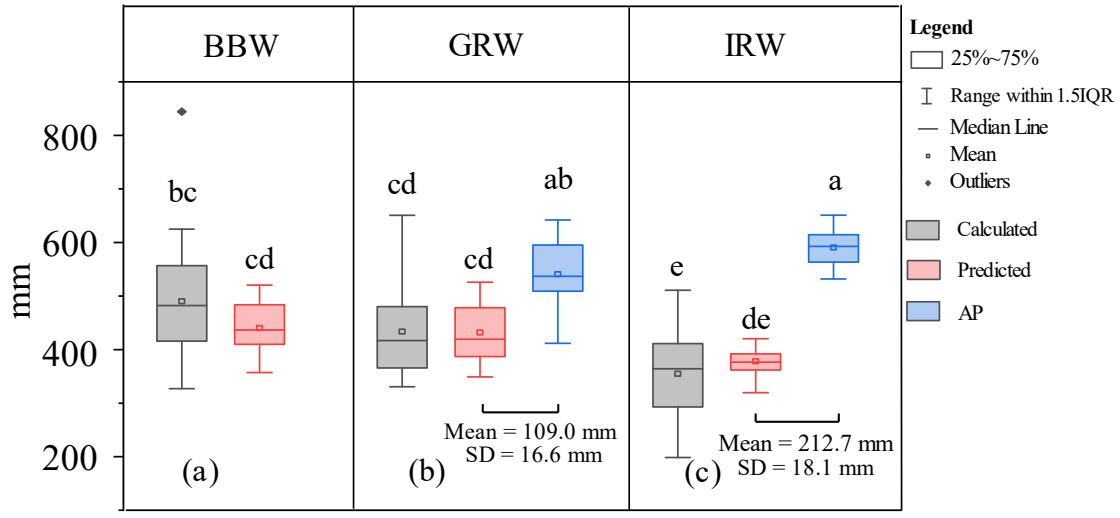

Fig. 4.6 Comparisons between field-based calculations and SWAT-based predictions of annual mean ET governed by parameters acquired from the individual calibrations of model projects for the three watersheds (represented as 'predicted') and agriculture-based parameters (i.e., AP), separately. Different letters above each boxplot represent the statistical significance at a critical *p*-level of 0.01; IQR stands for the interquartile range. Differences in mean and standard deviation (SD) for the various simulations of ET for both GRW and IRW are also provided.

4.4 Discussion

4.4.1 Model performance

SWAT performed reasonably well for BBW, exhibiting satisfactory to very good accuracy during both model calibration and validation. However, when associated parameter values (i.e., AP) were directly applied to the model projects for the two neighboring forested watersheds, SWAT failed to accurately predict stream discharge (Fig. 4.3 and 4.4) by severely underestimating the flow rate. This was consistent with the measured streamflow data acquired from the three watersheds, as illustrated in Fig. 4.5a, 4.5b and 4.5c. We found that the ET-parameters (i.e., EP) were generally responsible for the observed prediction biases, owing to the underestimation of late-summer low flow events (Fig. 4.3a and 4.4a). Also, the SNO-parameters (i.e., SP) were responsible for the

error observed in SWAT-based predictions of spring peak flow for the two forested watersheds (Fig. 4.3b and 4.4b).

A final model performance with the set of FP showed improved agreement between measured and predicted streamflow in terms of *PBIAS* for both forested watersheds, i.e., 0.4 and -3.6% for GRW and IRW, respectively (Fig. 4.3c and 4.4c). These results highlight the suitability of the current structure of SWAT for Atlantic Canada (Qi et al., 2017a; Liang et al., 2019). However, the underestimation of SWAT-based predictions of streamflow based on the AP-set of parameters indicates potential issues in the definition of hydrological characterization of forests within the model. This emphasizes the potential risk of current practices associated with assessing the impacts of reforestation and deforestation on streamflow dynamics by directly changing landcover types in the model.

4.4.2 Hydrological response in agricultural and forested watersheds

4.4.2.1 Streamflow and evapotranspiration

My results revealed that both measured and SWAT-based predictions of streamflow exhibited greater rates in forested watersheds because ET at the watershed scale was lower (Fig. 4.6). These results contradict the general belief that forests evaporate more water (e.g., Wang et al., 2014; Dias et al., 2015; Zhang et al., 2017; Zhang and Wei., 2021) due to the large, exposed leaf surface area and deeper roots (Breil et al., 2021). Differences in plant physiology of forested watersheds, for example, may cause variations in stomatal aperture and conductance in response to environmental conditions may substantially affect rates of transpiration. For instance, conifers like spruce, pine, and fir species, are largely adapted to cold, dry conditions and generally have lower transpiration rates than many food plants. They have various adaptations, such as waxy needles and thick cuticles, to help minimize

water losses (Shepherd and Wynne, 2006). However, as shown in Fig. 4.6, predictions of ET per hydrological year for GRW (with needleleaf and deciduous forests accounting for 35.7 and 24.5% of the total drainage area) was greater than the rate predicted for IRW (with mixedwood and deciduous forests accounting for 40.4 and 36.8% of the total drainage area, Table S4.1). This may have been caused by adjustment to the ET-parameters, including available soil water (SOL_AWC.sol) and soil evaporation compensation factor (ESCO.hru) to reduce the discrepancy between measured and predicted streamflow rates (Fig. 4.3 and 4.4). These adjustments resulted in lower available soil water in the forested areas of IRW, compared to GRW (Table S4.3). Such modifications were necessary due to the absence of relevant biophysical parameters in SWAT governing stomatal conductance in cold regions, highlighting the need for enhancements to SWAT's capacity to simulate forest growth.

In addition, the soils in forested regions are often low in nutrients and have a high proportion of peat, which can retain a great deal of water that may not be readily released for plant consumption. In contrast, agricultural soils are often amended with fertilizers and managed to improve soil structure and water availability, which can cause ET to increase. In this study, hydrology in BBW is controlled by several land management practices, including tillage, flow diversion terracing, and differences in crop rotation. This can lead to ET being greater for BBW compared to forested watersheds with no or limited levels of management.

4.4.2.2 Peak and low flows

Snow is a crucial influencing factor in Atlantic Canada, with forest cover interacting with snowfall to determine maximum snowpack thickness and spring runoff (Schmidt et al., 1998). During the snowmelt season, forested watersheds displayed elevated measured

and predicted accumulated flows compared to agricultural watersheds, with an increase ranging from 2.8–15.6% and a delayed peak flow of 7–17 days. High peak flows were found to occur in the agricultural watershed (Fig. 4.5 and Table 4.4), in contrast with the two forested watersheds. Forested watersheds provide greater shading of the snowpack below the canopy, causing snowmelt processes to proceed at a much slower and extended rate. This is reflected in an overall improvement in model-project performance with modification to the snow-based parameters and associated processes during the snowmelt season (Fig. 4.3 and 4.4). The snowmelt base temperature (SMTMP.bsn) was seemingly greater in the forested watersheds (Table S4.3), leading to a delay in snowmelt during the winter as compared with the higher and earlier peak flow observed for the agricultural watershed. SWAT still has some shortfalls when predicting streamflow rates during the snowmelt season, particularly as it pertains to the forested watersheds (Fig. 4.5).

Accordingly, landcover conversion can help mitigate the timing of peak flow and, as a result, alleviate flooding during the snowmelt season. This finding is consistent with the research conducted by Jin et al. (2023) for a significant part of the USJR basin, revealing that the loss of forests can lead to an increase in peak flow and a decrease in low flows during the warm season of each year. Also, reductions in forest cover can lead to a reduced lag between the timing of peak flow and maximum snow cover thickness (Jin et al., 2023).

When detecting accumulated low flow during the dry, warm season, forested watersheds exhibited significantly greater flows compared to the agricultural watershed (Fig. 4.5). This can be attributed to the fact that forested watersheds may account for a thick forest-floor litter mat, typically not present in agriculture-dominated watersheds. Flow originating from forested watersheds is composed of lateral flow or shallow groundwater

return flow, with lesser amounts of water flowing directly as surface runoff. Although SWAT does not address the effects of litter dynamics directly in its treatment of streamflow, we managed to improve model simulations regarding baseflow during the warm seasons by adjusting ET-based parameters related to soil water capacity (Fig. 4.3 and 4.4). In general, a decrease in ET meant an increase in streamflow, and during the warm seasons, contribution of baseflow to stream discharge was shown to be significant. Jin et al. (2023) also illustrates this point for the larger USJR basin outline in Fig. 4.1.

4.4.3 Limitations and future work

In this study, we do not calibrate parameters separately for the agriculture- and forest-dominated HRUs of watersheds, which could include varying landcover. This is because the forested area in BBW is quite small, resulting in their parameters having minimal control on outlet discharge. The same situation was noted for the forested watersheds. Despite its wide application, SWAT may have limitations when applied to studies of hydrological processes in forested watersheds (Haas et al., 2022 and Karki et al., 2023). This study highlights some of these inherent limitations in the model, which obscures the assessment of hydrological differences across various watersheds, including the simulation of ET (Wu et al., 2012a, 2012b) and in- and outflow of groundwater (May and Mazlan, 2014; Zhang et al., 2016; Liu et al., 2020). Future enhancements of SWAT's forest-growth module, with more accurate representation of physiological processes and litter dynamics, are anticipated to improve the simulation of hydrological responses at the watershed scale for watersheds of variable landcover. This will facilitate the detection of hydrological response of watersheds resulting from differences in landcover.

4.5 Conclusions

This research examined the variation in hydrological response between agricultural and forested watersheds in Atlantic Canada with the help of an established, integrated hydrological model (SWAT) to disentangle the complex interactions between biophysical factors that are known to influence hydrological processes at the watershed level. Distinct differences were found in hydrological response between forested and agricultural watersheds. These results contradict the general belief that forests evaporate more water, leading to the reductions in streamflow. We found that forested watersheds in Atlantic Canada generally yielded more streamflow on an annual basis, which could be attributed to a net reduction in ET. We also found that forested watersheds generated more streamflow during dry, warm seasons largely as baseflow, which is likely caused by increased infiltration and groundwater recharging. In addition, during the snowmelt season, the peak flow in forested watersheds was observed to be delayed by approximately 7–17 days with higher accumulated flow due to shading provided by intact forests. We also found that the total cumulative streamflow in forested watersheds during the snowmelt season was greater than the streamflow from an agricultural watershed, with corresponding peak flow rates being reduced.

Acknowledgements

The authors would like to acknowledge (i) the Natural and Science and Engineering Council (NSERC), New Brunswick Environmental Trust Fund (NBETF) and Environment and Climate Change Canada (ECCC) for funding this project; (ii) the Faculty of Forestry and Environmental Management, University of New Brunswick, for license and computer support for ESRI ArcGIS™ and other software employed in this study. Authors are

thankful to Sylvie Lavoie, Yulia Kupriyanovich, John Monteith, and Lionel Stevens for their technical support in data collection and sample analyses.

References

Abbaspour, K. C., Johnson, C. A., and Van, G. M. T. (2004). Estimating uncertain flow and transport parameters using a sequential uncertainty fitting procedure. Vadose Zone Journal, 3(4), 1340–1352. https://doi.org/10.2136/vzj2004.1340.

Abbaspour, K. C., Rouholahnejad, E., Vaghefi, S., Srinivasan, R., Yang, H., and Kløve, B. (2015). A continental-scale hydrology and water quality model for Europe: Calibration and uncertainty of a high-resolution large-scale SWAT model. Journal of Hydrology, 524, 733–752. https://doi.org/10.1016/j.jhydrol.2015.03.027.

Aloui, S., Mazzoni, A., Elomri, A., Aouissi, J., Boufekane, A., and Zghibi, A. (2023). A review of Soil and Water Assessment Tool (SWAT) studies of Mediterranean catchments: Applications, feasibility, and future directions. Journal of Environmental Management, 326(B), 116799. https://doi.org/10.1016/j.jenvman.2022.116799.

Arnold, J. G., Srinivasan, R., Muttiah, R. S., and Williams, J. R. (2007). Large area hydrologic modeling and assessment part I: Model Development. Journal of the American Water Resources Association, 34 (1), 73–89. https://doi.org/10.1111/j.1752-1688.1998.tb05961.x.

Arnold, J.G., Moriasi, D.N., Gassman, P.W., Abbaspour, K.C., White, M.J., Srinivasan, R., Santhi, C., Harmel, R., Van Griensven, A., and Van Liew, M.W. (2012). SWAT: Model use, calibration, and validation. Transactions of the ASABE, 55(4), 1491–1508. https://doi.org/10.13031/2013.42256

Bearup, L. A., Maxwell, R. M., Clow, D. W., and McCray, J. E. (2014). Hydrological effects of forest transpiration loss in bark beetle-impacted watersheds. Nature Climate Change, 4, 481–486. https://doi.org/10.1038/nclimate2198.

Breil, M., Davin, E. L., and Rechid, D. (2021). What determines the sign of the evapotranspiration response to afforestation in European summer? Biogeosciences, 18(4), 1499–1510. https://doi.org/10.5194/bg-18-1499-2021.

Brown, A. E., Zhang, L., McMahon, T. A., Western, A. W., and Vertessy, R. A. (2005). A review of paired catchment studies for determining changes in water yield resulting from alterations in vegetation. Journal of Hydrology, 310(1–4), 28–61. https://doi.org/10.1016/j.jhydrol.2004.12.010.

Carlyle-Moses, D.E., and Gash, J.H.C. (2011). Rainfall Interception Loss by Forest Canopies. In: Levia, D., Carlyle-Moses, D., Tanaka, T. (eds). Forest Hydrology and Biogeochemistry (pp. 407–423). Ecological Studies, Vol 216. Springer, Dordrecht. https://doi.org/10.1007/978-94-007-1363-5_20

Chen, Y., Wang, L., Shi, X., Zeng, C., Wang, Y., Wang, G., Qiangba, C., Yue, C., Sun, Z., Renzeng, O., and Zhang, F. (2023). Impact of climate change on the hydrological regimes of the midstream section of the Yarlung Tsangpo River Basin based on SWAT model. Water, 15(4), 685. https://doi.org/10.3390/w15040685.

Chow, L., Xing, Z., Benoy, G., Rees, H.W., Meng, F.-R., Jiang, Y., and Daigle, J.L. (2011). Hydrology and water quality across gradients of agricultural intensity in the Little River watershed area, New Brunswick, Canada. Journal of Soil and Water Conservation, 66(1), 71–84. https://doi.org/10.2489/jswc.66.1.71

Chow, T. and Rees, H. (2006). Impacts of intensive potato production on water yield and sediment load (Black Brook Experimental Watershed: 1992–2002 summary). Potato Research Centre, AAFC, Fredericton, NB, Canada.

Crockford, R. H. and Richardson, D. P. (2000). Partitioning of rainfall into throughfall, stemflow and interception: effect of forest type, ground cover and climate. Hydrological Processes, 14(16–17), 2903–2920. https://doi.org/10.1002/1099-1085(200011/12)14:16/17<2903::AID-HYP126>3.0.CO;2-6

Dias, L. C. P., Macedo, M. N., Costa, M. H., Coe, M. T., and Neill, C. (2015). Effects of land cover change on evapotranspiration and streamflow of small catchments in the Upper Xingu River Basin, Central Brazil. Journal of Hydrology: Regional Studies, 4(B), 108–122. https://doi.org/10.1016/j.ejrh.2015.05.010.

Duveiller, G., Hooker, J., and Cescatti, A. (2018). The mark of vegetation change on Earth's surface energy balance. Nature communications, 9, 679. https://doi.org/10.1038/s41467-017-02810-8.

Dwarakish, G. S. and Ganasri, B. P. (2015). Impact of landuse change on hydrological systems: A review of current modeling approaches. Cogent Geoscience, 1(1), 1115691. https://doi.org/10.1080/23312041.2015.1115691.

Fisher, J.B., Tu, K.P., and Baldocchi, D.D. (2018). Global estimates of the land–atmosphere water flux based on monthly AVHRR and ISLSCP-II data, validated at 16 FLUXNET sites. Remote Sense Environment, 112, 901-919. https://doi.org/10.1016/j.rse.2007.06.025.

Garna, R. K., Fuka, D. R., Faulkner, J. W., Collick, A. S., and Easton, Z. M. (2023). Watershed model parameter estimation in low data environments. Journal of Hydrology: Regional Studies, 45, 101306. https://doi.org/10.1016/j.ejrh.2022.101306.

Gunacti, M. C., Gul, G. O., Cetinkaya, C. P., Gul, A., and Barbaros, F. (2023). Evaluating impact of land use and land cover change under climate change on the Lake Marmara System. Water Resources Management, 37, 2643–2656. https://doi.org/10.1007/s11269-022-03317-8.

Haas, H., Reaver, N. G. F., Karki, R., Kalin, L., Srivastava, P., Kaplan, D. A., and Gonzalez-Benecke, C. (2022). Improving the representation of forests in hydrological models. Science of The Total Environment, 812, 151425. https://doi.org/10.1016/j.scitotenv.2021.151425.

Hurkmans, R. T. W. L., Terink, W., Uijlenhoet, R., Moors, E. J., Troch, P. A., and Verburg, P. H. (2009). Effects of landuse changes on streamflow generation in the Rhine basin. Water Resources Research, 45(6), W06405. https://doi.org/10.1029/2008WR007574.

Jin, C., Zha, T., Guo, X., Li, X., Liu, X., Jiang, Y., Guo, Z., and Bourque, C. P.-A. (2023). Forest-cover-loss control on year-round river flow dynamics in the upper Saint John River (Wolastoq) basin, Northeastern North America from 2001 to 2019. Journal of Hydrology, 623, 129776. https://doi.org/10.1016/j.jhydrol.2023.129776.

Johnson, M. F. and Wilby, R. L. (2015). Seeing the landscape for the trees: Metrics to guide riparian shade management in river catchments. Water Resources Research, 51(5), 3754–3769. https://doi.org/10.1002/2014WR016802.

Johnson, R. S. H. and Alila, Y. (2023). Nonstationary stochastic paired watershed approach: Investigating forest harvesting effects on floods in two large, nested, and snow-dominated watersheds in British Columbia, Canada. Journal of Hydrology, 625(A), 129970. https://doi.org/10.1016/j.jhydrol.2023.129970.

Karki, R., Qi, J., Gonzalez-Benecke, C. A., Zhang, X., Martin, T. A., and Arnold, J. G. (2023). SWAT-3PG: Improving forest growth simulation with a process-based forest model in SWAT. Environmental Modelling and Software, 164, 105705. https://doi.org/10.1016/j.envsoft.2023.105705.

Kiptala, J. K., Mohamed, Y., Mul, M. L., and Van der Zaag, P. (2013). Mapping evapotranspiration trends using MODIS and SEBAL model in a data scarce and heterogeneous landscape in Eastern Africa. Water Resources Research, 49(12), 8495–8510. https://doi.org/10.1002/2013WR014240.

Knoben, W. J. M., Freer, J. E., and Woods, R. A. (2019). Technical note: Inherent benchmark or not? Comparing Nash–Sutcliffe and Kling–Gupta efficiency scores. Hydrology and Earth System Sciences, 23(10), 4323–4331. https://doi.org/10.5194/hess-23-4323-2019.

Liang, K., Qi, J., Liu, E. Y., Jiang, Y., Li, S., and Meng, F.-R. (2019). Estimated potential impacts of soil and water conservation terraces on potato yields under different climate conditions. Journal of Soil and Water Conservation, 74(3), 225–234. https://doi.org/10.2489/jswc.74.3.225.

Liu, W., Park, S., Bailey, R. T., Molina-Navarro, E., Andersen, H. E., Thodsen, H., Nielsen, A., Jeppesen, E., Jensen, J. S., Jensen, J. B., and Trolle, D. (2020). Quantifying the streamflow response to groundwater abstractions for irrigation or drinking water at catchment scale using SWAT and SWAT–MODFLOW. Environmental Sciences Europe, 32, 113. https://doi.org/10.1186/s12302-020-00395-6.

Lu, C., Zhao, T., Shi, X., and Cao, S. (2018). Ecological restoration by afforestation may increase groundwater depth and create potentially large ecological and water opportunity costs in arid and semiarid China. Journal of Cleaner Production, 176, 1213–1222. https://doi.org/10.1016/j.jclepro.2016.03.046.

May, R. and Mazlan, N. S. B. (2014). Numerical simulation of the effect of heavy groundwater abstraction on groundwater–surface water interaction in Langat Basin, Selangor, Malaysia. Environmental Earth Sciences, 71, 1239–1248. https://doi.org/10.1007/s12665-013-2527-4.

Mellerowicz, K.T. (1993). Soils of Black Brook Watershed St. Andre Parish, Madawaska County, New Brunswick. [Fredericton]: New Brunswick Department of Agriculture. https://sis.agr.gc.ca/cansis/publications/surveys/nb/nbbb/index.html

Mengistu, A. G., van Rensburg, L. D., and Woyessa, Y. E. (2019). Techniques for calibration and validation of SWAT model in data scarce arid and semi-arid catchments in South Africa. Journal of Hydrology: Regional Studies, 25, 100621. https://doi.org/10.1016/j.ejrh.2019.100621.

Mu, Q. Z., Zhao, M. S., and Running, S. W. (2011). Improvements to a MODIS global terrestrial evapotranspiration algorithm, Remote Sensing of Environment, 115(8), 1781-1800. https://doi.org/10.1016/j.rse.2011.02.019.

Moriasi, D. N., Arnold, J. G., Van Liew, M. W., Bingner, R. L., Harmel, R. D., and Veith, T. L. (2007). Model evaluation guidelines for systematic quantification of accuracy in watershed simulations. Transactions of the ASABE, 50(3), 885–900, https://doi.org/10.13031/2013.23153.

Neitsch, S., Arnold, J., Kinry, J. R., and Williams, J. R. (2011). Soil and Water Assessment Tool Theoretical Documentation, Version 2011. https://swat.tamu.edu/media/99192/swat2009-theory.pdf

Qi, J., Zhang, X., and Cosh, M. H. (2019). Modeling soil temperature in a temperate region: A comparison between empirical and physically based methods in SWAT. Ecological Engineering, 129, 134–143. https://doi.org/10.1016/j.ecoleng.2019.01.017.

Qi, J., Kang, X., Li, S., and Meng, F.-R. (2022). Evaluating impacts of detailed land use and management inputs on the accuracy and resolution of swat predictions in an experimental watershed. Water, 14(15), 23–52. https://doi.org/10.3390/w14152352.

Qi, J., Li, S., Bourque, C. P.-A., Xing, Z., and Meng, F.-R. (2018). Developing a decision support tool for assessing landuse change and BMPs in ungauged watersheds based on decision rules provided by SWAT simulation. Hydrology and Earth System Sciences, 22(7), 3789–3806. https://doi.org/10.5194/hess-22-3789-2018.

Qi, J., Li, S., Yang, Q., Xing, Z., and Meng, F.-R. (2017a). SWAT setup with long-term detailed landuse and management records and modification for a micro-watershed influenced by freeze-thaw cycles. Water Resources Management, 31, 3953–3974. https://doi.org/10.1007/s11269-017-1718-2.

Qi, J., Li, S., Jamieson, R., Hebb, D., Xing, Z., and Meng, F.-R. (2017b). Modifying SWAT with an energy balance module to simulate snowmelt for maritime regions. Environmental Modelling and Software, 93, 146–160. https://doi.org/10.1016/j.envsoft.2017.03.007.

Qi, J., Li, S., Li, Q., Xing, Z., Bourque, C. P.-A., and Meng, F.-R. (2016a). Assessing an enhanced version of SWAT on water quantity and quality simulation in regions with seasonal snow cover. Water Resources Management, 30, 5021–5037. https://doi.org/10.1007/s11269-016-1466-8.

Qi, J., Li, S., Li, Q., Xing, Z., Bourque, C. P.-A., and Meng, F.-R. (2016b). A new soil-temperature module for SWAT application in regions with seasonal snow cover. Journal of Hydrology, 538, 863–877. https://doi.org/10.1016/j.jhydrol.2016.05.003.

Ricciardi, L., D'Odorico, P., Galli, N., Chiarelli, D. D., and Rulli, M. C. (2022). Hydrological implications of large-scale afforestation in tropical biomes for climate change mitigation, Philosophical transactions of the Royal Society of London. Series B, Biological sciences, 377(1857), 20210391, https://doi.org/10.1098/rstb.2021.0391.

Rocha, A. K. P., de Souza, L. S. B., de Assunção Montenegro, A. A., de Souza, W. M., and da Silva, T. G. F. (2023). Revisiting the application of the SWAT model in

arid and semi-arid regions: a selection from 2009 to 2022. Theoretical and Applied Climatology, 154, 7–27. https://doi.org/10.1007/s00704-023-04546-6.

Saravanan, S., Singh, L., Sathiyamurthi, S., Sivakumar, V., Velusamy, S., and Shanmugamoorthy, M. (2022). Predicting phosphorus and nitrate loads by using SWAT model in Vamanapuram River Basin, Kerala, India. Environmental Monitoring and Assessment, 195, 186. https://doi.org/10.1007/s10661-022-10786-2.

Scheff, S. W. (2016). Fundamental Statistical Principles for the Neurobiologist: A Survival Guide, https://doi.org/10.1016/C2015-0-02471-6.

Schmidt, R. A., Troendle, C. A., and Meiman, J. R. (1998). Sublimation of snowpacks in subalpine conifer forests. Canadian Journal of Forest Research, 28(4), 501–513, https://doi.org/10.1139/x98-033

Shepherd, T. and Wynne Griffiths, D. (2006). The effects of stress on plant cuticular waxes. New Phytologist, 171(3), 469–499, https://doi.org/10.1111/j.1469-8137.2006.01826.x

Tang, F. F., Xu, H. S., and Xu, Z. X. (2012). Model calibration and uncertainty analysis for runoff in the Chao River Basin using sequential uncertainty fitting. Procedia Environmental Sciences, 13, 1760–1770, https://doi.org/10.1016/j.proenv.2012.01.170.

Teo, H. C., Raghavan, S. V., He, X., Zeng, Z., Cheng, Y., Luo, X., Lechner, A. M., Ashfold, M. J., Lamba, A., Sreekar, R., Zheng, Q., Chen, A., and Koh, L. P. (2022). Large-scale reforestation can increase water yield and reduce drought risk

for water-insecure regions in the Asia-Pacific. Global Change Biology, 28(21), 6385–6403, https://doi.org/10.1111/gcb.16404.

Thornton, M.M., R. Shrestha, Y. Wei, P.E. Thornton, S. Kao, and B.E. Wilson. (2020). Daymet: Daily Surface Weather Data on a 1-km Grid for North America, Version 4. ORNL DAAC, Oak Ridge, Tennessee, USA. https://doi.org/10.3334/ORNLDAAC/1840

Truong, N. C., Khoi, D. N., Nguyen, H. Q., and Kondoh, A. (2022). Impact of forest conversion to agriculture on hydrologic regime in the Large Basin in Vietnam. Water, 14(6), 854. https://doi.org/10.3390/w14060854 .

Viney, N. R., Bormann, H., Breuer, L., Bronstert, A., Croke, B. F. W., Frede, H., Gräff, T., Hubrechts, L., Huisman, J. A., Jakeman, A. J., Kite, G. W., Lanini, J., Leavesley, G., Lettenmaier, D. P., Lindström, G., Seibert, J., Sivapalan, M., and Willems, P. (2009). Assessing the impact of landuse change on hydrology by ensemble modelling (LUCHEM) II: Ensemble combinations and predictions. Advances in Water Resources, 32(2), 147–158, https://doi.org/10.1016/j.advwatres.2008.05.006.

Von Randow, C., Manzi, A. O., Kruijt, B., de Oliveira, P. J., Zanchi, F. B., Silva, R. L., Hodnett, M. G., Gash, J. H. C., Elbers, J. A., Waterloo, M. J., Cardoso, F. L., and Kabat, P. (2004). Comparative measurements and seasonal variations in energy and carbon exchange over forest and pasture in South West Amazonia. Theoretical and Applied Climatology, 78, 5–26, https://doi.org/10.1007/s00704-004-0041-z.

Wang, C., Shang, S., Jia, D., Han, Y., Sauvage, S., Sánchez-Pérez, J.-M., Kuramochi, K., and Hatano, R. (2018). Integrated effects of land use and topography on streamflow response to precipitation in an agriculture-forest dominated northern watershed. Water, 10(5), 633. https://doi.org/10.3390/w10050633.

Wang, K., Dickinson, R.E., Wild, M., and Liang, S. (2010). Evidence for decadal variation in global terrestrial evapotranspiration between 1982 and 2002, Journal of Geophysical Research, 115. https://doi.org/10.1029/2010JD013847.

Wang, Q., Qi, J., Qiu, H., Li, J., Cole, J., Waldhoff, S., and Zhang, X. (2021). Pronounced increases in future soil erosion and sediment deposition as influenced by Freeze–Thaw cycles in the Upper Mississippi River Basin. Environmental Science and Technology, 55(14), 9905–9915. https://doi.org/10.1021/acs.est.1c02692.

Wang, Q., Qi, J., Wu, H., Zeng, Y., Shui, W., Zeng, J., and Zhang, X. (2020). Freeze-Thaw cycle representation alters response of watershed hydrology to future climate change. Catena, 195, 104767. https://doi.org/10.1016/j.catena.2020.104767

Wang, R., Kalin, L., Kuang, W., and Tian, H. (2014). Individual and combined effects of landuse/cover and climate change on Wolf Bay watershed streamflow in southern Alabama. Hydrological Processes, 28(22), 5530–5546, https://doi.org/10.1002/hyp.10057

Williams, C. A., Reichstein, M., Buchmann, N., Baldocchi, D., Beer, C., Schwalm, C., Wohlfahrt, G., Hasler, N., Bernhofer, C., Foken, T., Papale, D., Schymanski, S., and Schaefer, K. (2012). Climate and vegetation controls on the surface water

balance: Synthesis of evapotranspiration measured across a global network of flux towers. Water Resources Research, 48(6), https://doi.org/10.1029/2011WR011586.

Wu, Y., Liu, S., and Abdul-Aziz, O. I. (2012a). Hydrological effects of the increased CO_2 and climate change in the Upper Mississippi River Basin using a modified SWAT. Climatic Change, 110, 977–1003. https://doi.org/10.1007/s10584-011-0087-8.

Wu, Y., Liu, S., and Gallant, A. L. (2012b). Predicting impacts of increased CO_2 and climate change on the water cycle and water quality in the semiarid James River Basin of the Midwestern USA. Science of The Total Environment, 430, 150–160. https://doi.org/10.1016/j.scitotenv.2012.04.058.

Xia, J., Zhang, Y., Xiong, L., He, S., Wang, L., and Yu, Z. (2017). Opportunities and challenges of the Sponge City construction related to urban water issues in China. Science China Earth Sciences, 60, 652–658. http://doi.org/10.1007/s11430-016-0111-8

Yang, D., Yang, Y., and Xia, J. (2021). Hydrological cycle and water resources in a changing world: A review. Geography and Sustainability, 2(2), 115–122. https://doi.org/10.1016/j.geosus.2021.05.003

Yang, J., Reichert, P., Abbaspour, K. C., Xia, J., and Yang, H. (2008). Comparing uncertainty analysis techniques for a SWAT application to the Chaohe Basin in China. Journal of Hydrology, 358(1–2), 1–23. https://doi.org/10.1016/j.jhydrol.2008.05.012.

Yang, Q. and Zhang, X. (2016). Improving SWAT for simulating water and carbon fluxes of forest ecosystems. Science of The Total Environment, 569–570, 1478–1488. https://doi.org/10.1016/j.scitotenv.2016.06.238.

Yao, Y.J., Liang, S., Cheng, J., Liu, S.M., Fisher, J.B., Zhang, X.D., Jia, K., Zhao, X., Qing, Q.M., Zhao, B., Han, S.J., Zhou, G.S., Zhou, G.Y., Li, Y.L., and Zhao, S.H. (2013). MODIS-driven estimation of terrestrial latent heat flux in China based on a modified Priestley-Taylor algorithm. Agricultural and Forest Meteorology, 171, 187-202. https://doi.org/10.1016/j.agrformet.2012.11.016 .

Yao, Y., Liang, S., Li, X., Hong, Y., Fisher, J.B., Zhang, N., Chen, J., Cheng, J., Zhao, S., Zhang, X., Jiang, B., Sun, L., Jia, K., Wang, K., Chen, Y., Mu, Q., and Feng, F. (2014). Bayesian multimodel estimation of global terrestrial latent heat flux from eddy covariance, meteorological, and satellite observations, Journal of Geophysical Research: Atmospheres, 119, 2013JD020864. https://doi.org/10.1002/2013JD020864.

Yaseef, N. R., Yakir, D., Rotenberg, E., Schiller, G., and Cohen, S. (2010). Ecohydrology of a semi-arid forest: partitioning among water balance components and its implications for predicted precipitation changes. Ecohydrology, 3(2), 143–154. https://doi.org/10.1002/eco.65.

Yu, X. and Bourque, C. P.-A. (2022). Controls of contemporary (2001–2018) springtime waterflow dynamics in a large, snowmelt-dominated basin in northeastern North America. Journal of Hydrology X, 14, 100117. https://doi.org/10.1016/j.hydroa.2021.100117.

Yuan, W.P., Liu, S.G., Yu, G.R., Bonnefond, J.-M., Chen, J. Q., Davis, K., Desai, A. R., Goldstein, A. H., Gianelle, D., Rossi, F., Suyker, A. E. and Verma, S. B. (2010). Global estimates of evapotranspiration and gross primary production based on MODIS and global meteorology data. Remote Sensing of Environment, 114 (7), 1416-1431. https://doi.org/10.1016/j.rse.2010.01.022 .

Zhang, M. and Wei, X. (2021). Deforestation, forestation, and water supply. Science, 371(6533), 990–991. https://doi.org/10.1126/science.abe7821.

Zhang, M., Liu, N., Harper, R., Li, Q., Liu, K., Wei, X., Ning, D., Hou, Y., and Liu, S. (2017). A global review on hydrological responses to forest change across multiple spatial scales: Importance of scale, climate, forest type and hydrological regime. Journal of Hydrology, 546, 44–59. https://doi.org/10.1016/j.jhydrol.2016.12.040.

Zhang, X., Ren, L., and Kong, X. (2016). Estimating spatiotemporal variability and sustainability of shallow groundwater in a well-irrigated plain of the Haihe River basin using SWAT model. Journal of Hydrology, 541(B), 1221–1240. https://doi.org/10.1016/j.jhydrol.2016.08.030

Zhou, G., Wei, X., Chen, X., Zhou, P., Liu, X., Xiao, Y., Sun, G., Scott, D. F., Zhou, S., Han, L., and Su, Y. (2015). Global pattern for the effect of climate and land cover on water yield. Nature communications, 6, 5918. https://doi.org/10.1038/ncomms6918.

SUPPLEMENTARY MATERIAL

Table S4.1 Percent area of specific landcover types in two forested watersheds, GRW and IRW.

Landcover type	GRW	IRW
Temperate or sub-polar needleleaf forests	35.7	13.4
Temperate or sub-polar broadleaf deciduous forests	24.5	36.8
Mixedwood forests	16.6	40.4
Wetlands	6.5	0.1
Temperate or sub-polar shrublands	5.7	5.0
Temperate or sub-polar grasslands	4.4	1.2
Barren lands	3.3	0.1
Croplands	2.0	1.3
Urban and buildup areas	1.0	1.5
Water	0.2	0.2

Table S4.2 Sensitivity analysis based on the model-project specific to BBW.

Rank	Parameter	Description	Range	Sensitivity	
				t-Stat	*p*-value
1	v__SMTMP.bsn	Snowmelt base temperature [ºC]	[-10,10]	-2.67	0.008***
2	r__SOL_K.sol	Saturated hydraulic conductivity [mm/hr]	[-0.2,0.2]	-2.10	0.036**
3	v__ESCO.hru	Soil evaporation compensation factor	[0,1]	-2.05	0.040**
4	r__SOL_AWC.sol	Available water capacity of the soil layer [mm H_2O/mm soil]	[-0.2,0.2]	2.03	0.042**
5	v__ALPHA_BF.gw	Baseflow alpha factor [days]	[0.5,1]	1.28	0.048**
6	r__SOL_Z.sol	Depth from soil surface to bottom of layer [mm]	[-0.2,0.2]	1.42	0.158
7	v__GW_DELAY.gw	Groundwater delay [days]	[0,500]	-52.26	0.211
8	v__SMFMX.bsn	Melt factor for snow on June 21 [mm H_2O/ºC-day]	[0,20]	1.17	0.241
9	v__TIMP.bsn	Snowpack temperature lag factor	[0,1]	-1.14	0.254
10	v__GWQMN.gw	Threshold depth of water in the shallow aquifer required for return flow to occur [mm]	[0,1000]	0.88	0.378
11	v__CH_N2.rte	Manning's n value for main channel	[-0.01,0.3]	-0.86	0.390
12	v__CH_K2.rte	Effective hydraulic conductivity [mm/hr]	[-0.01,500]	0.60	0.550
13	v__SFTMP.bsn	Snowfall temperature [ºC]	[-20,10]	-0.51	0.612
14	v__EPCO.hru	Plant uptake compensation factor	[0,1]	-0.50	0.619
15	v__CANMX.hru	Maximum canopy storage [mm]	[0,10]	-0.37	0.713
16	v__SMFMN.bsn	Melt factor for snow on December 21 [mm H_2O/ºC-day]	[0,20]	0.18	0.855

Note: v_ and r_ represent replace default values or relative change in these parameters

Table S4.3 Best-fitted parameters following calibration of model projects for the three watersheds.

Parameter No.	Parameter Grouping	Parameter	Default	BBW	GRW	IRW
1	ET-based	v__ESCO.hru	0.95	0.80	0.80	0.95
2	ET-based	r__SOL_AWC.sol	-	0	-0.78	-0.85
3	GW-based	v__ALPHA_BF.gw	0.004	0.95	0.95	0.95
4	SNO-based	v__SMTMP.bsn	0.5	2	5	5

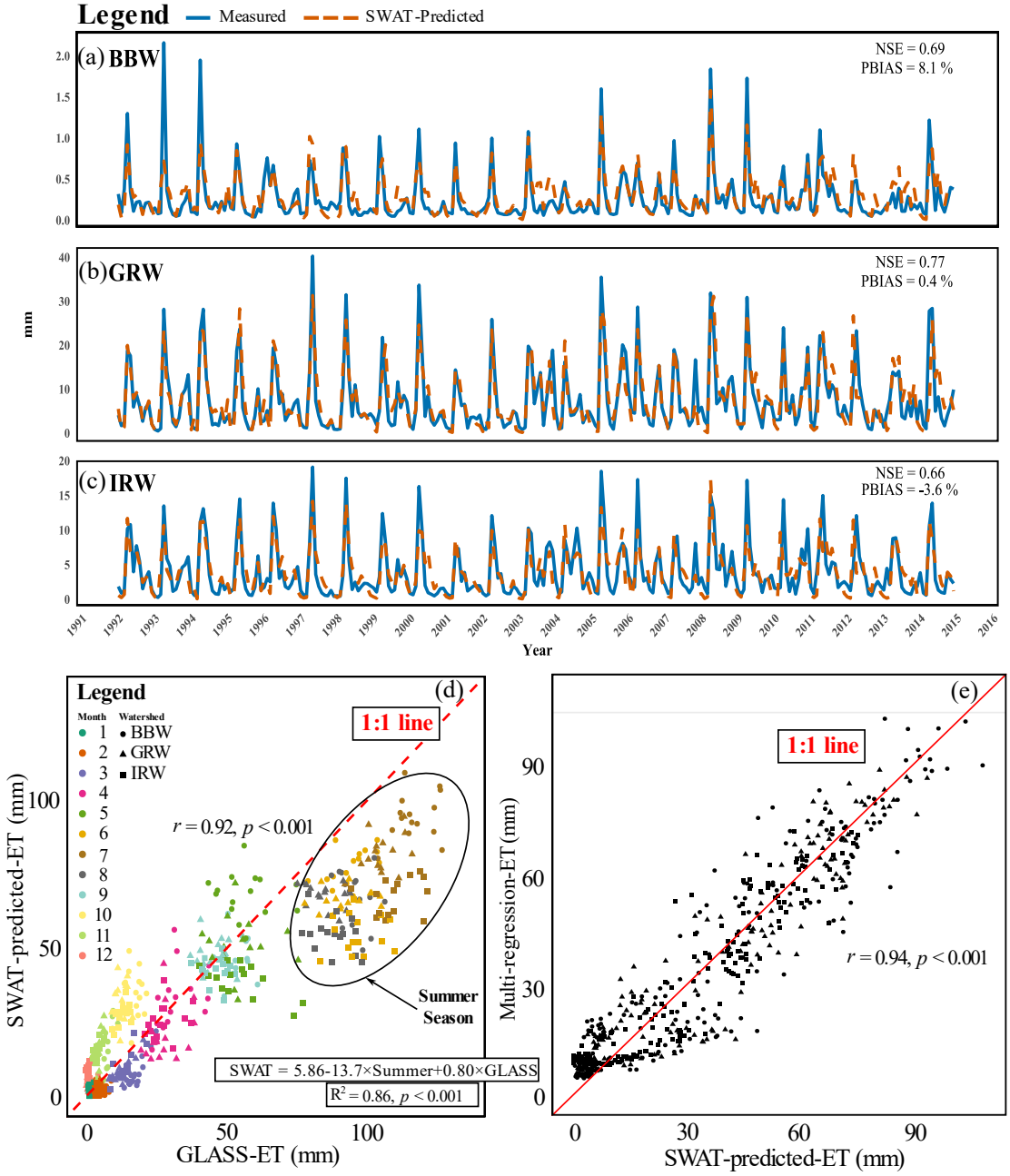

Fig. S4.1 Measured and SWAT-predicted discharge rates for the 1992–2014 period for the three target watersheds [i.e., BBW(a), GRW(b) and IRW(c)] with model performance indicated as a function of NSE and *PBIAS*. (d) Scatterplots between GLASS-ET and SWAT-predicted-ET from 2000–2018 and (e) SWAT-predicted-ET and multi-regression-based estimates of ET from the model created in (d); r in (d) and (e) represents the correlation coefficient with the multiple regression model developed in (d) indicating the relationship between GLASS-ET and SWAT-predicted-ET accounting for seasonal variability.

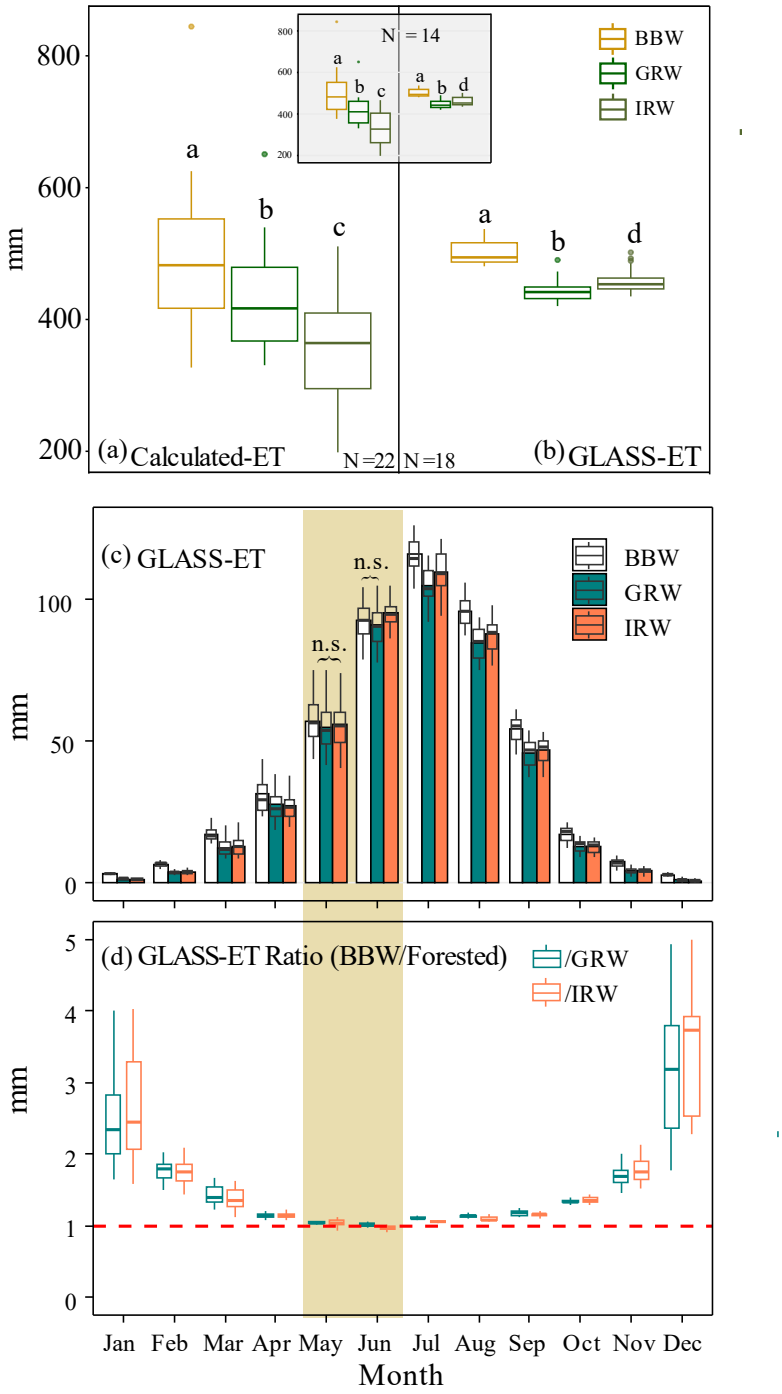

Fig. S4.2 Boxplots for annual (a) 'Calculated-ET' (1993–2014) and (b) 'GLASS-ET' (2001–2018) for the three target watersheds [i.e., BBW(a), GRW(b) and IRW(c)]. (c) Bar charts for average monthly GLASS-ET with boxplots. (d) Bar charts based on a ratio of agricultural-to-forest based GLASS-ET. Paired t-tests were applied among watersheds at a P-value < 0.001 in (c) and (d). n.s. in (c) stands for 'not significant'.

CHAPTER 5

CONCLUDING REMARKS

5.1 Scientific Contributions

Systems models are useful in the study of environmental impact caused by variances in many of the more common process variables, such as those associated with biophysical processes influenced by prevailing monthly weather, existing physiography, and differences in landcover. In many situations, many of the associated variables are correlated and confounded, rendering their assessment in the field, as to their specific contribution to environmental impact, rather challenging. Watershed-scale characterizations of stomatal conductance (related to changes in ambient CO_2 concentrations) and plant transpiration could conceivably be acquired with eddy-covariance techniques that can capture biospheric gas and energy exchanges at moderate spatial, field-level scales. However, installation of eddy-covariance equipment for such research is very time-consuming, and logistically and financially expensive, although practical in model parameterization. Application of systems models, as demonstrated in this dissertation, can help address some of these problems with some level of success.

In **Chapter 2**, crop yield under future climate change is projected with the direct application of SWAT calibrated and validated for BBW, along with downscaled simulation ensembles based on five GCMs. The impact of soil water stress and ET on crop yields were assessed directly with SWAT. Specific results of the study include: (i) significant reduction in crop yields are expected under RCP 8.5 from 2060–2099, with 13–23% declines from historical yields; (ii) elevated ambient CO_2 concentrations could help increase crop yields because of CO_2 fertilization. This increase, however, is small compared to the negative impact on crop yields anticipated to accompany soil water deficits and associated

environmental stress on crops; and (iii) adjusting GHG emissions to below RCP 4.5 levels can benefit future crop production and yields.

It is commonly known that systems models inherently do not incorporate all conceivable factors and processes in their design, and as a result these models have a limited scope in their application. In this dissertation, by way of **Chapter 3**, we show how a well-established, integrated model of watershed hydrology (in this case, SWAT) can be used to examine the contribution of several unaccounted variables (i.e., ambient CO_2 concentrations and annual construction of flow diversion terraces) in shaping streamflow dynamics in an agricultural watershed. The related variables due to their watershed-scale characterizations are very difficult to measure *in-situ*, limiting the incorporation of these variables and associated processes in hydrological models. To avoid the shortcomings of SWAT, we use the model initially to define a baseline scenario that captures the more common processes in defining the contribution of variances in landuse practices and monthly weather on waterflow dynamics at the watershed scale. The baseline calculations generated are compared against field-based measurements of stream/river flow via an analysis of residuals. The decomposition of the residuals with Bayesian statistical techniques provides an innovative way of isolating the contribution of individual variables unaccounted for in the model. This development is one contribution to the scientific literature that may help identify processes that are not currently addressed in existing watershed models. This approach may benefit the continued refinement of models, subject to the availability of *in-situ* measurements in informing module development and guiding its integration in models.

A second approach is developed in **Chapter 4** to analyze differences in the hydrological response of watersheds dominated by either agricultural or forest cover. The approach uses model regionalization, with the parameter values generated through automatic calibration of the agriculture-dominated model project in forcing the forest-dominated model-project simulations. Differences in watershed model outputs are attributed to variances in landcover type. With subsequent manual adjustments of the forest-based-model parameters, the primary processes that govern streamflow dynamics in watersheds of variable vegetation cover for both the snowmelt and warm seasons of the year are analyzed. Intact forest cover in watersheds caused the length of the snowmelt season and peak flow to vary from corresponding variables in an agricultural watershed. There is a message in this chapter about the role of forests in moderating streamflow dynamics year-round, consistent with the results of Jin et al. (2023) for the larger upper Saint John River (Wolastoq) basin (Fig. 4.1) using very different analytical techniques, involving machine learning and wavelet analysis. Caution should be used to limit the disruptive effects of open terrain on streamflow and water-quality dynamics further downstream.

5.2 Potential Future Work

i. Combination of field and modeling experiments is needed. With limited experimental data, the approaches developed herein can direct future decision-making as to the level of sampling and environmental impact conceivably possible.

ii. Evaluation of the effectiveness of current integrated hydrological models as to their parameter values and hydrological processes should be considered, especially as they relate to the watershed scale.

iii. Research described here should not be restricted to the application of SWAT but to other comparable models (e.g., WetSpa) in cross-model comparisons to acquire a better understanding of cause-and-effect relationships embraced by individual models.

CURRICULUM VITAE

Candidate's Full Name Xiaoyu Kang

PhD Candidate, University of New Brunswick (Fredericton)

Research Fields: Water Resource Management, Hydrological Modelling

---

Universities Attended

2019–2024	Doctor of Philosophy, University of New Brunswick, Canada
2016–2019	Master of Science, Beijing Forestry University, China
2012–2016	Bachelor of Science, Beijing Forestry University, China

Publications (accepted and in review)

(1) **Kang, X.,** Qi, J., Bourque, C. P.-A., Li, S., Jin, C., Hao, S., and Meng, F.-R. (2024). An inter-watershed comparison of hydrological response in agriculture- and forest-dominated watersheds in Atlantic Canada. *Under Revision.*

(2) **Kang, X.,** Qi, J., Bourque, C. P.-A., Li, S., Jin, C., and Meng, F.-R. (2024). Assessing watershed-scale impacts of best management practices and elevated atmospheric carbon dioxide concentrations on water yield. Science of the Total Environment, 926, 171629. https://doi.org/10.1016/j.scitotenv.2024.171629.

(3) Qi, J., **Kang, X.,** Li, S., and Meng, F.-R. (2022). Evaluating impacts of detailed land use and management inputs on the accuracy and resolution of SWAT predictions in an experimental watershed. Water, 14(15), 23–52. https://doi.org/10.3390/w14152352.

(4) **Kang, X.,** Qi, J., Li, S., and Meng, F.-R. (2022). A watershed-scale assessment of climate change impacts on crop yields in Atlantic Canada. Agricultural Water Management, 269, 107680. https://doi.org/10.1016/j.agwat.2022.107680.

(5) **Kang, X.,** Zhang, Z., Chen, L., Leng, M., and Yang, F. (2019). Baseflow variation and driving factors for the last six decades in a watershed on the Loess Plateau, northern China. Journal of Natural Resources, 34(3), 563–572. https://doi.org/10.31497/zrzyxb.20190310.

(6) **Kang, X.,** Zhang, Z., Chen, L., Xu, H., and Leng, M. (2019). Analysis of the applicability of automatic baseflow in Xinshui River of Loess Plateau. Journal of Beijing Forestry University, 41(1), 92–101. https://doi.org/10.13332/j.1000-1522.20180087.

Conference Presentations

(1) American Geophysical Union (AGU23, San Francisco, USA, in-person oral) 2023.12

(2) American Geophysical Union (AGU22, Chicago, USA, online iposter) 2022.12

(3) Chinese Ecohydrology Conference (Chengdu, China, in-person oral) 2018.10